# SOLUTION PROCESSABLE BENZOTRIAZOLE AND FLUORENE CONTAINING COPOLYMERS FOR PHOTOVOLTAIC APPLICATIONS

A THESIS SUBMITTED TO
THE GRADUATE SCHOOL OF NATURAL AND APPLIED SCIENCES
OF
MIDDLE EAST TECHNICAL UNIVERSITY

BY

EMİNE KAYA

IN PARTIAL FULFILLMENT OF THE REQUIREMENTS
FOR
THE DEGREE OF MASTER OF SCIENCE
IN
CHEMISTRY

SEPTEMBER 2011

Approval of the thesis:

**SOLUTION PROCESSABLE BENZOTRIAZOLE AND FLUORENE CONTAINING COPOLYMERS FOR PHOTOVOLTAIC APPLICATIONS**

submitted by **EMİNE KAYA** in partial fulfillment of the requirements for the degree of **Master of Science in Chemistry Department, Middle East Technical University** by,

Prof. Dr. Canan Özgen
Dean, Graduate School of **Natural and Applied Sciences** _____

Prof. Dr. İlker Özkan
Head of Department, **Chemistry** _____

Assist. Prof. Dr. Ali Çırpan
Supervisor, **Chemistry Dept., METU** _____

Prof. Dr. Levent Toppare
Co-Supervisor, **Chemistry Dept., METU** _____

**Examining Committee Members:**

Prof. Dr. Ahmet M. Önal _____
Chemistry Dept., METU

Assist. Prof. Dr. Ali Çırpan
Chemistry Dept., METU _____

Prof. Dr. Levent Toppare _____
Chemistry Dept., METU

Assoc. Prof. Dr. Metin Ak _____
Chemistry Dept., Pamukkale University

Dr. Bilge Emre _____
Chemistry Dept., METU

**Date:** 12.09.2011

**I hereby declare that all information in this document has been obtained and presented in accordance with academic rules and ethical conduct. I also declare that, as required by these rules and conduct, I have fully cited and referenced all material and results that are not original to this work.**

Name, Last Name: EMİNE KAYA

Signature

# ABSTRACT

SOLUTION PROCESSABLE BENZOTRIAZOLE AND FLUORENE CONTAINING COPOLYMERS FOR PHOTOVOLTAIC APPLICATIONS

Kaya, Emine

M. Sc., Department of Chemistry

Supervisor: Assist. Prof. Dr. Ali Çırpan

Co-Supervisor: Prof. Dr. Levent Toppare

September 2011, 87 pages

2-Dodecyl benzotriazole and 9,9-dioctylfluorene containing alternating copolymers poly((9,9-dioctylfluorene)-2,7-diyl-(2-dodecyl-benzo[1,2,3]triazole)) (P1), poly((9,9-dioc-tylfluorene)-2,7-diyl-(4,7-bis(thien-2-yl) 2-dodecyl benzo[1,2,3]triazole)) (P2), poly((9,9 dioctylfluorene)-2,7-diyl-(4,7-bis(3-hexylthien-5-yl) 2-dodecyl-benzo[1,2,3]triazole)) (P3) were synthesized via Suzuki polycondensation. Synthesized monomers and copolymers were characterized by Nuclear Magnetic Resonance ($^{1}$H-NMR, $^{13}$C-NMR). Optical and electronic properties of resulting alternating copolymers were investigated by means of Cyclic Voltammetry (CV), Ultraviolet–Visible Spectroscopy and spectroelectrochemistry. All three polymers showed both p and n doping behaviors and multicolored electrochromic states. In order to learn switching

times and percent transmittance changes kinetic studies were also performed. Thermal properties of the polymers were investigated via Thermogravimetric Analysis (TGA) and Differential Scanning Calorimetry (DSC). Due to the convenient HOMO and LUMO levels, band gaps, strong absorptions in the visible region and thermal stability, polymers were tested in Organic Solar Cell (OSC) device applications. The preliminary investigation indicated that polymers had promising power conversion efficiencies.

**Keywords:** Benzotriazole, Fluorene, Optoelectronic, Organic Solar Cells, Conjugated Copolymers, Donor–Acceptor.

# ÖZ

FOTOVOLTAİK UYGULAMALAR İÇİN ÇÖZÜNEBİLEN
BENZOTRİAZOL VE FLUORENE İÇEREN KOPOLİMERLER

Kaya, Emine
Yüksek Lisans, Kimya Bölümü
Tez Yöneticisi: Yrd. Doç. Dr. Ali Çırpan
Ortak Tez Yöneticisi: Prof. Dr. Levent Toppare

September 2011, 87 sayfa

2-Dodecyl benzotriazol ve 9,9-dioctylfluorene içeren kopolimerler poly((9,9-dioctylfluorene)-2,7-diyl-(2-dodecyl-benzo[1,2,3]triazole)) (P1), poly((9,9-dioc-tylfluorene)-2,7-diyl-(4,7-bis(thien-2-yl) 2-dodecyl benzo[1,2,3]triazole)) (P2) ve poly((9,9 dioctylfluorene)-2,7-diyl-(4,7-bis(3-hexylthien-5-yl) 2-dodecyl-benzo[1,2,3]triazole)) (P3), Suzuki birleşme yöntemi kullanılarak sentezlenmiştir. Sentezlenen monomer ve kopolimerler $^{1}H$, $^{13}C$ Nükleer Manyetik Rezonans Spektroskopisi (NMR) kullanılarak karakterize edilmiştir. Dönüşümlü Voltammetre (CV) ve UV-Vis Spektrofotometresi kullanılarak polimerlerin elektronik ve optik özellikleri araştırılmıştır. Bütün polimerlerin n ve p tip katkılanabilme ve multikromizm özelliklerine sahip oldukları gözlemlenmiştir. Renk geçiş süreleri ve % geçirgenlik değişimlerini öğrenmek için, kinetik çalışmalar yapılmıştır. Polimerler, HOMO ve LUMO enerji seviyeleri, bant

aralıkları, görünür bölgedeki güçlü soğurmaları ve ısısal kararlılıklarına bağlı olarak Organik Güneş Pili cihaz çalışmalarında kullanılmıştır. Öncü çalışmalar, polimerlerin umut verici güç çevirim verimlerine sahip olduğunu göstermiştir.

**Anahtar kelimeler**: Benzotriazol, Fluorene, Optoelektronik, Organik Güneş Pilleri, Konjuge kopolimerler, Donör–Akseptör

To My Family

## ACKNOWLEDGMENTS

I would like to express my sincere thanks to my supervisor Prof. Dr. Ali Çırpan and my co-supervisor Prof. Dr. Levent Toppare for their guidance, support, encouragement, patience, advice and criticism throughout this study.

I would like to thank my dear friend Melike Karakuş for her endless support and invaluable friendship.

I would like to thank to Abidin Balan, Derya Baran and Doğukan Hazar Apaydın for their experimental helps besides their friendships.

I would like thank to all Toppare Research Group members for their cooperation and their friendships.

Words fail to express my eternal gratitude to my family for believing in me and giving me endless support.

**TABLE OF CONTENTS**

ABSTRACT ..... iv
ÖZ ..... vi
ACKNOWLEDGMENTS ..... ix
TABLE OF CONTENTS ..... x
LIST OF TABLES ..... xiv
LIST OF FIGURES ..... xv
ABBREVATIONS ..... xix
CHAPTERS
1. INTRODUCTION ..... 1
1.1 Conjugated Polymer ..... 1
1.2 Band Theory ..... 2
1.3 Electrochemical Doping ..... 7
1. 4 Applications of Conjugated Polymers ..... 8
1.4.1 Electrochromism ..... 8
1.4.2 Organic Solar Cells ..... 9
1.4.2.1 Advantages of Organic Semiconductors ..... 10
1.4.2.2 Concept of Bulk Heterojunction Solar Cells ..... 10
1.4.2.3 Principles of Bulk Heterojunction Solar Cells ..... 11
1.4.2.5 Optimization of Organic Solar Cells ..... 15
1.5 Bandgap Engineering ..... 17
1.5.1 Donor-Acceptor Theory ..... 19
1.6 Polymerization Methods ..... 20
1.7 New Materials for OSCs ..... 21
1.7.1 Benzotriazole Based Conjugated Copolymers ..... 24

1.7.2 Fluorene Based Conjugated Copolymers ..... 27
1.8 Aim of This Study ..... 29
2. EXPERIMENTAL ..... 30
2.1 Materials ..... 30
2.2 Equipment ..... 30
2.3 Procedure ..... 31
2.3.1 Synthesis ..... 31
2.3.1.1 2-Dodecylbenzotriazole ..... 31
2.3.1.2 4,7-Dibromo-2-dodecylbenzotriazole ..... 32
2.3.1.3 Tributyl(thiophen-2-yl)stannane and Tributyl(4-hexylthiophen-2 yl)stannane ..... 33
2.3.1.4 2-dodecyl-4,7-di(thiophen-2-yl)-2H-benzo[d][1,2,3]triazole (TBT) ..... 33
2.3.1.5 2-Dodecyl-4,7-bis(4-hexylthiophen-2-yl) 2Hbenzo[d][1,2,3]triazole (HTBT) ..... 34
2.3.1.6 4,7-bis(5-bromothien-2-yl)-2-dodecylbenzo[1,2,3]triazole ..... 35
2.3.1.7 4,7-bis(5-bromo-4-hexylthien-2-yl)-2-dodecylbenzo[1,2,3]triazole ..... 35
2.4 Synthesis of the Polymers ..... 36
2.4.1 Poly((9,9-dioctylfluorene)-2,7-diyl-(2-dodecyl-benzo[1,2,3]triazole)) (P1) ..... 37
2.4.3 Poly((9,9-dioctylfluorene)-2,7-diyl-(4,7-bis(3-hexylthien-5-yl) 2-dodecyl-benzo[1,2,3]triazole)) (P3) ..... 37
2.5 Characterization of the Polymers ..... 38
2.5.1 Cyclic Voltammetry (CV) ..... 38
2.5.2 Spectroelectrochemistry ..... 40
2.5.3 Kinetic Studies ..... 41
2.5.4 Gel Permeation Chromatography (GPC) ..... 41
2.5.5 Thermal Properties ..... 42
2.6 Characterization of the Solar Cells ..... 42
3. RESULTS AND DISCUSSION ..... 44
3.1 Characterization ..... 44

3.1.1 2-Dodecylbenzotriazole ..... 44
3.1.2 4,7-Dibromo-2-dodecylbenzotriazole ..... 46
3.1.3 TBT ..... 47
3.1.42-Dodecyl-4,7-bis(4-hexylthiophen-2-yl)-2Hbenzo[d][1,2,3]triazole (HTBT) .... 49
3.1.5 4,7-Bis(5-bromothien-2-yl)-2-dodecylbenzo[1,2,3]triazole ..... 50
3.1.6 4,7-Bis(5-bromo-4-hexylthien-2-yl)-2-dodecylbenzo[1,2,3]triazole ..... 52
3.1.7 Poly((9,9-dioctylfluorene)-2,7-diyl-(2-dodecyl-benzo[1,2,3]triazole)) (P1) ..... 53
3.1.8Poly((9,9-dioctylfluorene)-2,7-diyl-(4,7-bis(thien-2-yl) 2-dodecyl benzo[1,2,3]triazole)) (P2) ..... 54
3.1.9 Poly((9,9-dioctylfluorene)-2,7-diyl-(4,7-bis(3-hexylthien-5-yl) 2-dodecyl-benzo[1,2,3]triazole)) (P3) ..... 55
3.2 Poly((9,9-dioctylfluorene)-2,7-diyl-(2-dodecyl-benzo[1,2,3]triazole)) (P1) ..... 56
3.2.1 Cyclic Voltammetry (CV) ..... 56
3.2.2 Spectroelectrochemistry ..... 58
3.2.3 Kinetic Studies ..... 60
3.3Poly((9,9-dioctylfluorene)-2,7-diyl-(4,7-bis(thien-2-yl)2-dodecyl benzo[1,2,3]triazole)) (P2) ..... 61
3.3.1 Cyclic Voltammetry (CV) ..... 61
3.3.2 Spectroelectrochemistry ..... 63
3.3.3 Kinetic Studies ..... 65
3.4Poly((9,9-dioctylfluorene)-2,7-diyl-(4,7-bis(3-hexylthien-5-yl) 2-dodecyl-benzo[1,2,3]triazole)) (P3) ..... 66
3.4.1 Cyclic Voltammetry (CV) ..... 66
3.4.2 Spectroelectrochemistry ..... 68
3.4.3 Kinetic Studies ..... 69
3.5 Thermal Properties (DSC) & (TGA) ..... 69
3.6 Photovoltaic Studies ..... 70
3.6.1 Optical Properties ..... 70
3.6.2 Photoluminescence Studies ..... 71

3.6.3 Photovoltaic properties ..... 72
4. CONCLUSION ..... 77
REFERENCES ..... 79
APPENDIX
A. DSC and TGA DATA ..... 85

## LIST OF TABLES

**TABLES**

**Table 1** Oxidation potentials and onset values for both p- and n-type doping, estimated HOMO–LUMO energies and band gaps of synthesized polymers P1 ..... 58

**Table 2** Oxidation potentials and onset values for both p- and n-type doping, estimated HOMO–LUMO energies and band gaps of synthesized polymers P2 ..... 63

**Table 3** Oxidation potentials and onset values for both p- and n-type doping, estimated HOMO–LUMO energies and band gaps of synthesized polymers P3 ..... 67

**Table 4** Photovoltaic performance of the solar cells based on P1:PCBM, P2:PCBM and P3:PCBM..... 75

## LIST OF FIGURES

**FIGURES**

Figure 1.1 Molecular structure of polyacetylene ..... 1
Figure 1.2 Common organic conducting polymers ..... 2
Figure 1.3 Representation of band structure in organic semiconductors ..... 3
Figure 1.4 Conductivity range of conducting polymers ..... 3
Figure 1.5 The degenerate ground states of PA ..... 4
Figure 1.6 Soliton structures of polyacetylene ..... 5
Figure 1.7 Aromatic and quinoid configurations for polythiophene ..... 6
Figure 1.8 Charge carriers in PPy and its corresponding energy bands ..... 7
Figure 1.9 Fullerene (1) derivatives PC61BM (2) and PC71BM (3) used as electron acceptors in OSCs ..... 11
Figure 1.10 Photoinduced charge (electron) transfer from photoexcited PPV to C60 fullerene ..... 12
Figure 1.11 Device architecture of a typical Bulk Heterojunction Solar Cell ..... 13
Figure 1.12 Schematic current–voltage characteristics a BHJ solar cell showing the Voc, Jsc, and FF ..... 14
Figure 1.13 Band structure diagram illustrating the HOMO and LUMO energies of MDMO-PPV, P3HT, and an “ideal” donor relative to the band structure of PCBM [38] ..... 16
Figure 1.14. Ideal structure of a bulk heterojunction solar cell ..... 17
Figure 1.15 Structural factors determining the band gap of materials derived from linear π conjugated systems ..... 19
Figure 1.16 Mechanism for Suzuki reaction ..... 21
Figure 1.17 Structures of P1 and P2 ..... 23

Figure 1.18 Structures of the Polymer and $PC_{71}BM$ ..... 24
Figure 1.19 Structure of Benzotriazole ..... 25
Figure 1.20 Typical J–V curves of the polymer solar cells based on..... 26
PCDTBTz:PC60BM ..... 26
Figure 1.21 Medium band gap fluor containing copolymer..... 27
Figure 1.22 Polyfluorene homopolymer and copolymer ..... 28
Figure 2.1 Synthetic route for 2-dodecylbenzotriazole..... 31
Figure 2.2 Synthetic route for 4,7-dibromo-2-dodecylbenzotriazole..... 32
Figure 2.3 Synthetic pathway for stannylation of thiophene and 3-hexylthiophene. 33
Figure 2. 4 Synthetic route for TBT..... 33
Figure 2.5 Synthetic pathway for HTBT..... 34
Figure 2.6 Synthetic route for 4,7-bis(5-bromothien-2-yl)-2 dodecylbenzo
[1,2,3]triazole ..... 35
Figure 2.7 Synthetic route for 4,7-bis(5-bromo-4-hexylthien-2-yl)
2dodecylbenzo[1,2,3]triazole ..... 35
Figure 2.8 Synthetic route for P1, P2, and P3 ..... 36
Figure 2.9 Cyclic voltammetry waveform ..... 38
Figure 2.10 A cyclic voltammogram for a reversible redox process ..... 39
Figure 3.1 $^{1}$H-NMR and $^{13}$C NMR of 2-dodecylbenzotriazole..... 45
Figure 3.2 $^{1}$ H-NMR and $^{13}$C NMR of 4,7- Dibromo-2-dodecylbenzotriazole..... 47
Figure 3.3 $^{1}$H-NMR and $^{13}$C NMR of spectrum of TBT..... 48
Figure 3.4 $^{1}$H and $^{13}$C-NMR of 2-Dodecyl-(4,7-bis(4-hexylthio phen-2-yl) -
2Hbenzo[d] [1,2,3]triazole (HTBT) ..... 50
Figure 3.5 $^{1}$H-NMR and $^{13}$C NMR of spectrum of 4,7-bis(5-bromothien-2-yl)-2-
dodecylbenzo[1,2,3]triazole ..... 51
Figure 3.6 $^{1}$H-NMR and $^{13}$C NMR of spectrum of 4,7-bis(5-bromo-4-hexylthien-2-
yl)-2-dodecylbenzo[1,2,3]triazole ..... 53
Figure 3.7 $^{1}$H-NMR spectrum of P1 ..... 54
Figure 3.8 $^{1}$H-NMR spectrum of P2 ..... 55

Figure 3.9 $^{1}$H-NMR spectrum of P3 ..... 56
Figure 3.10 Cyclic voltammogram of P1 for both p and n type doping in the presence of 0.1 M $TBAPF_6$/MeCN solution at a scan rate of 50 mV/s..... 57
Figure 3.11 Electrochemical p-type doping electronic absorption spectra of P1 between 0.0 and 1.3 V with 0.1 V potential intervals ..... 59
Figure 3.12 Kinetic switching results in both visible and NIR regions for P1 ..... 61
Figure 3.13 Cyclic voltammogram for spray coated polymer film of P2 in ACN/$TBAPF_6$ solution at a scan rate of 50 mV/s ..... 62
Figure 3.14 Electrochemical p-type doping electronic absorption spectra of P2 between 0.5 and 1.45 V with 0.1 V potential intervals ..... 64
Figure 3.15 HOMO/LUMO levels and band gaps of related polymers [76] ..... 65
Figure 3.16 Kinetic switching results in both visible and NIR regions for P2 ..... 66
Figure 3.17 Cyclic voltammogram for spray coated polymer film of P3 in ACN/TBAPF6 solution at a scan rate of 50 mV/s ..... 67
Figure 3.18 Electrochemical p-type doping electronic absorption spectra of P2 between 0.5 and 1.3 V with 0.1 V potential intervals ..... 68
Figure 3.19 Normalized absorption spectra of P1, P2, P3 in chloroform solution (a) and in thin film (b) ..... 70
Figure 3.20 Optical emission spectrum of the targeted polymers in chloroform solutions ..... 71
Figure 3.21 Current density-voltage (*J*-*V*) characteristics of the P1/PCBM blends of 1:1 under white light illumination (AM 1.5 G conditions) ..... 73
Figure 3.22 Current density-voltage (*J*-*V*) characteristics of the P2/PCBM blends of 1:1 under white light illumination (AM 1.5 G conditions) ..... 74
Figure 3.23 Current density-voltage (*J*-*V*) characteristics of the P3/PCBM blends of 1:2 under white light illumination (AM 1.5 G conditions) ..... 75
Figure A.1 TGA result of P1 ..... 85
Figure A.2 DSC result of P1 ..... 85
Figure A.3 TGA result of P2 ..... 86

Figure A.4 DSC result of P2 ..... 86
Figure A.5 TGA result of P3 ..... 87
Figure A.6 DSC result of P3 ..... 87

## ABBREVATIONS

**ACN** Acetonitrile

**BHJ** Bulk Heterojunction

**CB** Conduction Band

**CP** Conjugated Polymer

**CV** Cyclic Voltammetry

**DA** Donor Acceptor

**DCM** Dichloromethane

**ECD** Electrochromic Device

**$E_g$** Band Gap Energy

**Fc** Ferrocenyl

**HOMO** Highest Occupied Molecular Orbital

**ITO** Indium Tin Oxide

**LUMO** Lowest Unoccupied Molecular Orbital

**NMR** Nuclear Magnetic Resonance

**OFET** Organic Field Effect Transistors

**OLED** Organic Light Emitting Diode

**OSC** Organic Solar Cell

**$PC_{61}BM$** [6,6]-phenyl-$C_{61}$-butyric acid methyl ester

**$P_3HT$** Poly (3-Hexylthiophene)

**PEDOT:PSS** Poly(3,4-ethylenedioxythiophene)

**PL** Photoluminescence

**PTh** Polythiophene

**$TBAPF_6$** Tetrabutylammonium hexafluorophosphate

**VB** Valence Band

# CHAPTER 1

# INTRODUCTION

## 1.1 Conjugated Polymer

Plastics are known as typical organic polymers and generally used as outstanding electrical insulators. However a new era started with the appearance of conducting polymers which has opened new roads in chemistry and physics [1]. Conducting polymer story started in 1970s with the accidental discovery that insulating π conjugated polyacetylene (PA) (Figure 1.1) could gain conductivity by doping process [2]. This new class included materials which combined the properties of a physical mixture of a non-conductive polymer with a conducting material such as metal.

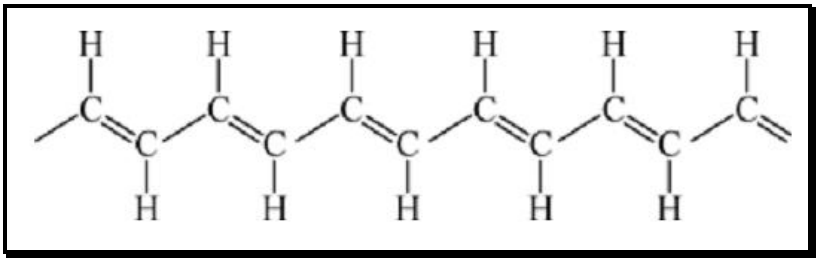

**Figure 1.1** Molecular structure of polyacetylene

Three scientists, Alan J. Heeger, Alan G. MacDiarmid and Hideki Shirakawa, played a chief role in this breakthrough, and they were awarded with the Nobel Prize in Chemistry in 2000 "*for the discovery and development of electronically conductive polymers*" [3]. With the help of the electrochemistry and electrochemical techniques, preparation and characterization of novel materials have been achieved

successfully. The more scientists analyzed the relationship between structure and property, the more complex conducting polymers like polythiophenes and polypyrroles and many others superior to PA have been developed [4-6] (Figure 1.2).

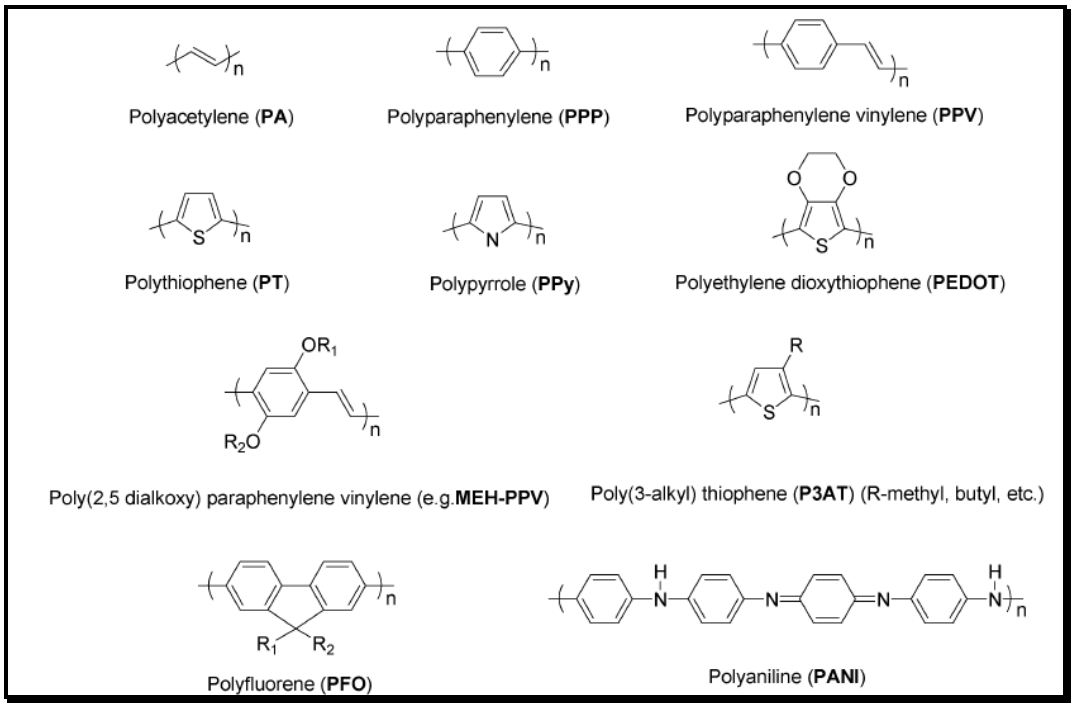


**Figure 1.2** Common organic conducting polymers

## 1.2 Band Theory

Band theory explains energy transition processes in conjugated polymers (The excitation and/or removal/insertion of electrons). In the most simple form conjugated polymers have two discrete energy bands, the highest occupied molecular orbital (HOMO), also known as the valence band (VB); and the lowest unoccupied molecular orbital (LUMO), known as the conduction band (CB). The energy spacing between HOMO and LUMO is defined as band gap (Eg) (Figure

1.3). The Eg of conjugated polymers can be calculated from the onset of the π-π* transition in the UV-Vis spectrum.

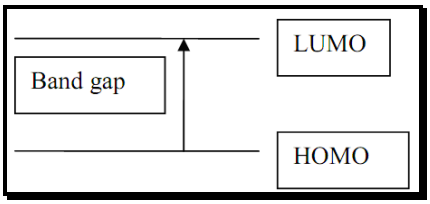


**Figure 1.3** Representation of band structure in organic semiconductors

In their neutral form, conjugated polymers are intrinsic semiconductors having a filled valence band due to delocalized π electrons and an empty conduction band with Eg values ranging from 1.5 to 4 eV [7]. Due to their band structures it is possible for electrons to move to conduction band for example by light absorption. Additionally, with doping process which can be done in two ways; oxidation or reduction, interband transitions between the VB and CB can be formed. These newly formed interbands lower the effective band gap leading to formation of charge carriers throughout the polymer backbone. Charge carriers can be either holes (p-type) or electrons (n-type) depending on the type of dopant used [8]. It is possible for CPs to have conductivity values from the range of insulators to metals as shown in the Figure 1.4.

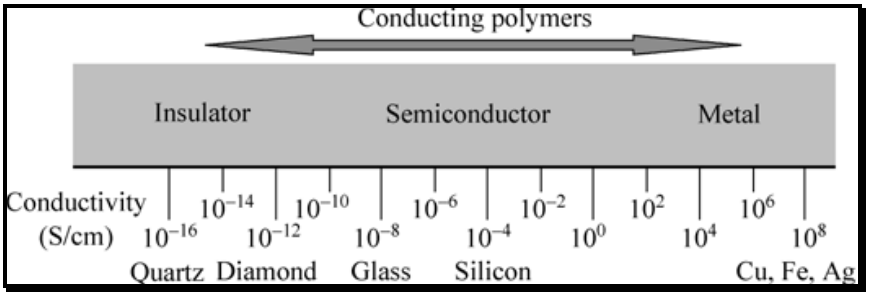


**Figure 1.4** Conductivity range of conducting polymers

In order to understand the band theory of CPs, PA is the simplest structure to examine. PA develops two degenerate resonance structures meaning that the ground states are thermodynamically equivalent (Figure 1.5). Moreover, extensive delocalization causes all the bond lengths to be equal.

**Figure 1.5** The degenerate ground states of PA

This degenerate ground state configurations lead to the formation of a structural defect which is called *Soliton* consisting of a single unpaired electron [9]. Solitons are the main charge carriers in PA case and three types of soliton can form (Figure 1.6). Charged solitons have no spin; however, neutral solitons have spin but no charge. Positively charged soliton is attained by the insertion of acceptor band (p-type doping) or removal of an electron from localized state of a neutral soliton by oxidation. Negatively charged soliton is produced when an electron, donor band is inserted by reduction [10].

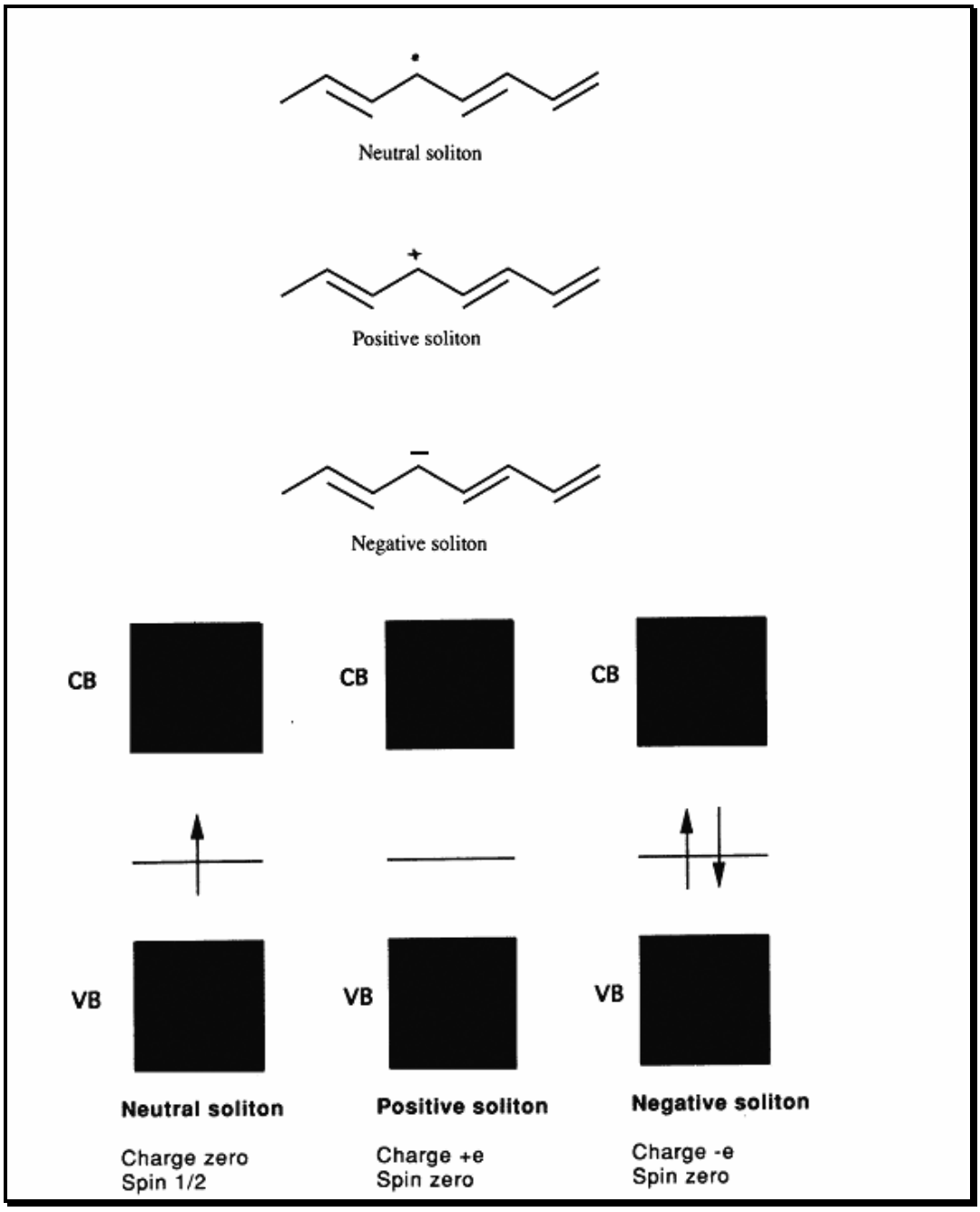


**Figure 1.6** Soliton structures of polyacetylene

Conjugated polymers which have more complex structures differ in terms of band theory. These types of CPs have non-degenerate ground states. In other words, they

have nonequivalent bond alternation structures [11]. For example in polythiophene which is an aromatic compound both quinoid and aromatic structures form (Figure 1.7) [12].

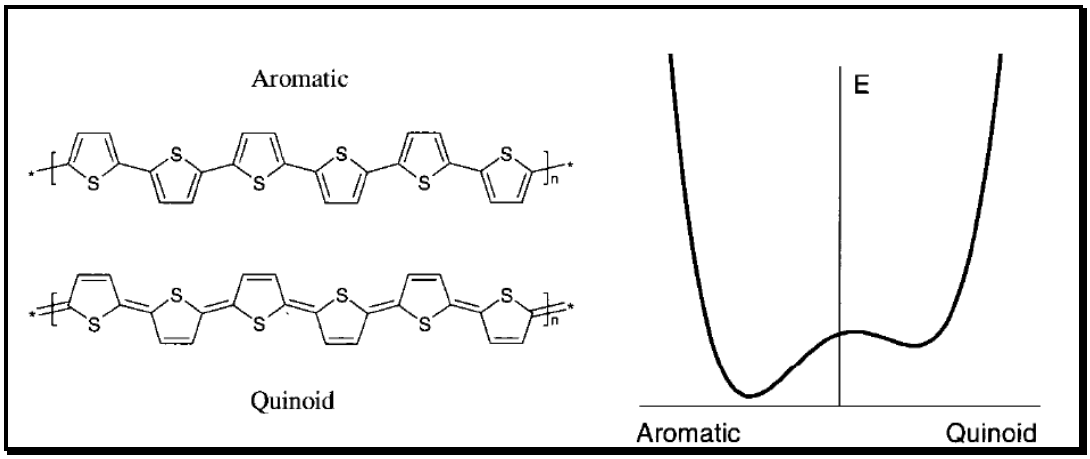


**Figure 1.7** Aromatic and quinoid configurations for polythiophene

For non-degenerate systems main charge carriers are polarons which can be defined as the radical cations for the oxidation process. Further oxidation of the polymer chain leads to the formation of bipolarons meaning dications. Bipolaron can both be produced by the removal of electron from the polaron or remaining neutral part of the polymer chain. The formation of bipolaron is thermodynamically more favorable since it generates a larger decrease in ionization energy rather than the formation of two polarons [13]. Charge carrier formation of the polypyrrole is given in the Figure 1.8.

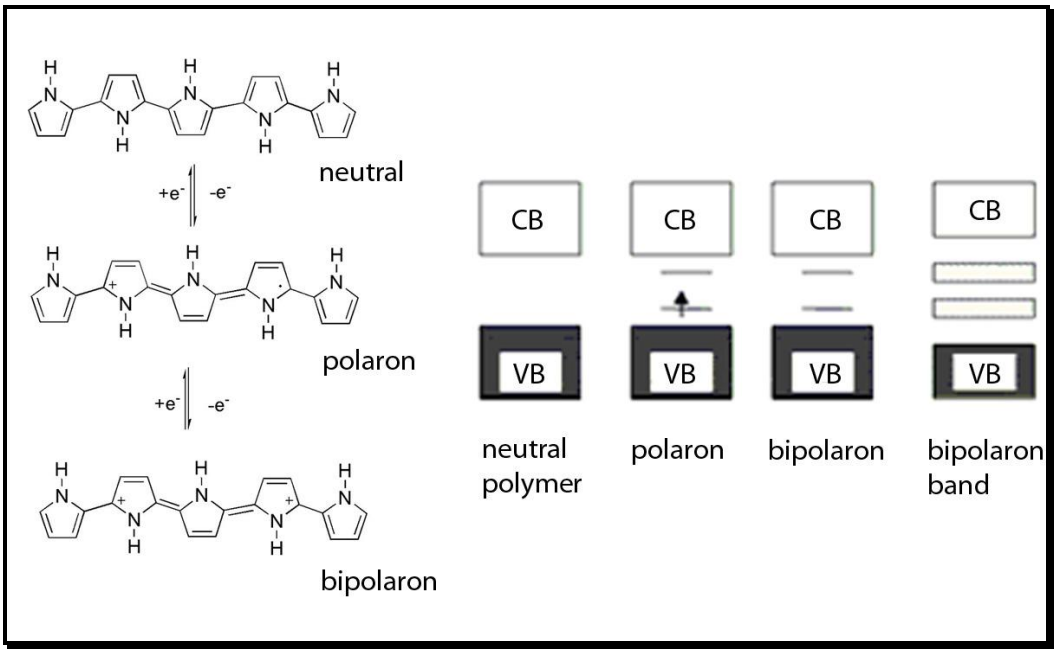


**Figure 1.8** Charge carriers in PPy and its corresponding energy bands

### 1.3 Electrochemical Doping

Conjugated polymers in their undoped forms have relatively large band gaps with a low concentration of charge carriers. By applying electrochemical doping with appropriate potentials to the polymer in a suitable medium, it is possible to increase the number of the charge carriers. Increasing charge carriers which are formed either through oxidation or reduction modify electronic and optical structure of the CPs. The oxidation of a neutral polymer by removing an electron from its valence band is referred to *p*-doping and the reduction of a polymer by adding an electron to its conduction band is referred to *n*-doping [14].

Doping is a reversible process so it does not change the chemical structure of the polymer. Moreover, by arranging the doping level different conductivities can be

achieved [15]. Besides changing the conductivity, doping can also alter optical, magnetic, and mechanical properties. When the literature is examined, it is seen that the p-doping process has been observed to a much greater extent than n-doping due to the requirement of stringently dry and oxygen-free conditions [16]. However, there exist vast amount of publications on the n-doping process [17-20].

### 1. 4 Applications of Conjugated Polymers

The ability of doping and changing the properties of conducting polymers from insulator to metal created a new and exciting research field concerning chemistry and condensed matter physics. Solutions of CPs can be thought as ‘‘*inks*’’ with electronic functionality. Therefore, ‘‘*printed plastic electronics*’’ has become a central point of the science and technology of semiconducting polymers [21]. Moreover, CPs can be produced with relatively facile synthetic pathways and they have environmental stability and solution processability [22].

Due to these qualifications, they have been extensively studied for their potentials as active materials in numerous industrial applications namely, electrochromics (ECDs) [23], organic light emitting diodes (OLEDs) [24], organic photovoltaic devices (OPVs) [25], and thin film transistors (OFETs) [26].

#### 1.4.1 Electrochromism

Electrochromic materials have attracted attention of the researchers for their applicability in display areas and smart windows for several decades [27]. Electrochromism is simply defined as the reversible and visible change in the color of a material upon applied potential. Color changes can be between a transparent (bleached) state and a colored state or between two or more colored states. Materials

showing more than one colored state are named as multichromic materials [28]. In the neutral state, the color depends on the band gap of the polymer. The change in the color is provided by the doping process. With doping process, new energy states between valance and conduction bands are formed. Formation of these lower energy transitions, when they are in the visible region, causes observable color changes. When this newly formed energy states reach to near-IR region, then it is possible to get transmissive state.

Conjugated polymers are extensively used electrochromic materials since it is easy to tune their band gaps with structural modifications and getting different colors. Examples from the literature indicates that it is possible to get fully solution processable multichromic materials using different synthetic approaches such as donor-acceptor approach and substituents like a variety of alkyl and alkoxy groups [29]. Moreover, they have good performance at other parameters such as switching time, high contrast ratio between oxidized and reduced states, coloration efficiency**,** stability and optical memory which is significant for ECD [30].

### 1.4.2 Organic Solar Cells

The usage of the photovoltaic effect to produce electricity from the sun has become a remarkable solution for the need of clean and renewable energy sources. On the other hand, amount of energy produced from the sun remains very low due to the high costs of silicon based solar cells [31]. Organic solar cells (OSCs) are accepted as one of the best solutions for low cost device fabrication [32]. Conjugated polymer based solar cells have received great interest as the third generation solar cells because of their advantages like being flexible and processable [33]. They have been intensely studied during the past decade and for this purpose many low band gap conjugated polymers have been synthesized [34].

#### 1.4.2.1 Advantages of Organic Semiconductors

Usage of organic materials in solar cells offers many advantages compared to inorganic ones. First of all, it is possible to use several synthetic approaches to synthesize countless organic compounds which will make them always available. Secondly, via tailoring organic materials meaning functionalizing them with different substituents, requirements for an efficient device can be provided. Thirdly, most organic compounds are soluble in common organic solvents. This makes them processable for low cost and large area production using different methods such as roll to roll or inkjet printing. Lastly, flexibility, lightweight and semi transparency of OSCs qualifies them with a high application potential compared to conventional ones. These application areas can be windows, mobile applications e.g. charging for mobile phones or laptops [35].

#### 1.4.2.2 Concept of Bulk Heterojunction Solar Cells

Organic semiconductors in energy conversion have been used since 1970s [36].
Tang's discovery of the donor-acceptor heterojunction with a double layer device concept enabled the fabrication of more efficient OPVCs [37]. Since then many approaches have been developed for achieving higher power conversion efficiencies (PCE). Bulk heterojunction approach (BHJ) from solution processed polymer-fullerene mixtures has been extensively utilized. In this respect, a blend of an electron donor polymer and electron accepting fullerene derivative (Figure 1.9) is used as active layer [38]. In such a solid state blend, it is possible for materials to form bicontinuous and interpenetrating networks which will allow the excitons (bound electron-hole pair) to reach regarding phases within their lifetimes and dissociate there forming free charges. Recently, PCE of 6- 8 % have been achieved by means of this approach [39].

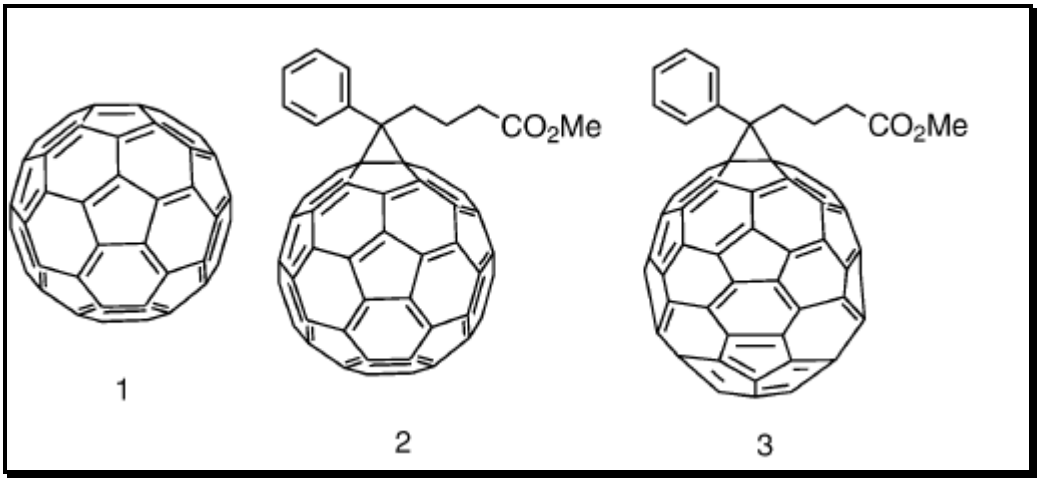


**Figure 1.9** Fullerene (1) derivatives $PC_{61}BM$ (2) and $PC_{71}BM$ (3) used as electron acceptors in OSCs

### 1.4.2.3 Principles of Bulk Heterojunction Solar Cells

In order to generate electricity from sun light, solar cells must provide three steps;

- Absorption of light
- Generation of charge carriers
- Transportation of opposite charges to opposite contacts.

These are main steps which apply to all kinds of solar cells but the discussion is based on polymer-fullerene solar cells in this thesis.

Absorption of the most of the solar spectrum is the first necessity for a solar cell. This situation generates two requirements. First, the band gap of the donor material must be small enough to allow the absorption of a large portion of the solar spectrum. Second, the film must have sufficient thickness to absorb the most of the light. It

cannot exceed a certain limit since charge carriers have limited mobility. After the absorption of the light, exciton formation takes place. Excitons can travel a distance of 5-10 nm in most semiconducting polymers before recombination. Therefore it is necessary for the exciton to find a donor acceptor interface within this distance to be able to generate free charges. Photoinduced charge transfer from polymer to fullerene derivative is the most efficient way for charge generation (Figure 1.10). Finally, the free carriers must reach to corresponding electrodes through their respective phases in order to produce electricity.

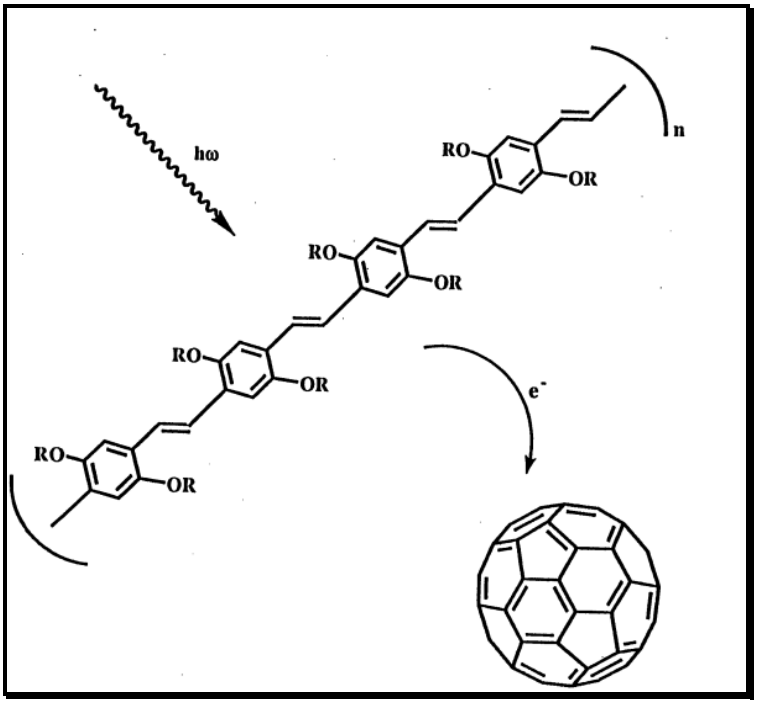


**Figure 1.10** Photoinduced charge (electron) transfer from photoexcited PPV to $C_{60}$ fullerene

### 1.4.2.4 Device Fabrication and Characterization

A typical BHJ solar cell is shown in Fig. 1.11. Active layer which consists of a donor-acceptor blend is sandwiched between two electrodes. Anode is a transparent

conductive oxide coated on glass substrate. Indium tin oxide (ITO) is generally the choice. It has a high work function. A layer of poly(3,4-ethylene dioxythiophene): poly(styrene sulfonate) (PEDOT:PSS) is spin coated as a hole transporter layer. It also smoothes the surface of the ITO and even enhances the work function. After that, active layer is spin coated. The top electrode usually consists of a low work function metal or lithium fluoride (LiF), topped with a layer of aluminum, all of which are deposited by thermal deposition in vacuum through a shadow mask.

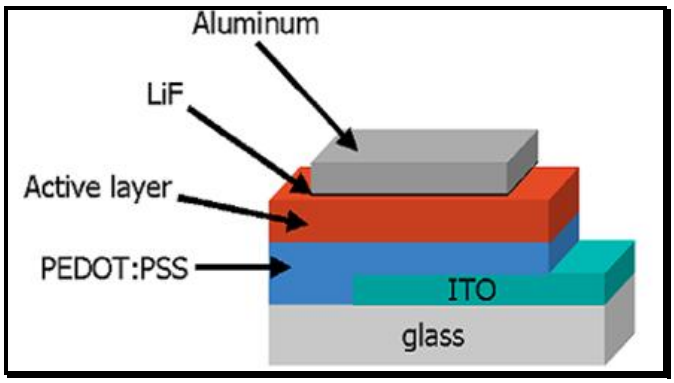


**Figure 1.11** Device architecture of a typical Bulk Heterojunction Solar Cell

In order to determine the performance and electrical characteristics of the photovoltaic devices, current-voltage (I-V) measurements are performed both in dark and under illumination. A typical I-V curve of a solar cell under illumination is shown in Figure 1.12. The most significant figure of this equation is the power conversion efficiency η. It depends on three parameters which are open circuit voltage (Voc), short circuit current density (Jsc) and fill factor (FF). The current density under illumination at zero applied voltage is called the short-circuit current density. The maximum voltage that the cell can supply is designated as the open-circuit voltage. The fill factor indicates the '*squareness'* of the device's current–voltage characteristics and it is the quotient of maximum power (yellow rectangle) and the product of Voc and Jsc (white rectangle).

The efficiency is the ratio of maximum power to incident radiant power $P_L$- typically radiated by the sun:

$$FF = \frac{(J_m)(V_m)}{(J_{sc})(V_{oc})} \qquad \eta = \frac{FF\, j_{sc} V_{oc}}{P_L} \tag{1}$$

The efficiencies should be measured under standard test conditions. The conditions include the temperature of the cell (25°C), the light intensity (1000 $W/m^2$) and the spectral distribution of light (AM 1.5).

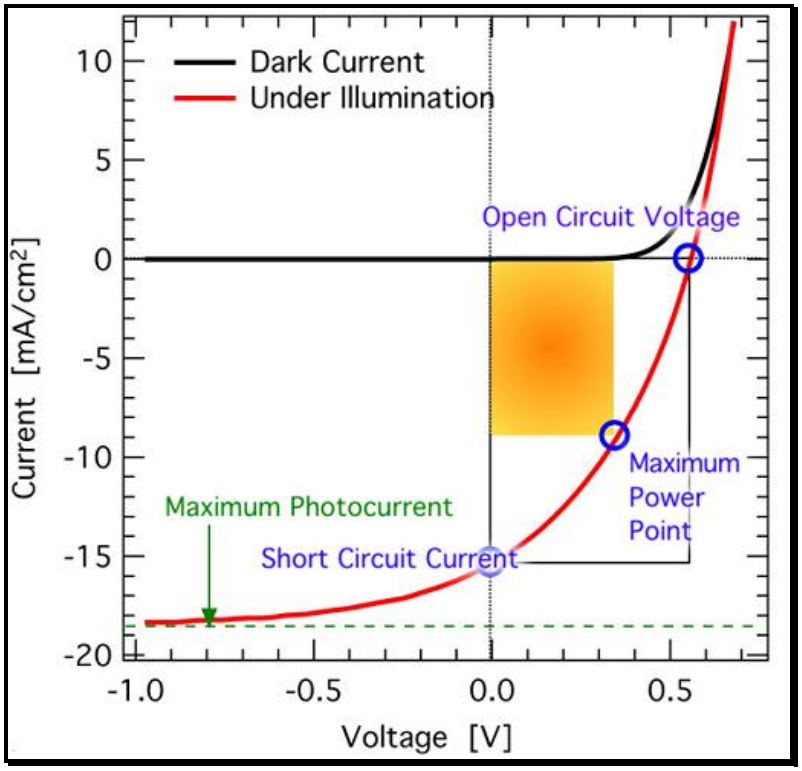


**Figure 1.12** Schematic current–voltage characteristics a BHJ solar cell showing the Voc, Jsc, and FF

#### 1.4.2.5 Optimization of Organic Solar Cells

In order for solar cells to become marketable, their efficiencies must reach 10% levels. To achieve this, it is significant to realize the importance of concepts like the band gap i.e. the absorption range of the conjugated polymer, energy levels of HOMO and LUMO, morphology of the active layer and device architecture.

Design of an efficient organic solar cell involves achieving respectable values of voltage and extracted current since the power generated by a cell depends on these two parameters. In order to get high Voc values HOMO-LUMO energy levels of the donor and acceptor should be considered. Voc is theoretically expressed as the energetic difference between the HOMO of the donor and the LUMO of the acceptor [40]. Therefore donor materials having deep lying HOMO levels such as carbazole and fluorene have been extensively preferred [41]. However, HOMO level of an ideal polymer should be determined by analyzing the band gap of the polymer since it controls the amount of the spectral overlap with the sun's photon flux which has a maximum at 1.8 eV (700 nm). A band gap of 1.5 eV can be considered as an optimal value for a donor material [42]. LUMO level is also significant; there should be a minimum energy difference of 0.3 eV between the LUMOs of the donor and the acceptor corresponding to a value of 3.9 eV compare to the PCBM. Energy difference larger than this amount does not offer any advantage, since it cannot contribute to the device performance [43]. Ideal HOMO level is about 5.4 eV (Figure 1.13). These energy levels give an attainable 1.2 V of Voc.

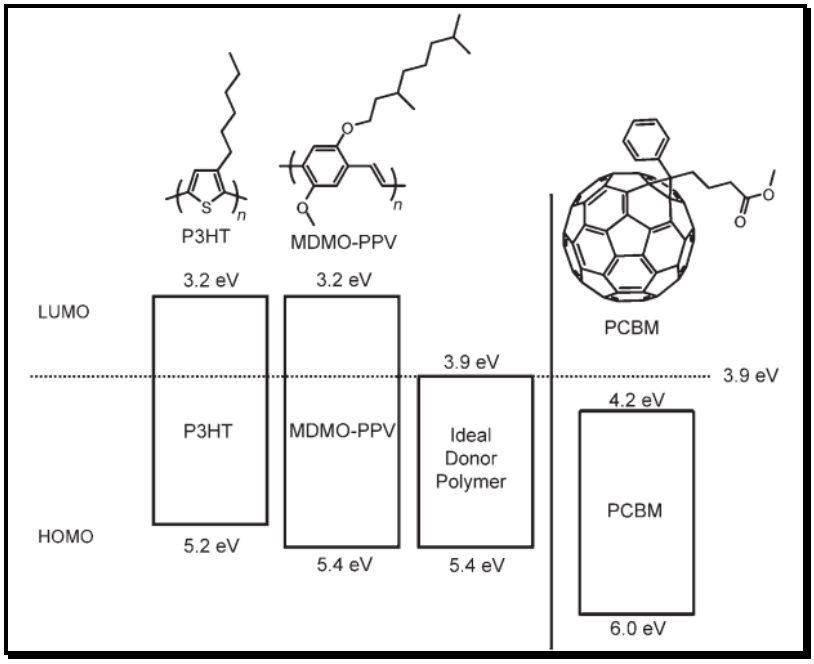


**Figure 1.13** Band structure diagram illustrating the HOMO and LUMO energies of MDMO-PPV, P3HT, and an "ideal" donor relative to the band structure of PCBM [38]

Morphology is a crucial parameter as it determines the magnitude of the photoactive volume where the excitons can be dissociated [44]. The ideal morphology of a BHJ solar cell is described as bicontinuous and interpenetrating networks which will allow the dissociation of excitons within their diffusion length (5-10 nm). In other words, when there is phase segregation between donor and acceptor with proper lengths, free charges can be effectively transported to the respective electrodes. This minimizes the recombination of the free charges and increases the PCE. Figure 1.14 shows morphology of an ideal solar cell. The morphology of the photoactive layer also depends on many other factors which can be categorized as intrinsic and extrinsic properties. Intrinsic properties which depend on the chemical nature of the donor and acceptor are crystallinity and miscibility. Extrinsic properties depend on the device fabrication parameters such

as the choice of the proper solvent, annealing process, solvent evaporation rate and deposition technique [45].

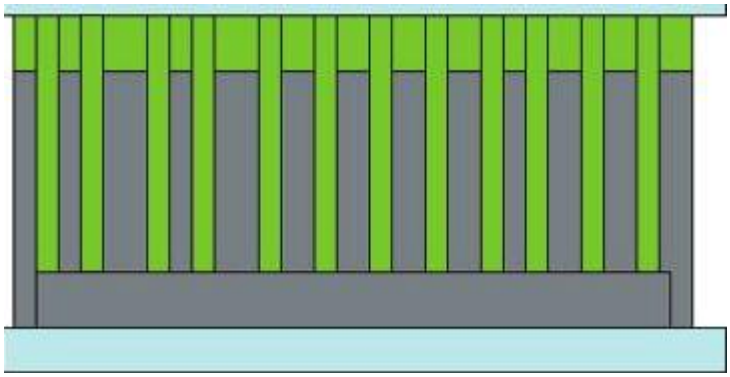

**Figure 1.14.** Ideal structure of a bulk heterojunction solar cell

Device architecture, the choice of the electrode materials has a significant effect on the resulting PCE of the OSC. As the anode material, in most of the cases ITO is used. Due to its properties like having high cost and brittleness, alternative materials for replacing it is a popular research topic. To satisfy this need, carbon nanotubes, graphene and conducting polymers can be utilized [46]. Usage of buffer layers to increase the charge collection at electrodes is mostly resorted. Despite the fact that the exact mechanism behind buffer layers is still unclear, a very thin layer of LiF (less than 1nm) below the mostly used cathode material Al enhances the PCE by lowering the work function [47]. Furthermore, PEDOT: PSS is used as the anode material and it acts as the surface smoother and electron blocking layer.

## 1.5 Bandgap Engineering

Control of band-gap of the π conjugated polymers is significant since this will make them suitable for many optoelectronic applications such as organic solar cells, electrochromic devices, light-emitting diodes and transistors. As well as controlled band gap, active materials for electronic and photonic applications must possess

proper absorption or emission properties, HOMO and LUMO energy levels and charge carrier properties.

Polyacetylene, the first conducting polymer, had some stability issues in atmospheric conditions. With the emergence of other conjugated polymers resulting from heteroaromatic units such as polythiophene or polypyrrole, more stable polymers were synthesized. Especially, thiophene based π conjugated polymers became popular since they presented conductivity, environmental stability, moderate band gap and structural flexibility [48].

Band gap of this type of polymers depends on 5 factors [49].

$$Eg = E_{BLA} + E_{Res} + E_{Sub} + E_u + E_{Int}$$

$E_{BLA}$, represents bond length alternation. It is possible to decrease the band gap of the resulting polymer by using synthetic methods which will end up with reduced BLA.

$E_{Res}$, means resonance effect. This type of polymers has non-degenerate ground states confining them to have two forms namely aromatic and quinoid. Generally, the aromatic form demonstrates higher stabilization energy and therefore the higher band gap.

$E_{Sub}$, represents the substituent effect. By incorporating electron deficient and electron rich groups, it is achievable to directly change the HOMO and LUMO energy levels. Electron donating groups raise the HOMO level and electron withdrawing groups lower the LUMO.

$E_u$, represents the dihedral angle between consecutive units. By limiting the delocalization of p electrons along the chain, it contributes to increase the band gap.

These four factors play a significant role on determining which synthetic approach should be used for the molecular engineering of the HOMO-LUMO of an isolated system.

$E_{Int}$, represents inter chain effects. It becomes important when the individual molecules or polymer chains assemble into a material. Figure 1.15 shows these effects.

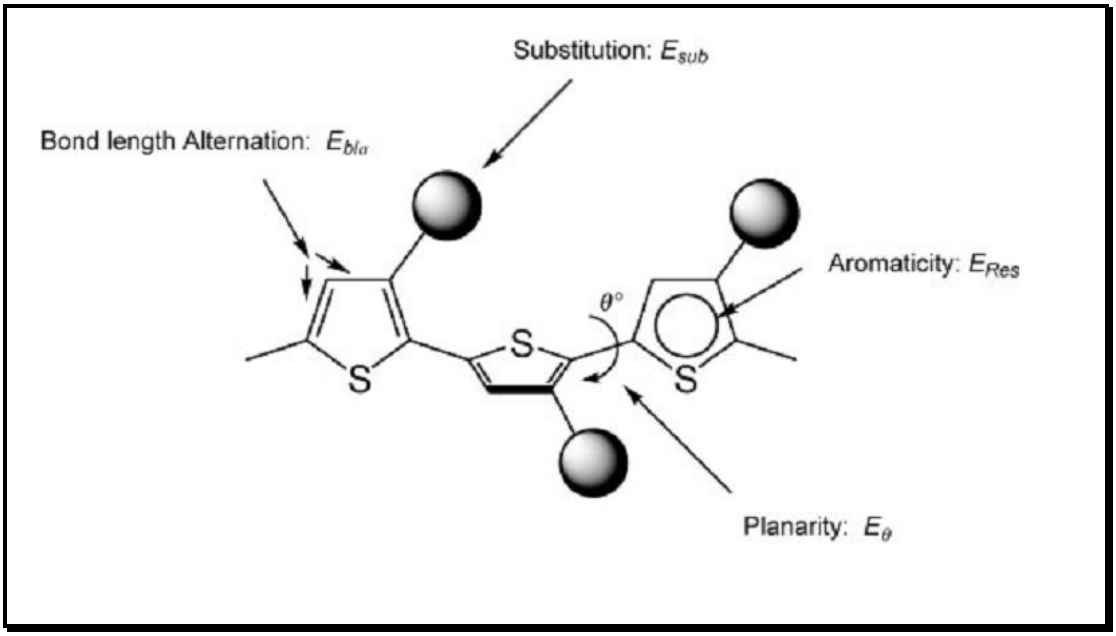


**Figure 1.15** Structural factors determining the band gap of materials derived from linear π conjugated systems

In order to modify the band gap, there are several synthetic approaches. Donor-acceptor theory has been extensively used.

### 1.5.1 Donor-Acceptor Theory

Donor-acceptor approach has been extensively used for tuning the band gap of resulting conjugated polymers by arranging donor and acceptor molecules in an alternating manner which will enable intermolecular charge transfer [50]. The hybridization of HOMO of the donor and the LUMO of the acceptor provides a means for modifying electronic and optoelectronic properties by enabling a stronger double bond character between the donor and acceptor units. A Good match of these groups provides desired properties. By combining the high lying HOMO level of the donor and low lying level of LUMO of the acceptor in the same polymer, it is possible to get lower band gap.

The use of DA type CPs as active layers became more popular over time due to their variation of optical properties via structural alternations [51]. Possibility for applications of CPs to large and flexible display devices makes their development significant for future display technologies [52].

Suzuki Coupling is one of the coupling reactions used to synthesize donor-acceptor type polymers.

### 1.6 Polymerization Methods

There are different types of aryl-aryl bond formation reactions. Suzuki coupling has been widely utilized [53]. This polymerization method has advantages such as mildness of the reaction environments, tolerance towards a variety of functional groups, insensitiveness to the presence of water and insensitiveness to the need for truly catalytic amount of palladium (Pd) catalyst [54].

The precursors of the reaction are aryl halide and boronic acid or ester derivative of an aryl compound. Reaction takes place in a weakly basic medium in order to

enhance the reactivity of boron. Pd catalyst can be used either as Pd(II) and Pd(0). The mechanism of the reaction involves the usage of palladium catalyst. Firstly, aryl halide is added to the palladium catalyst via oxidative addition. Then basic medium activates this intermediate for the reaction with aryl-boronate compound. The last step is the releasing of the precursor palladium catalyst by formation of the desired aryl-aryl compound via reductive elimination.

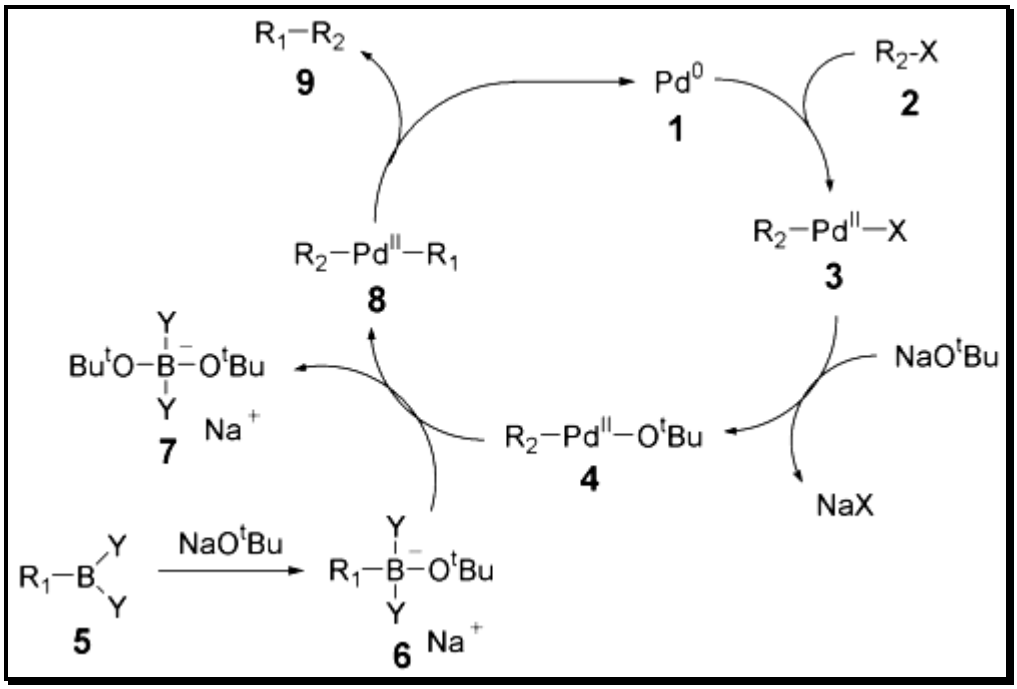


**Figure 1.16** Mechanism for Suzuki reaction

### 1.7 New Materials for OSCs

The current-state-of-the-art OSCs are basically formed of fullerene derivatives as the electron accepting materials. There are many reasons for preferring them as acceptors. They have high electron affinity and electron mobility, ultrafast charge transfer (50 fs) and better phase segregation in the blend film [55]. As donor materials a large variety of different oligomers and conjugated polymers have been

designed and in the past fifteen years, an important advancement has been carried out on the PCE of BHJ solar cells. The attained efficiencies have developed from less than 1% in the poly(phenylene vinylene) (PPV) system in 1995, to 4–5% in the poly(3 hexylthiophene) (P3HT) system in 2005 [56]. However, due to its moderate band gap value (1.9 eV), its absorption is limited.

Moreover, P3HT shows a very high HOMO level (-5.1eV) confining the Voc (0.6 V) of the cell. Also, P3HT based BHJ OSCs requires solvent or thermal annealing for showing their best performance. This processes decreases applicability of P3HT to large area roll to roll production, since it is time consuming [57].

Therefore, new systems which have absorption ranges extended to near IR region have been searched for. This can be achieved via the usage of low band gap polymers. In many cases, these low band gap polymers form with alternating donor-acceptor blocks. Nowadays, efficiencies around 6% have been reported [58].

One example for that kind of high efficiency is the study of Alex K.-Y. Jen and his coworkers. The structures of the polymers which contain alternating donor acceptor blocks of dithienobenzoquinoxaline (P1) and dithienobenzopyridopyrazine (P2) as the electron-deficient units and an indenodithiophene (IDT) as the electron-rich unit, can be seen in figure 1.17. The existence of the fused dithiophene ring on top of the pyrazine part decreases steric hindrance and provides a more planar structure. By this way intermolecular stacking of polymers so the hole mobility is improved. The resulting polymers have low band gaps and outcomes from photovoltaic measurements presented a very promising PCE of 6.06 % for the P1/$PC_{71}$BM blend system without any thermal or solvent treatment which makes it a great candidate for the roll-to-roll manufacturing. Presence of pyridine group in P2 lowers the LUMO and has a negative effect on charge separation, by this means causes a lower Jsc and reduces PCE to a value of 3.21% [59].

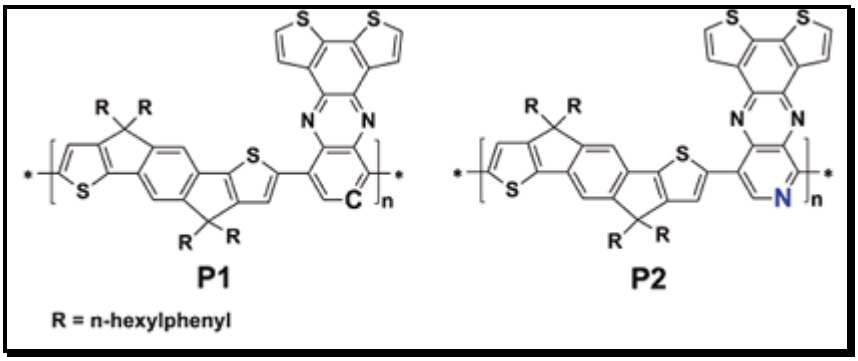


**Figure 1.17** Structures of P1 and P2

Furthermore, study of Luping Yu and coworkers brought out an efficiency of 7.4% by utilizing donor-acceptor type alternating ester substituted thienothiophene and benzodithiophene units (Figure 1.18). This polymer reveals a combination of superior properties that can make possible a brilliant result. First of all, it has a band gap of 1.6 eV meaning it can absorb around 700 nm region where the highest photon flux of the solar spectrum exists. Good hole mobility is provided by the rigid backbone and the side chains on the ester and benzodithiophene allow processability and proper miscibility with the acceptor. Also, the presence of fluorine in the thieno[3,4-b]thiophene lowers the HOMO level which provides enhanced Voc [60].

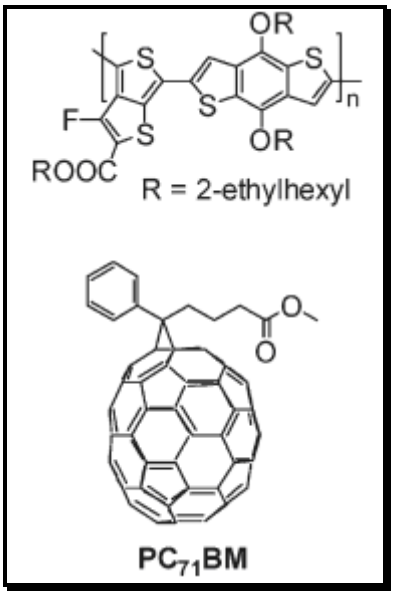


**Figure 1.18** Structures of the Polymer and $PC_{71}BM$

### 1.7.1 Benzotriazole Based Conjugated Copolymers

Quinoxaline, thienopyrazine and benzothiadiazole are some common acceptor groups frequently used for OSC applications. However, benzotriazole (BTz) which is similar to benzothiadiazole has been rarely used as the acceptor group especially in OSCs. BTz is an aromatic heterocycle having strong electron accepting characteristic due to presence of two imine groups (Figure 1.). Moreover, the presence of the N-H bond makes it possible to play with the structure and add solubilizing alkyl chains, altering the optical and electronic properties which will allow achieving processable multipurpose conjugated polymers [61].

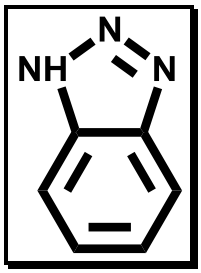


**Figure 1.19** Structure of Benzotriazole

Toppare Research Group indicated the application of BTz based CPs in OSCs. Donor-acceptor combination of BTz with hexylthiophene presented promising properties. Compared to P3HT, introduction of BTz increased the oxidation potential by lowering the HOMO level. By this way, an increase in Voc was achieved (0.85 V) [62].

Yingping Zou and coworkers synthesized a dithienyl benzotriazole and carbazole based CP by using Suzuki coupling (Figure 1.20). The polymer showed good solubility in common organic solvents such as chloroform and chlorobenzene. Moreover, it revealed great film quality and exhibited optimized energy levels of HOMO and LUMO. These properties lead to efficient photovoltaic outcomes combined with great thermal and air stability [63].

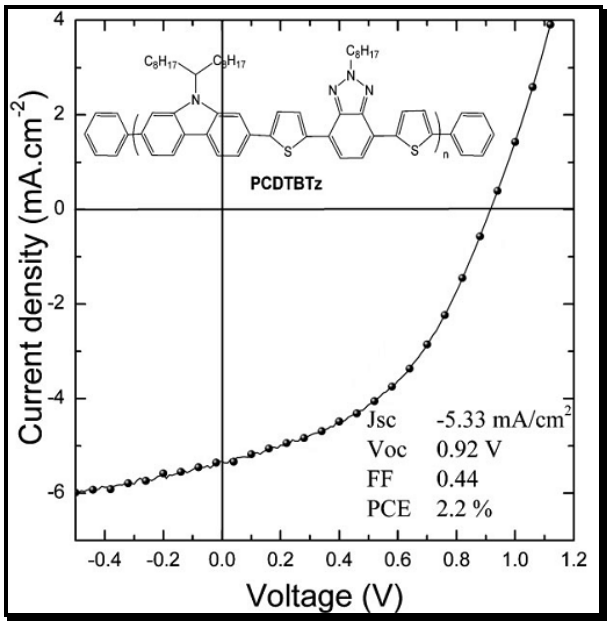


**Figure 1.20** Typical J–V curves of the polymer solar cells based on PCDTBTz:$PC_{61}BM$

The potential of BTz for OSCs has been further investigated by Wei You and coworkers. This study indicates that generating low band gap CPs is just one of the many parameters for ending up with high device efficiency. The synthesized polymers have moderate band gaps just like P3HT. However, they have excellent hole mobility and low HOMO and LUMO levels. The fluorinated copolymer presents efficiencies above 7% with an active layer thickness of 250 nm in a typical BHJ structure with $PC_{60}BM$. Substitution of fluor unit which is an electron withdrawing group, lower the HOMO and LUMO level of the resulting copolymer. By this way, fluorinated copolymer shows a higher Voc and Jsc values [57].

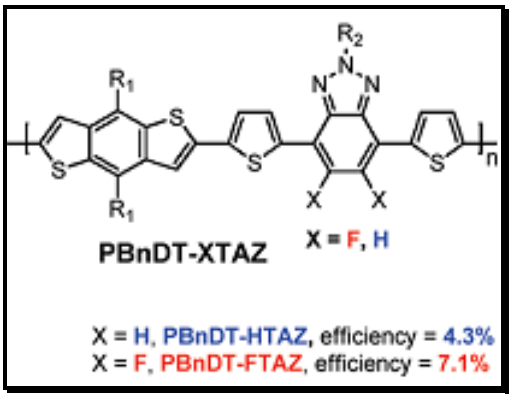


**Figure 1.21** Medium band gap fluor containing copolymer

### 1.7.2 Fluorene Based Conjugated Copolymers

Polyfluorene (PF) and its copolymers with different groups are considered as some of the most promising materials to be used in organic electronics and have been examined quite extensively up to date [64]. They are novel materials with their unique electro-optical properties and their availability for chemical modification. Fluorene and its derivatives are rigid, planar molecules that are usually associated with relatively large band gaps and low lying HOMO energy. Therefore, a high open circuit voltage is the characteristic of fluorene based cells [40]. The presence of the 9-position makes it available for easy dialkylation and selective bromination at the 2,7-positions of fluorene enable flexible molecular manipulation to improve solubility and extend conjugation easily via a transition-metal cross-coupling reaction [65]. Combination of PFs with an acceptor or a donor–acceptor–donor (DAD) group ensures that the band gap of the polymer can be modified according to device applications [66]. Poly-9,9-dialkylfluorene (PFO) based copolymers, particularly benzothiadiazole (BTd) derivatives, were used in optoelectronic applications and inserting BTd units in PFO chains resulted in highly efficient OPVs, OLEDs and OFETs [67].

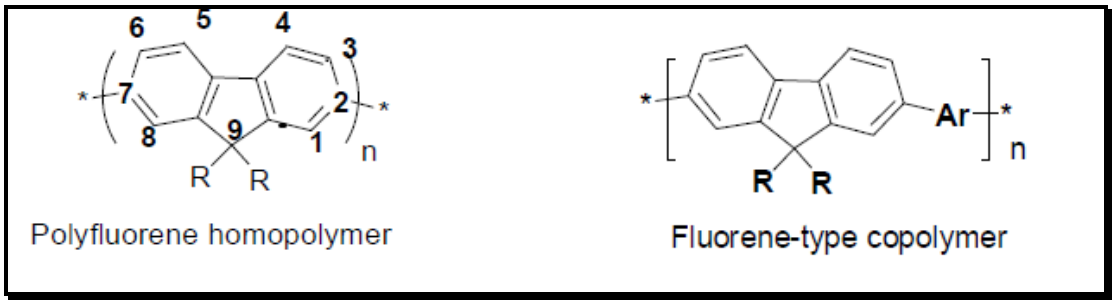


**Figure 1.22** Polyfluorene homopolymer and copolymer

A recent study conducted by Fengling Zhang and his coworkers investigates four fluorene- thiophene -benzothiadiazole-thiophene based alternating conjugated polymer differing in the presence and place of flexible side chains (Figure 1.23). The existence of side chains is significant since they enhance solubility thus, the processability of the polymers. The length and place of alkyl chains plays an important role on energy levels, molecular weights and morphology, thereby the photovoltaic responses of devices.

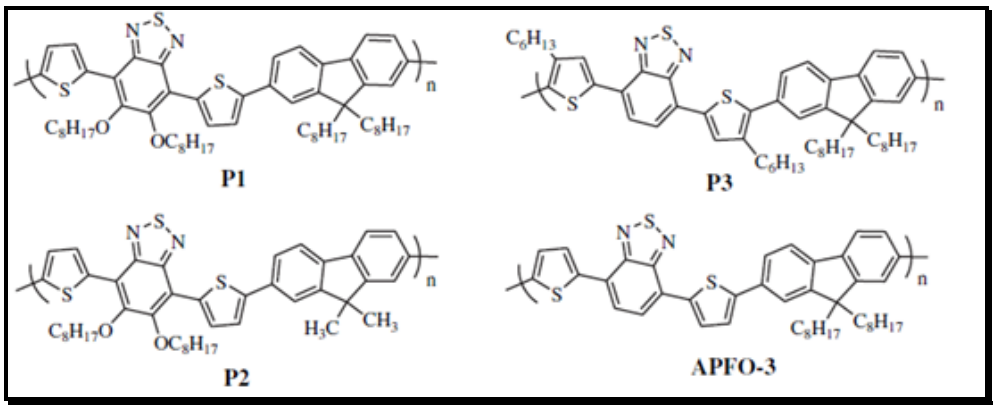


**Figure 1.23** Fluorene and benzothiadiazole containing copolymers

Under a device configuration of ITO/polymer:PC71BM blends/LiF/Al, P1 exhibits the best performance with a power conversion efficiency of 3.1%. When the results compared with APFO-3 which has no side chains on BTd unit, these two polymers have almost same photovoltaic properties. This means that the incorporation of octyloxy substituents to BTd does not alter the absorbance and carrier transport property of the conjugated polymer main chain. On the other hand, P3 based device shows decreased performance due to the existence of hexyl groups on the thiophene units which reduces planarity [68].

On the contrary, BTz was introduced to the PFOs in few studies where it was used as internal molecular additive [69]. However, properties of alternating copolymers with BTz groups with fluorene are yet lack of scientific inventory. The use of BTz may bring an improvement on the several properties of OSCs.

### 1.8 Aim of This Study

The purpose of this study is to synthesize three novel benzotriazole and fluoerene based donor acceptor type alternating copolymers; poly((9,9-dioctylfluorene)-2,7-diyl-(2-dodecyl benzo[1,2,3]triazole)) (P1), poly((9,9-dioctylfluorene)-2,7-diyl-(4,7-bis(thien-2-yl) 2-dodecyl-benzo[1,2,3]triazole)) (P2), poly((9,9-dioctylfluorene)-2,7-diyl-(4,7-bis(3 hexylthien-5-yl) 2-dodecyl-benzo[1,2,3]triazole)) (P3)) and investigate their electrochemical and photovoltaic properties. All three polymers were soluble in common solvents and they formed good quality films from their mixtures with [6,6]-phenyl-C61-butyric acid methyl ester (PCBM) which is the common acceptor group. Results exhibited that the polymers were multipurpose materials which gave great results both in electrochemistry and photovoltaic studies. Furthermore, these materials have high potentials to be used in OLEDs.

# CHAPTER 2

# EXPERIMENTAL

## 2.1 Materials

Tetrabutylammonium hexafluorophosphate ($TBAPF_6$) (Aldrich), PEDOT: PSS (H.C.Stark), PCBM (Solenne), Chloroform (Aldrich), Ethanol(Aldrich), dichloromethane (DCM) (Merck), HBr (Merck), Chlorobenzene (CB) (Aldrich), Acetonitrile (ACN) (Merck), methanol (Merck), tributyltin chloride (Aldrich), N-butyl lithium (Aldrich), thiophene (Merck), 3-hexylthiophene (Aldrich) and $MgSO_4$ (Aldrich) were used without further purification as they were purchased from commercial sources. THF (Fisher) was distilled before usage. Al (Kurt. J. Lester), LiF (Kurt. J. Lester), ITO (Visiontek Systems Ltd.) 2,2'-(9,9-dioctyl-9H-fluorene-2,7-diyl)bis(1,3,2-dioxaborinane) were used as received.

## 2.2 Equipment

Electrochemical studies were performed in a three-electrode cell consisting of an Indium Tin Oxide coated glass slide as the working electrode, platinum wire as the counter electrode, and Ag wire as the reference electrode under ambient conditions using a Voltalab 50 potentiostat. The value of Normal Hydrogen Electrode (NHE) was taken as -4.75 eV [70]. $^{1}$H- NMR and $^{13}$C-NMR spectra were recorded in $CDCl_3$ on Bruker Spectrospin Avance DPX-400 Spectrometer.Chemical shifts were given in ppm downfield from tetramethylsilane. Products were purified via column

chromatography with Merck Silica Gel 60 (particle size: 0.040–0.063 mm, 230–400 mesh ASTM).

Solvents were spectrophotometric grade. Varian Cary 11 5000 UV–Vis spectrophotometer was used to perform the spectroelectrochemical studies of the polymer. Average molecular weight was determined by gel permeation chromatography (GPC) via a METU Central Laboratory GPC 220 using dry THF as effluent. Differential scanning calorimetry (DSC) and thermal gravimetric analysis (TGA) were performed on Perkin Elmer Diamond DSC and Perkin Elmer Pyris 1 TGA. The current density-voltage **(J–V)** measurements were carried out in a nitrogen-filled glove box system (MBraun) (moisture <0.1 ppm; oxygen <0.1 ppm) under illumination of AM 1.5G simulated solar light at 100 mW/cm$^2$ using an Atlas solar simulator. The light intensity was measured with an Oriel radiant power meter. Current-voltage characteristics were recorded using a Keithley 2400 Source.

## 2.3 Procedure

### 2.3.1 Synthesis

#### 2.3.1.1 2-Dodecylbenzotriazole

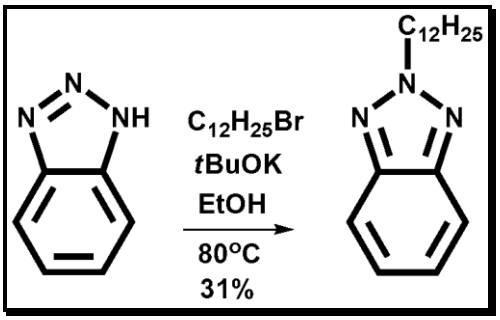


**Figure 2.1** Synthetic route for 2-dodecylbenzotriazole

Synthesis of 2-dodecylbenzotriazole was carried out using 1,2,3-benzotriazole (5.0 g, 42 mmol), potassium tert-butoxide (5.0 g, 44 mmol), and bromododecane (12.2 g, 49 mmol). All materials were dissolved in ethanol (50 mL) and the mixture was refluxed for 12 h. The reaction was monitored by TLC. After removal of the solvent by evaporation, the residue was dissolved in $CHCl_3$ and extracted with water. $MgSO_4$ was used to dry the organic extract. Then the solvent was evaporated under reduced pressure. The residue was subjected to column chromatography (3:2 chloroform:hexane; *R*f, 0.29) to obtain 2-dodecylbenzotriazole as a colorless oil (3.7 g, 31%).

### 2.3.1.2 4,7-Dibromo-2-dodecylbenzotriazole

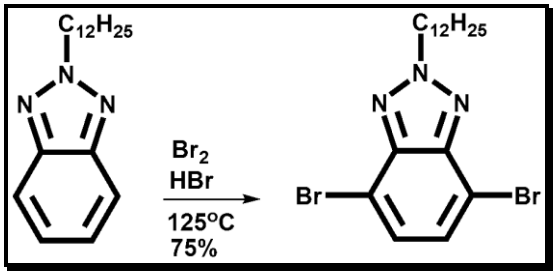


**Figure 2.2** Synthetic route for 4,7-dibromo-2-dodecylbenzotriazole

For the synthesis of 4,7-dibromo-2-dodecylbenzotriazole, 2-dodecylbenzotriazole (3.7 g, 13.1mmol) and an aqueous HBr solution (5.8 M, 15 mL) were added together and stirred for 1 h at 100 °C. Then bromine (5.9 g, 36 mmol) was added, the mixture was stirred for 12 h at 135 °C. After the reaction was completed, the mixture was allowed to cool to room temperature. After that a saturated solution of $NaHCO_3$ was added and the product was extracted with $CHCl_3$. The organic layer was dried over $MgSO_4$ and the solvent was evaporated under reduced pressure. By using column chromatography (1:1 chloroform:hexane; Rf, 0.33),

4,7- dibromo-2-dodecylbenzotriazole was obtained as light yellow oil (4.3 g, 75%).

### 2.3.1.3 Tributyl(thiophen-2-yl)stannane and Tributyl(4-hexylthiophen-2 yl)stannane

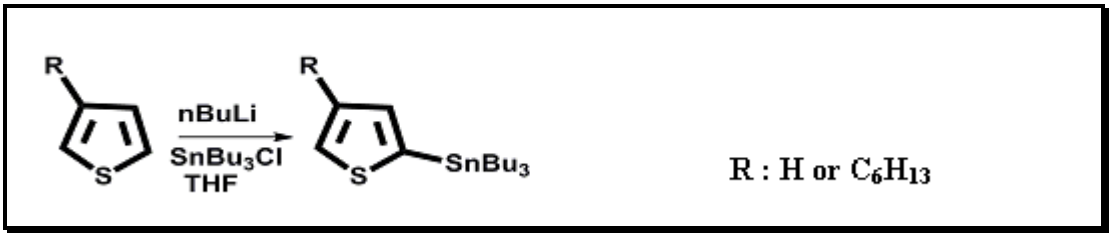


**Figure 2.3** Synthetic pathway for stannylation of thiophene and 3-hexylthiophene

Same procedure applies for the stannylation of thiophene and 3-hexylthiophene. Thiophene (1g, 0.95 mL) or 3-hexylthiophene (2 g, 2.13 mL) was dissolved in THF (20 mL), and the solution was cooled to -78$^{o}$C. n-Butyllithium (5.76 mL of 2.5 M for thiophene or 5.2 mL of 2.5 M for 3-hexyl thiophene) was added drop-wise. The mixture was stirred at -78$^{o}$C during 1 h. Then, tributyltin chloride (3.48 mL for thiophene or 3.5 mL for 3-hexylthiophene) was added at -78$^{o}$C via a syringe. Then the mixture was stirred at room temperature for 24 h. At the end of the reaction, water was added to the mixture. The phases were separated and organic layer was extracted with $CH_2Cl_2$. All the organic layers were then washed with water. The organic layer was dried over $MgSO_4$. After removal of the solvent, the product was obtained as a brown viscous liquid (70%).

### 2.3.1.4 2-dodecyl-4,7-di(thiophen-2-yl)-2H-benzo[d][1,2,3]triazole (TBT)

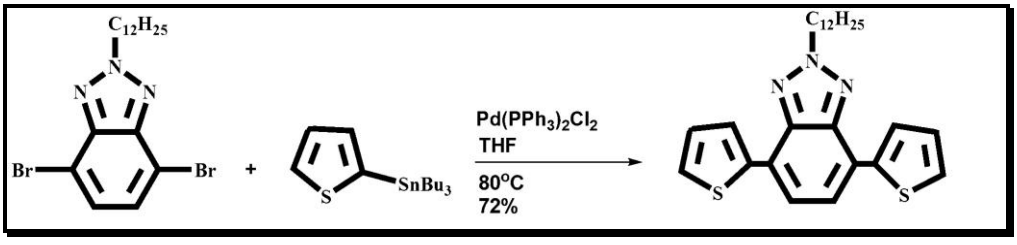


**Figure 2.4** Synthetic route for TBT

TBT was synthesized using the procedure utilized in the reference [71]. 4,7-Dibromo-2-dodecylbenzotriazole (100 mg, 0.224mmol), and tributyl(thiophen-2-yl) stannane were dissolved in anhydrous THF (100 ml) and as a necessity of Stille coupling, dichlorobis(triphenylphosphine)-palladium(II) (50 mg, 0.045 mmol) was added at room temperature. After 12 hours of reflux under argon atmosphere, the solvent of the reaction mixture was removed. The crude product was purified by column chromatography on silica gel to obtain 75 mg (74%) TBT.

### 2.3.1.5 2-Dodecyl-4,7-bis(4-hexylthiophen-2-yl) 2Hbenzo[d][1,2,3]triazole (HTBT)

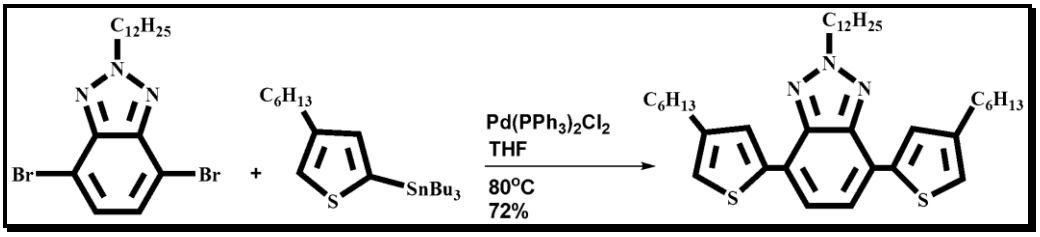


**Figure 2.5** Synthetic pathway for HTBT

HTBT was synthesized using the procedure utilized in the reference [72]. By means of Stille coupling, 4,7-Dibromo-2-dodecylbenzotriazole (100 mg, 0.224 mmol), and tributyl(4-hexylthiophen-2-yl)stannane (511 mg, 1.12 mmol) were dissolved in anhydrous THF (100 ml) and dichlorobis(triphenylphosphine)-palladium(II) (50 mg, 0.045 mmol) was added at room temperature. After 12 hours of reflux under argon atmosphere, the solvent of the reaction mixture was removed under reduced pressure. Finally, the crude product was purified by column chromatography on silica gel to obtain 95 mg (72 %) HTBT.

### 2.3.1.6 4,7-bis(5-bromothien-2-yl)-2-dodecylbenzo[1,2,3]triazole

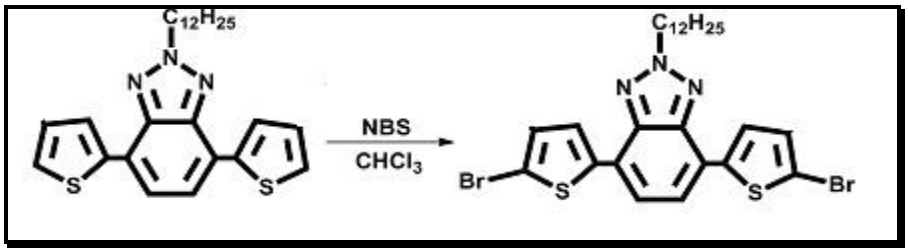


**Figure 2.6** Synthetic route for 4,7-bis(5-bromothien-2-yl)-2 dodecylbenzo [1,2,3]triazole

Bromination of TBT was done benefiting from the examples from the literature. 200 mg of TBT (0.44 mmol) and 190 mg of N-bromosuccinimide (1.07 mmol) were stirred in 100 ml of $CHCl_3$ at room temperature by preventing the mixture from exposure to light. After 12 h solvent was removed under reduced pressure and crude product was filtered over silica by 1:3 chloroform: hexane to obtain 250 mg (93%) as yellow solid.

### 2.3.1.7 4,7-bis(5-bromo-4-hexylthien-2-yl)-2-dodecylbenzo[1,2,3]triazole

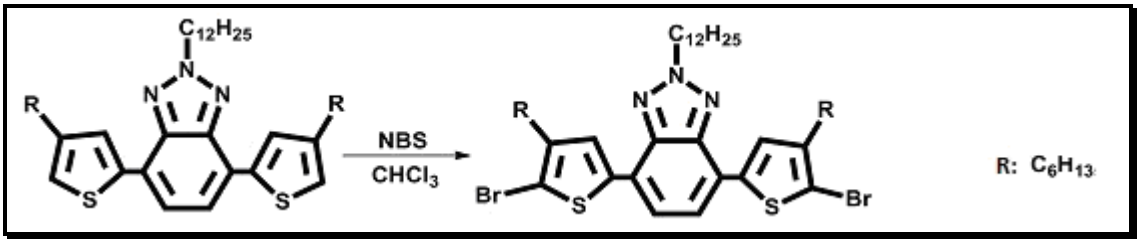


**Figure 2.7** Synthetic route for 4,7-bis(5-bromo-4-hexylthien-2-yl) 2dodecylbenzo[1,2,3]triazole

Bromination of HTBT was performed with the same procedure explained for TBT above. 200 mg of HTBT (0.32 mmol) and 138 mg of N-bromosuccinimide (0.77 mmol) were reacted to obtain 235 mg (94.4%) 8 as yellow solid.

### 2.4 Synthesis of the Polymers

All of the polymerizations were run with palladium (0) catalyzed Suzuki polycondensation reactions with equivalent molar ratios of dibrominated monomers and diboronic ester substituted fluorene compound under argon atmosphere. Special care was paid to the purification of the resulting polymers since remaining metal residues of catalyst might act as charge traps and cause an effect on electrical properties [73].

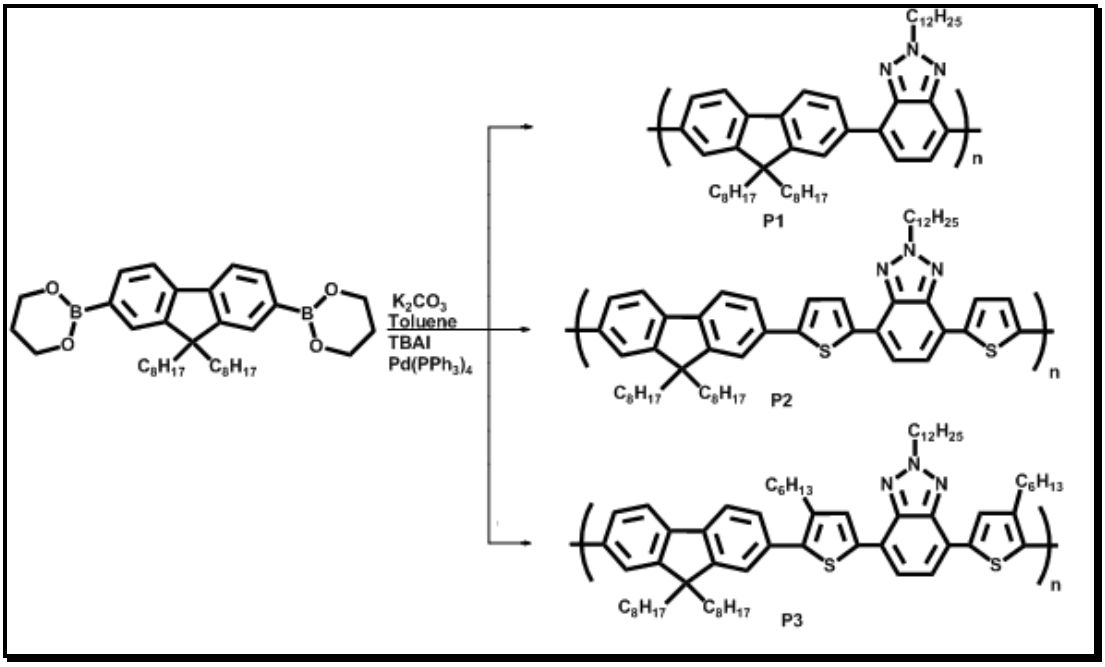


**Figure 2.8** Synthetic route for P1, P2, and P3

### 2.4.1 Poly((9,9-dioctylfluorene)-2,7-diyl-(2-dodecyl-benzo[1,2,3]triazole)) (P1)

4,7-Dibromo-2-dodecylbenzotriazole (1 mol equivalent), 2,2'-(9,9-dioctyl-9H-fluorene-2,7-diyl)bis(1,3,2-dioxaborinane) (1 mol equivalent), Pd(PPh3)4 (5 mol%), and tetrabutylammoniumiodide ($N(Bu)_4I$, 1 mol%) were added into a degassed mixture of potassium carbonate ($K_2CO_3$, 2M in $H_2O$). The mixture was refluxed at 115–120 $^{\circ}C$ for 48 h under argon. Solvent was removed under reduced pressure and extracted with $CHCl_3$:$H_2O$ mixture twice to remove alkali solution. Combined organic layers were dried over anhydrous $MgSO_4$ and evaporated under reduced pressure. The crude product was washed with methanol and Soxhlet extracted by acetone to obtain corresponding polymer.2.4.2 Poly((9,9-dioctylfluorene)-2,7-diyl-(4,7-bis(thien-2-yl) 2-dodecyl benzo[1,2,3]triazole)) (P2)

4,7-Bis(5-bromothien-2-yl)-2 dodecylbenzo[1,2,3]triazole (1 mol equivalent) and 2,2'-(9,9-dioctyl-9H-fluorene-2,7-diyl)bis(1,3,2-dioxaborinane) were reacted with the same manner as P1.

### 2.4.3 Poly((9,9-dioctylfluorene)-2,7-diyl-(4,7-bis(3-hexylthien-5-yl) 2-dodecyl-benzo[1,2,3]triazole)) (P3)

4,7-Bis(5-bromo-4-hexylthien-2-yl)-2-dodecylbenzo[1,2,3]triazole(1mol equivalent) and 2,2'-(9,9-dioctyl-9H-fluorene-2,7-diyl)bis(1,3,2-dioxaborinane) were reacted using the same procedure as in the synthesis of P1.

## 2.5 Characterization of the Polymers

### 2.5.1 Cyclic Voltammetry (CV)

Cyclic voltammetry is the most extensively utilized technique for providing qualitative information concerning electrochemical reactions. Redox potentials of electroactive species can be identified rapidly by means of this technique. In CV the normal three electrode configuration is used and voltage is applied to the working electrode sweeping between two values (Figure 2.9) at a fixed rate, when the voltage reaches $V_2$ the scan is reversed and the voltage is swept back to $V_1$.

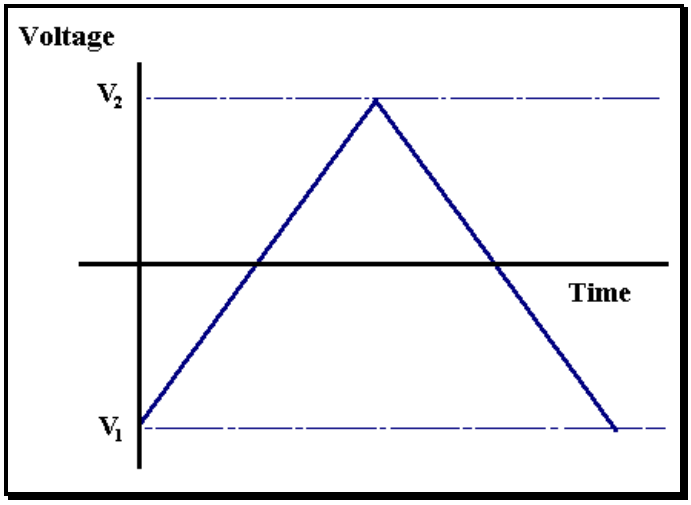


**Figure 2.9** Cyclic voltammetry waveform

Throughout the potential sweep, the resulting current values stemming from the applied potential is recorded by a potentiostat. Figure 2.10 indicates the estimated response of a reversible redox couple in a single scan. The potential is measured between the reference electrode and the working electrode and the current is

measured between the working electrode and the counter electrodes. This data is then plotted as current (i) vs. potential (V).

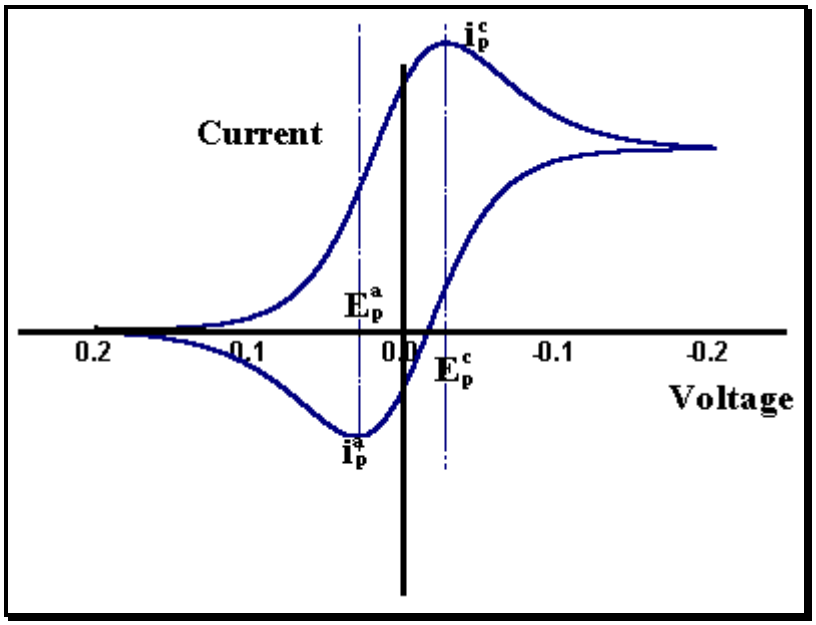


**Figure 2.10** A cyclic voltammogram for a reversible redox process

During the cathodic scan, the current will rise until the reduction potential of the analyte is reached. After that point, it will decrease due to the depleted concentration of the analyte close to electrode surface. When the applied potential is reversed, analyte will be reoxidized and generate a current of reverse polarity from the forward scan.

The formation of characteristic peaks in CV depends on the position of the diffusion layer with respect to the electrode surface. The observed peaks indicate the change in the concentration with time. The peak current for a reversible couple is calculated by Randles & Sevcik equation (2):

$$i_p = 0.4463\ n\ F\ A\ C\ (n\ F\ v\ D\ /\ R\ T)^{1/2} \qquad (2)$$

In this equation, $i_p$ means peak height, n indicates the number of electrons appearing in half-reaction for the redox couple, F is Faraday's constant (96485 C / mol), A is the electrode area ($cm^2$), C is the concentration, D is the analyte's diffusion coefficient ($cm^2$/sec), R is the universal gas constant (8.314 J / mol K) and T is the absolute temperature (K). If the temperature is assumed to be 25°C (298.15 K), the Randles-Sevcik equation can be expressed in a more brief form (3).

$$i_p = (2.687 \times 10^5)\, n^{3/2}\, v^{1/2}\, D^{1/2}\, A\, C \qquad (3)$$

Cyclic Voltammetry studies of polymers are conducted in a monomer free system.

### 2.5.2 Spectroelectrochemistry

Spectroelectrochemistry is a valuable method which simultaneously combines the techniques of electrochemistry and spectroscopy. A redox active compound is oxidized or reduced at electrode surface and with the changes in electronic transitions, changes in absorbance are observed. By utilizing this technique, it is possible to provide information about the bang gap, $\lambda_{max}$, intergap states (polarons and bipolarons) and colors of the polymer.

During the experiments, polymer coated ITO is immersed into a sample cell which includes liquid electrolyte. While potential is increased stepwise and the polymer is oxidized, the change in absorption spectrum is recorded by UV-Vis spectroscopy. Spectroelectrochemistry studies of conjugated polymers indicate that CPs are useful in electrochromic applications such as mirrors and smart windows since there is a strong change in their absorbance upon applied potential.

### 2.5.3 Kinetic Studies

Electrochromic applications such as displays require a very fast switching time accompanied by a remarkable color change. Kinetic studies allow monitoring these properties. Electrochromic switching time and contrast (percent transmittance change) are measured via square wave potential step method coupled with optical spectroscopy known as chronoabsorptometry. In this double potential step experiment, for a fixed time potential is set at an initial potential. After that, it reaches a second potential again for a fixed time and goes back the initial value.

In order to study switching properties of polymers, P1, P2 and P3 were spray coated on ITO-coated glass slides as homogenous thin films. After that the polymers were switched between their neutral and oxidized states during 5 second time intervals at their $\lambda_{max}$ values.

### 2.5.4 Gel Permeation Chromatography (GPC)

Gel permeation chromatography is a chromatographic technique in which particles are separated based on their size. In this method, organic solvents are used as the mobile phase and the stationary phase include beads of porous polymeric material. In this study, the average molecular weights ($M_n$ & $M_w$) of polymers were determined by means of a METU Central Laboratory GPC 220 calibrated with universal standard polystyrene.

### 2.5.5 Thermal Properties

The thermal stability of a polymer is significant for the device fabrication process. In this study, thermal properties of the polymers were investigated using Perkin Elmer diamond differential scanning calorimetry (DSC) and Perkin Elmer Pyris 1 thermal gravimetric analysis (TGA) instruments. DSC is used to identify the changes in polymers with applied heat. It is possible to observe thermal transitions, namely, glass transition temperature (Tg), melting temperature (Tm), and crystallinity temperature (Tc). The DSC experiments were conducted under nitrogen environment between 25-250 $^{0}$C temperature range with an 10 $^{o}$C/minute intervals. TGA analysis utilizes heat for creating physical changes and reactions in polymers. By this way, it is possible to obtain the mass change in relation to the thermal degradation in materials. By using TGA, decomposition temperature of materials can be found. The TGA experiments were conducted under nitrogen environment between 25-700 $^{0}$C temperature range and with 10 $^{o}$ C/minute intervals.

## 2.6 Characterization of the Solar Cells

The current density-voltage characteristics measurements were carried out in a nitrogen-filled glove box system (MBraun 200 B) (moisture <0.1 ppm; oxygen <0.1 ppm) under illumination of AM 1.5G Atlas solar simulator at 100 mW/cm$^2$.The light intensity was measured with an Oriel radiant power meter. Current-voltage characteristics were recorded using a Keithley 2400 Source by continuously sweeping from –0.5V to +1.0 V and recording data points in 10 mV steps. Short-circuit current density (Jsc), open-circuit potential (Voc), fill factor (FF) and power conversion efficiency (η) were calculated from J-V curves.

The solar cells were fabricated in the configuration of the traditional sandwich structure with an ITO/PEDOT: PSS/active layer/LiF/Al. Firstly, Indium tin oxide

(ITO) coated glass substrates were etched and cleaned by sequential ultrasonic treatment in toluene, detergent, acetone, and isopropanol and treated in Harrick Plasma Cleaner for 10 min. Then a thin layer of PEDOT/PSS was spin coated on top of cleaned ITO substrate at 5000 rpm/s and dried subsequently at 120 $^{\circ}$C for 10 min on a hotplate. A PEDOT:PSS layer enhances hole collection and increases open-circuit potential (Voc) due to improved ohmic contact with the photoactive layer. The active layer was prepared by spin coating the chlorobenzene solution of blend of P1 and P2 with $PC_{61}BM$ acceptor. Since homogenous films could not be achieved with CB, chloroform was used for P3 for the device fabrication. A high boiling point solvent is generally preferable since it has been shown to promote packing of the polymer offering a sufficient time for drying the film which increases charge transport between polymer chains. The resulting active layer films were dried for 24 h in a glove box and 6 h under vacuum before cathode evaporation to remove all residual solvent. The cathode was thermally evaporated with a 0.6 nm LiF layer, followed by 80 nm of aluminum at a pressure of $2.10^{-6}$ mbar through a shadow mask. Three OSCs were fabricated on one substrate and the effective area of one cell is 0.065 $cm^2$.

# CHAPTER 3

# RESULTS AND DISCUSSION

## 3.1 Characterization

$^{1}$H-NMR and $^{13}$C-NMR spectra of the synthesized materials were obtained in $CDCl_3$. Tetramethylsilane (TMS) was used as the internal standard to calculate the chemical shifts (δ). In order to characterize the conjugated polymers only $^{1}$H-NMR spectra were obtained.

### 3.1.1 2-Dodecylbenzotriazole

$^{1}$H (400 MHz, $CDCl_3$, δ): 7.76 (m, 2H), 7.26 (m, 2H), 4.62 (t, J) 7.1 Hz 2H), 2.12 (m, 2H), 1.25-1.15 (m, 18H), 0.78 (t, J) 6.0 Hz, 3H). $^{13}$C NMR (100 MHz, CDCl3, δ): 144.3, 126.1, 117.9, 56.6, 31.8, 30.0, 29.5, 29.4, 29.4, 29.3, 29.3, 29.0, 26.5, 22.6, 14.0.

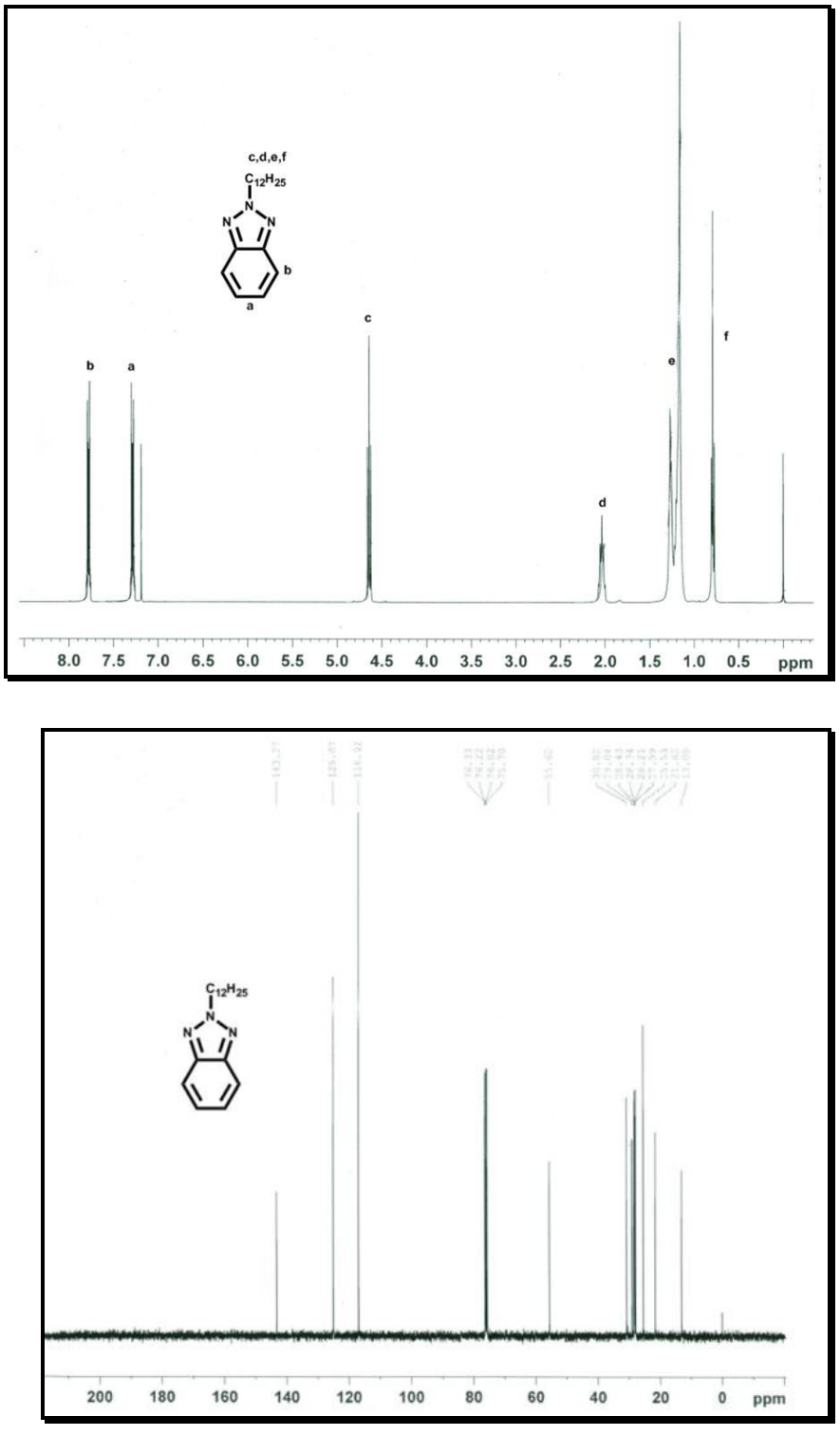


**Figure 3.1** $^{1}$H-NMR and $^{13}$C NMR of 2-dodecylbenzotriazole

### 3.1.2 4,7-Dibromo-2-dodecylbenzotriazole

$^{1}$H (400 MHz, $CDCl_3$, δ): 7.36 (s, 2H), 4.60 (t, J ) 7.0 Hz, 2H), 2.10 (m, 2H), 1.38-1.12 (m, 18H), 0.80 (t, J ) 6.9 Hz, 3H). $^{13}$CNMR (100 MHz, $CDCl_3$, δ): 143.7, 129.4, 109.9, 57.4, 31.8, 30.1, 29.5, 29.5, 29.4, 29.4, 29.3, 28.9, 26.4, 22.6, 14.0.

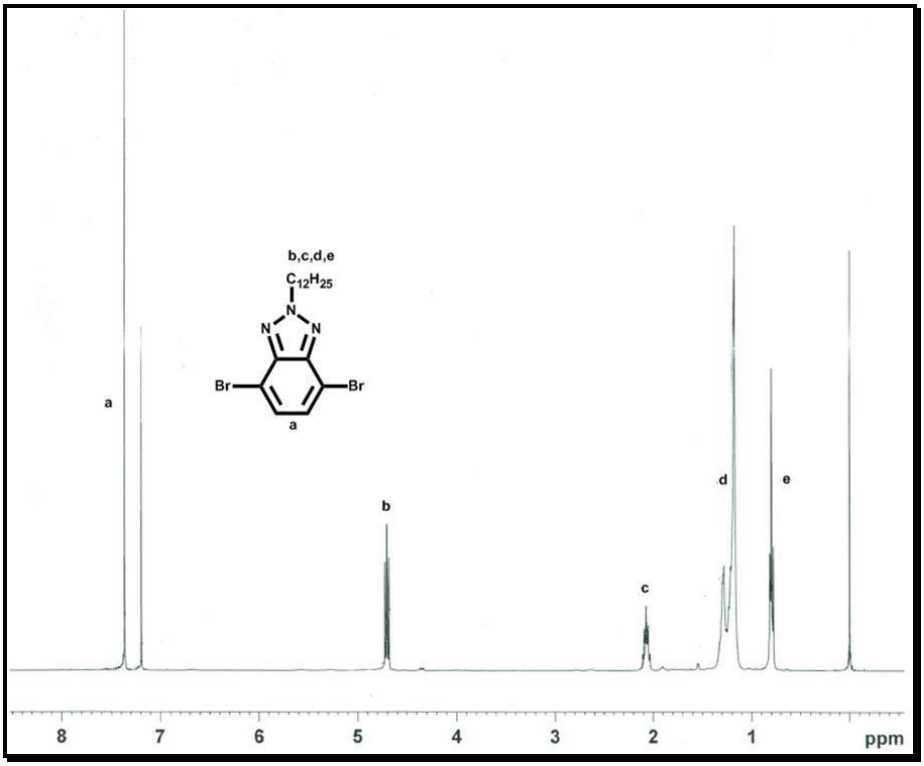


**Figure 3.2** $^{1}$ H-NMR and $^{13}$C NMR of 4,7- Dibromo-2-dodecylbenzotriazole

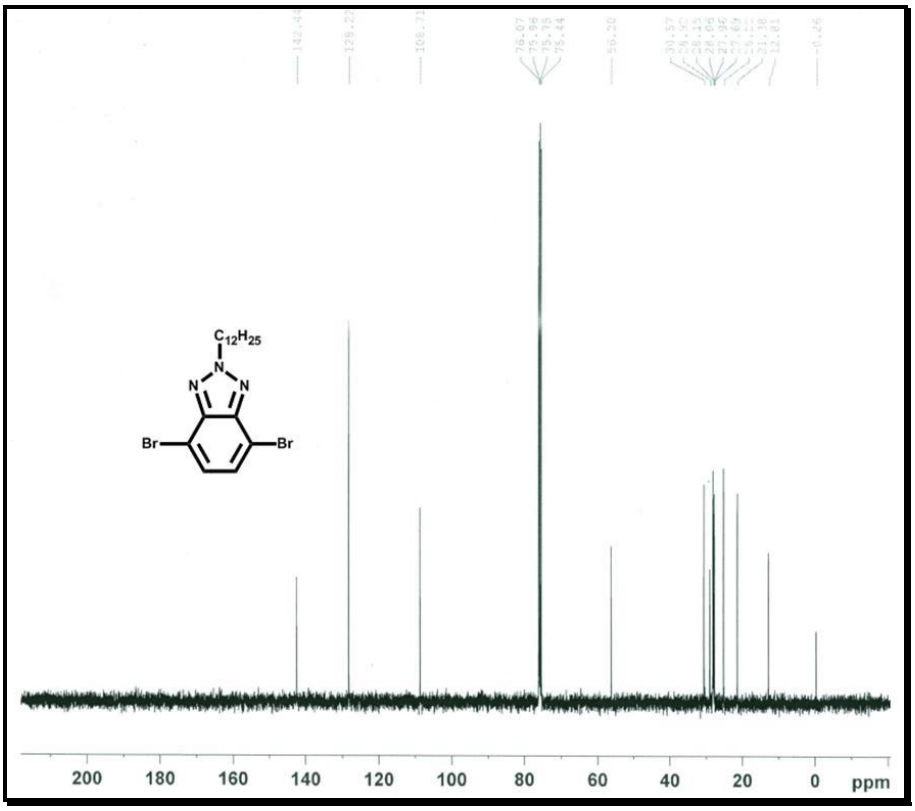


**Figure 3.2** [1] H-NMR and [13]C NMR of 4,7- Dibromo-2-dodecylbenzotriazole (continued)

### 3.1.3 TBT

$^{1}$H NMR (400MHz, $CDCl_3$, δ): 8.01 (d, J=5.6 Hz, 2H), 7.52 (s, 2H), 7.28 (d, J=6.0 Hz,2H), 7.09 (t, JA=8.8 Hz, JB = 4.8, 2H), 4.60 (t, J=7.0 Hz, 2H), 2.10 (m, 2H), 1.38-1.15 (m,18H), 0.80 (t, J=6.9 Hz, 3H); $^{13}$C NMR (100 MHz, DMSO-d6, δ): 142.4, 140.2, 128.4, 127.3, 125.8, 123.9, 123.0, 57.1, 32.2, 30.3, 29.9, 29.8, 29.7, 29.6, 29.5, 29.3, 26.9, 22.9, 14.4. MS (m/z): 451 [M+]

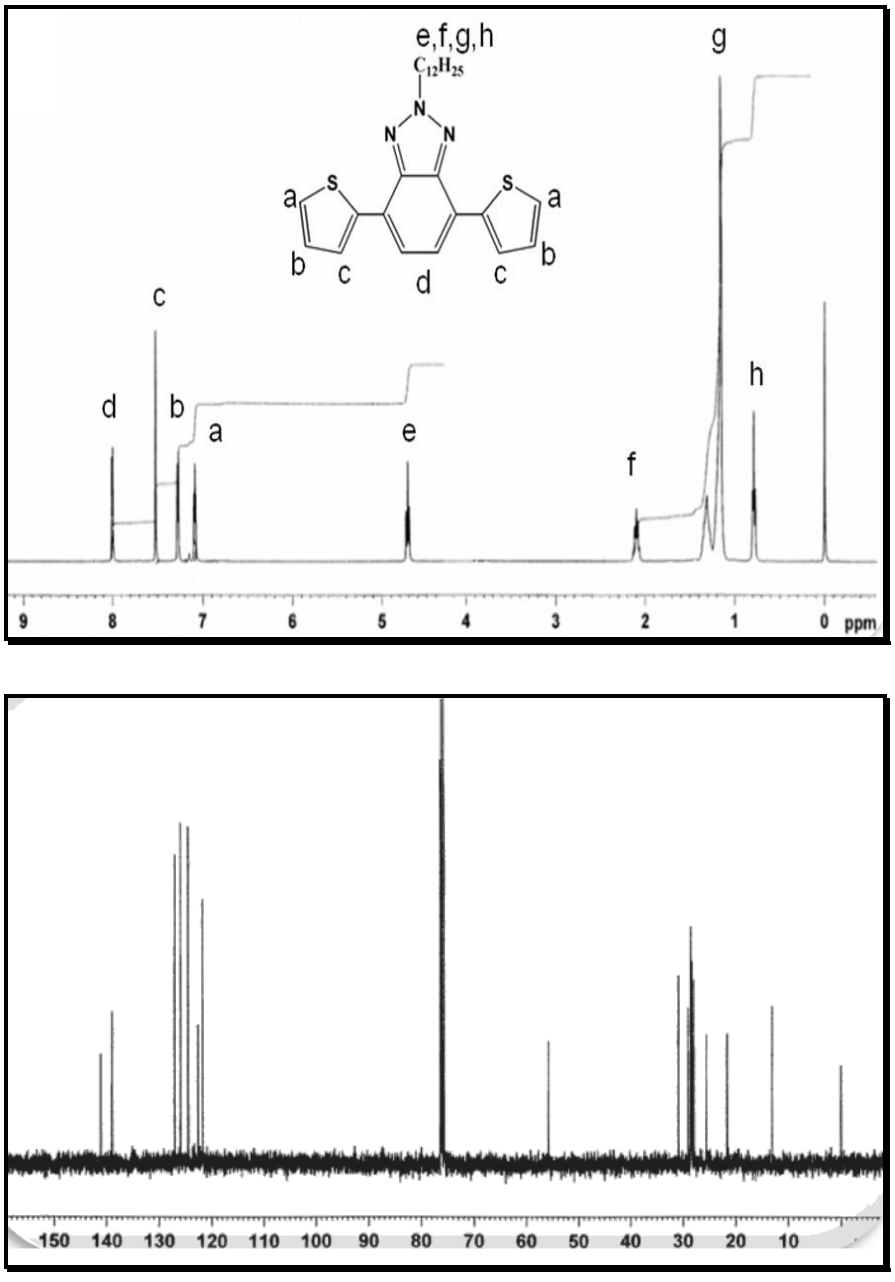


**Figure 3.3** $^{1}$H-NMR and $^{13}$C NMR of spectrum of TBT

### 3.1.42-Dodecyl-4,7-bis(4-hexylthiophen-2-yl)-2Hbenzo[d][1,2,3]triazole (HTBT)

$^{1}$H NMR (400MHz, $CDCl_3$, ): 7.9 (s, 2H), 7.5 (s, 2H), 6.9 (s,2H), 4.8 (t, J=7.0 Hz, 2H), 2.1 (m, 2H), 1.4-1.1 (m, 18H), 0.9 (t, J=6.9 Hz, 3H); $^{13}$C NMR (100 MHz, CDCl3, ): 143.1, 140.1, 138.3, 127.1, 122.4, 121.3, 119.0, 55.5, 30.6, 30.5, 29.5, 29.2, 28.8, 28.4, 28.2, 27.8, 25.49, 21.4, 12.8 MS (m/z): 619 [M+]

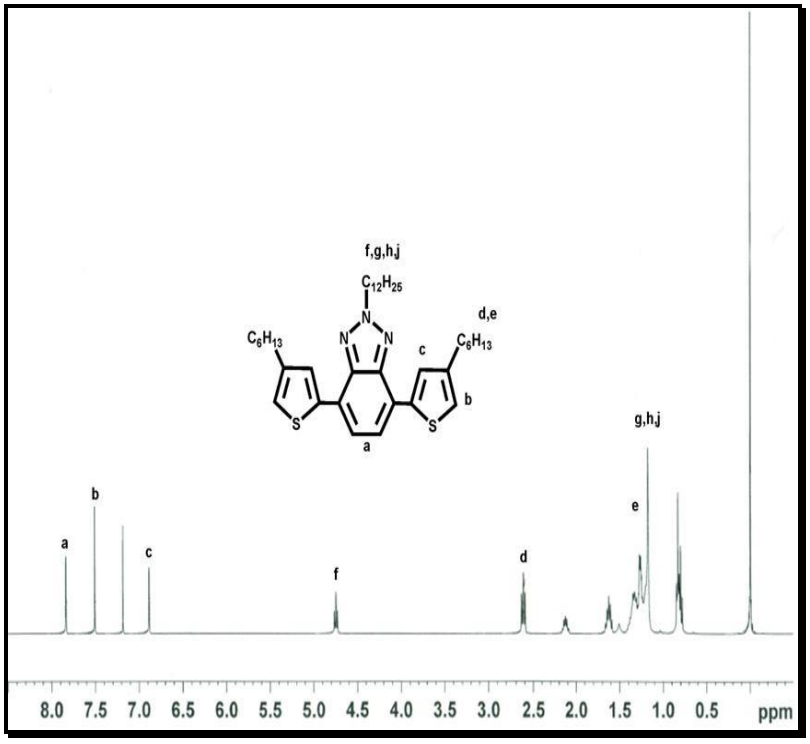


**Figure 3.4** $^{1}$H and $^{13}$C-NMR of 2-Dodecyl-(4,7-bis(4-hexylthio phen-2-yl) - 2Hbenzo[d] [1,2,3]triazole (HTBT)

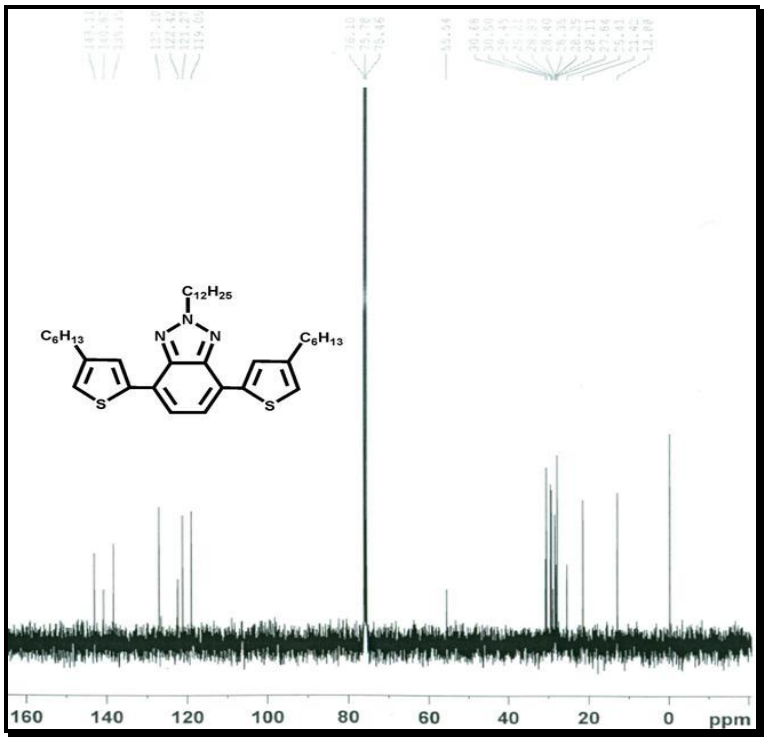


**Figure 3.4** $^{1}H$ and $^{13}C$-NMR of 2-Dodecyl-(4,7-bis(4-hexylthio phen-2-yl) -2Hbenzo[d] [1,2,3]triazole (HTBT) (continued)

### 3.1.5 4,7-Bis(5-bromothien-2-yl)-2-dodecylbenzo[1,2,3]triazole

$^{1}H$ NMR (400MHz, $CDCl_3$, δ): 7.72 (d, J=5.6 Hz, 2H), 7.44 (s, 2H), 7.04 (d, J=6.0 Hz, 2H), 4.72 (t, J=7.0 Hz, 2H), 2.10 (m, 2H), 1.32-1.17 (m,18H), 0.80 (t, J=6.9 Hz, 3H); $^{13}C$ NMR (100 MHz, CDCl3-d6, δ): 144.4, 142.2, 140.4, 127.3, 125.8, 123.9, 123.0, 57.1, 32.2, 30.3, 29.9, 29.8, 29.7, 29.6, 29.5, 29.3, 26.9, 22.9, 14.4. MS (m/z): 608 [M+]

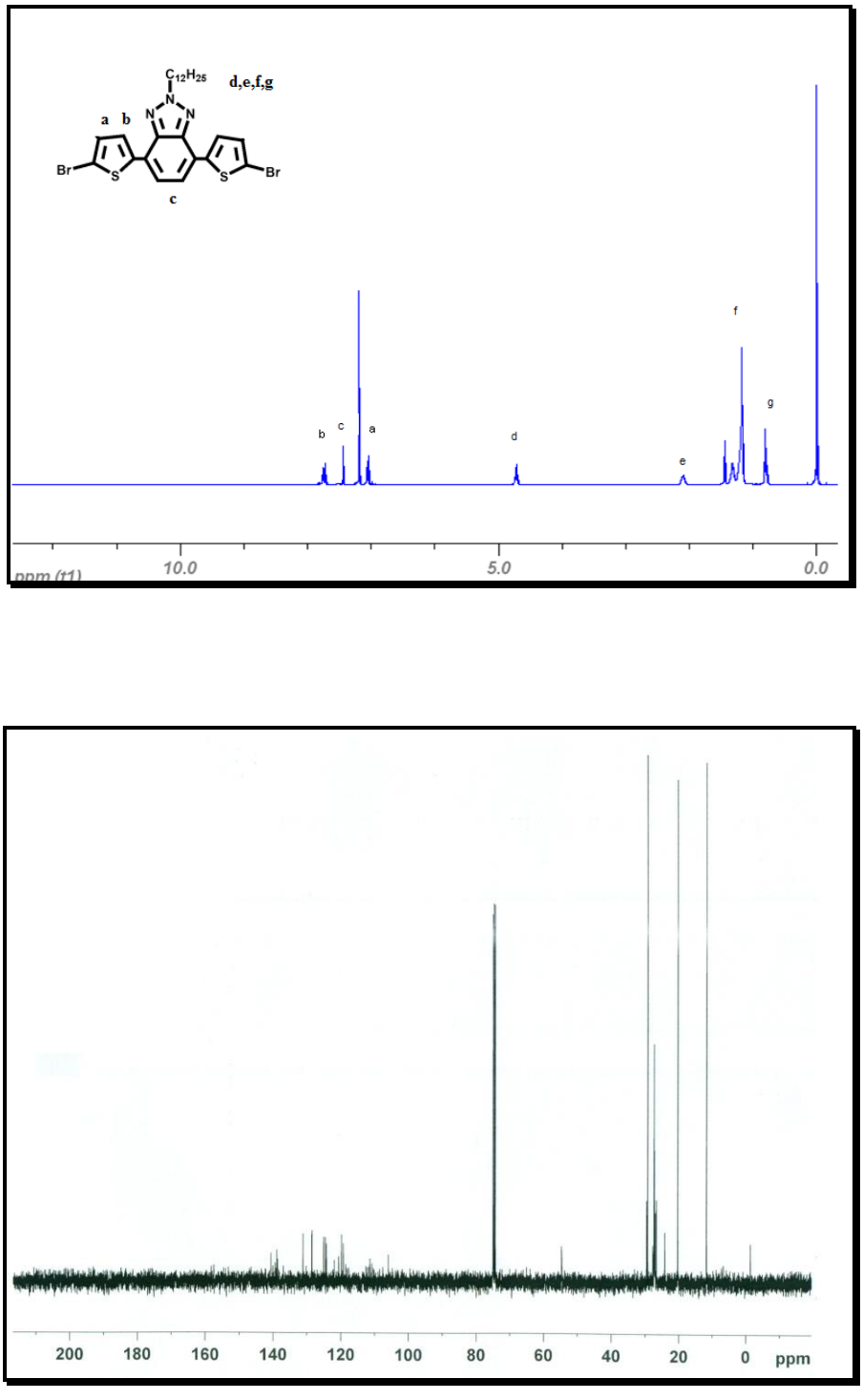


**Figure 3.5** $^{1}$H-NMR and $^{13}$C NMR of spectrum of 4,7-bis(5-bromothien-2-yl)-2-dodecylbenzo[1,2,3]triazole

### 3.1.6 4,7-Bis(5-bromo-4-hexylthien-2-yl)-2-dodecylbenzo[1,2,3]triazole

$^{1}$H NMR (400MHz, $CDCl_3$, δ): 7.69 (s, 2H), 7.41 (s, 2H), 4.77 (t, *J*=8.0 Hz, 2H), 2.61(t, *J*=8.0 Hz, 4H) 2.16 (m, 2H), 1.65 (m, 4H), 1.41-1.24 (m, 26H), 0.91-0.85 (m, 9H); $^{13}$C NMR (100 MHz, $CDCl_3$, δ): 143.1, 141.7, 139.2, 127.5, 123.0, 122.0, 110.1, 56.8, 32.0, 31.7, 30.0, 29.8, 29.7, 29.7 29.6, 29.5, 29.4, 29.1, 29.0, 26.7, 22.7 14.1. MS (*m*/*z*): 778 [M+].

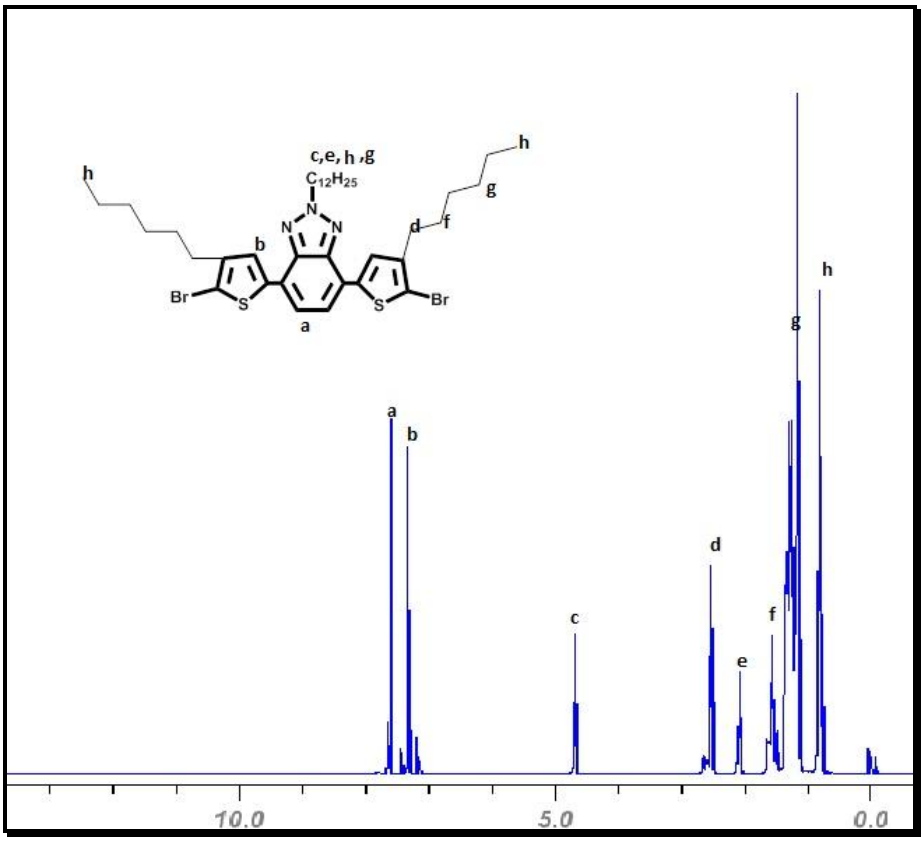


**Figure 3.6** $^{1}$H-NMR and $^{13}$C NMR of spectrum of 4,7-bis(5-bromo-4-hexylthien-2-yl)-2-dodecylbenzo[1,2,3]triazole

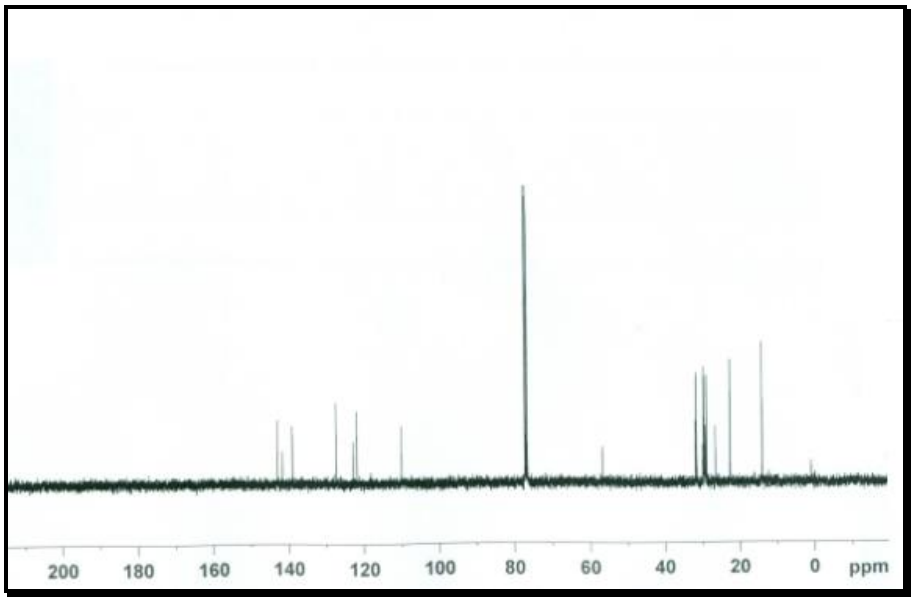


**Figure 3.6** $^{1}$H-NMR and $^{13}$C NMR of spectrum of 4,7-bis(5-bromo-4-hexylthien-2-yl)-2-dodecylbenzo[1,2,3]triazole (continued)

### 3.1.7 Poly((9,9-dioctylfluorene)-2,7-diyl-(2-dodecyl-benzo[1,2,3]triazole)) (P1)

$^{1}$H NMR (400 MHz, $CDCl_3$, d): 8.20 (benzotriazole), 8.1 (fluorene), 7.9 (fluorene), 7.7 (fluorene), 4.8 (N–CH2), 2.2 (C–CH2), 1.6–0.7 (pendant alkyl chains) GPC: Mn: 5900, Mw:10,600, PDI: 1.8.

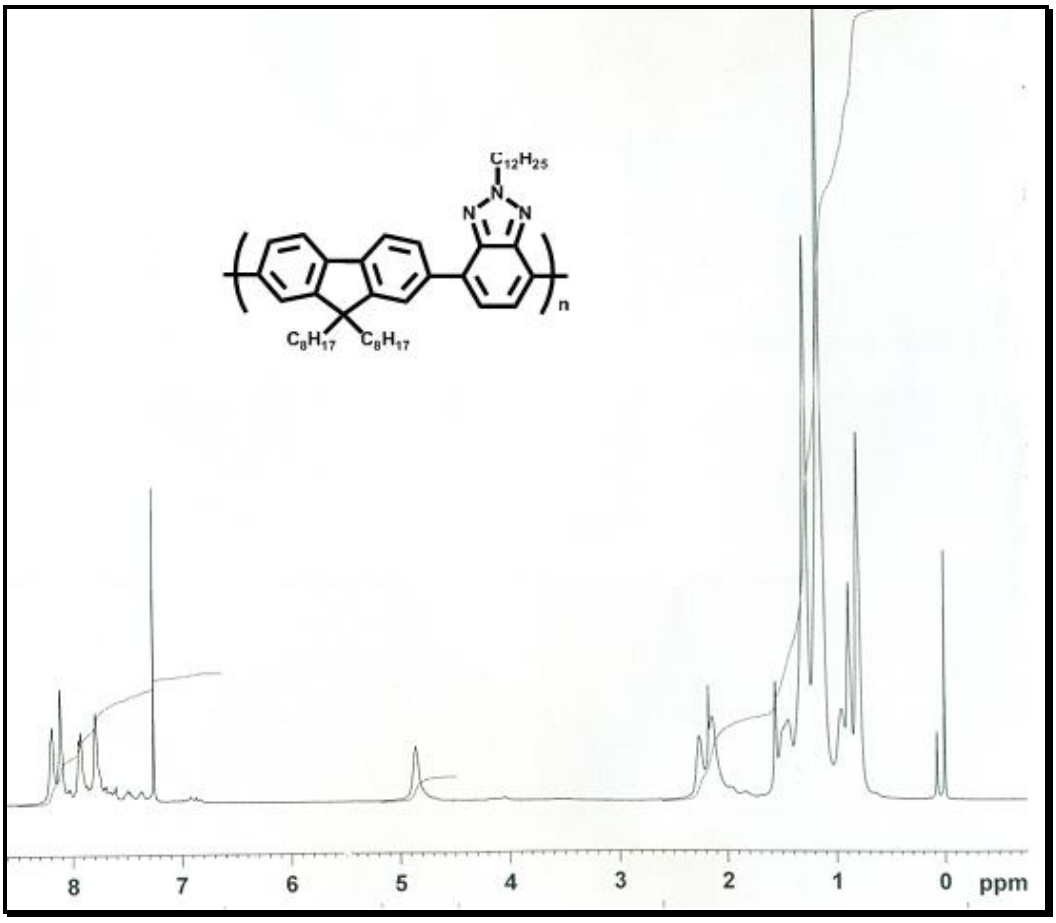


**Figure 3.7** $^{1}$H-NMR spectrum of P1

### 3.1.8 Poly((9,9-dioctylfluorene)-2,7-diyl-(4,7-bis(thien-2-yl) 2-dodecyl benzo[1,2,3]triazole)) (P2)

$^{1}$H NMR (400 MHz, $CDCl_3$, d): 8.1 (benzotriazole), 8.8–8.5 (fluorene, thiophene), 7.4 (thiophene), 4.8 (N–CH2), 2.2 (C–CH2), 1.6–0.7 (pendant alkyl chains).GPC: Mn: 6900, Mw: 17,500, PDI: 2.5.

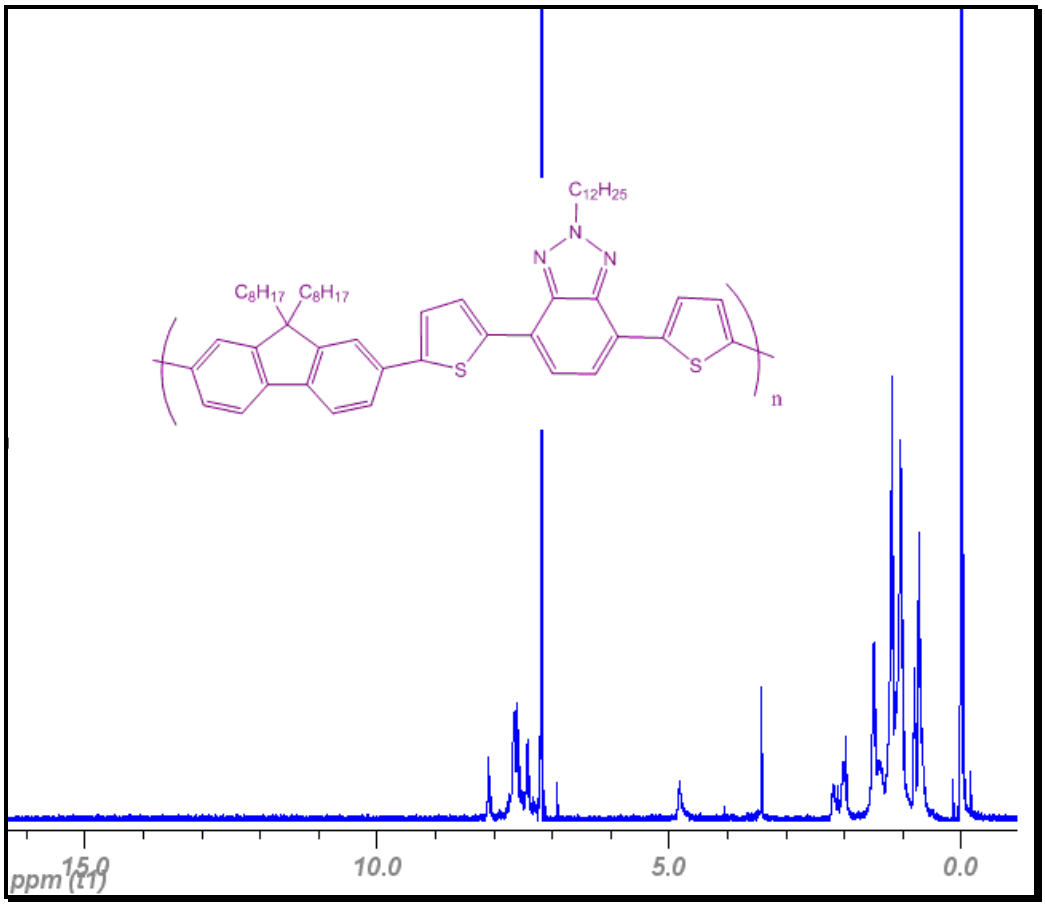


**Figure 3.8** $^{1}$H-NMR spectrum of P2

### 3.1.9 Poly((9,9-dioctylfluorene)-2,7-diyl-(4,7-bis(3-hexylthien-5-yl) 2-dodecyl-benzo[1,2,3]triazole)) (P3)

$^{1}$H NMR (400 MHz, $CDCl_3$, d): 8.00 (benzotriazole), 7.8 (fluorene), 7.6 (fluorene), 7.4 (fluorene, thiophene), 4.9 (N–CH2), 2.8 (CH2), 2.2 (C–CH2), 1.8–0.7 (pendant alkyl chains). GPC: Mn: 45,000, Mw: 183,000 PDI: 4.1.

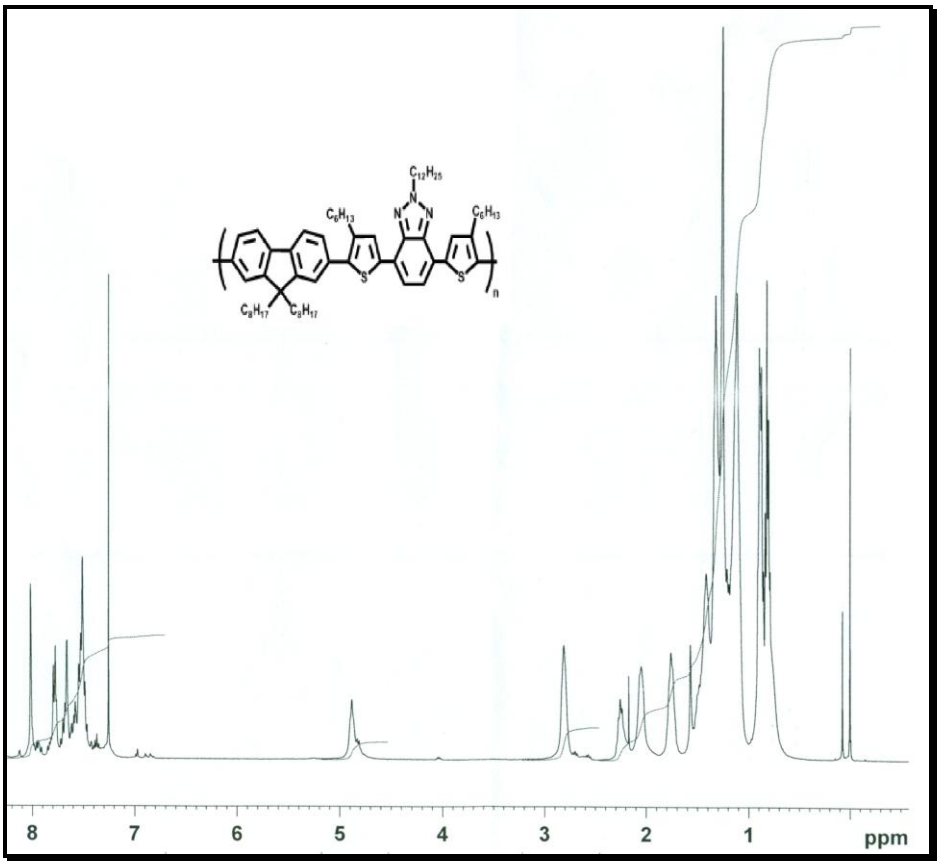


**Figure 3.9** $^{1}$H-NMR spectrum of P3

### 3.2 Poly((9,9-dioctylfluorene)-2,7-diyl-(2-dodecyl-benzo[1,2,3]triazole)) (P1)

#### 3.2.1 Cyclic Voltammetry (CV)

For electrochemical characterization, P1 was dissolved in chloroform to a concentration of 5 mg/mL and spray coated on indium tin oxide (ITO) coated glass slide. The polymer film on ITO was subjected to cyclic voltammetry (CV) in ambient conditions to determine the redox potentials in 0.1 M

tetrabutylammonium hexafluorophosphate (TBAPF6)/acetonitrile (ACN) solution at a scan rate of 50 mV/s. Initially, polymer film was subjected to a repeated cycling to obtain electrochemically stable and reproducible doping–dedoping. After that, potentials were swept between 1.5 and - 2.4 V versus Ag wire pseudo-reference electrode (50 mV versus $Fc/Fc^{+}$). (Figure 3.10).

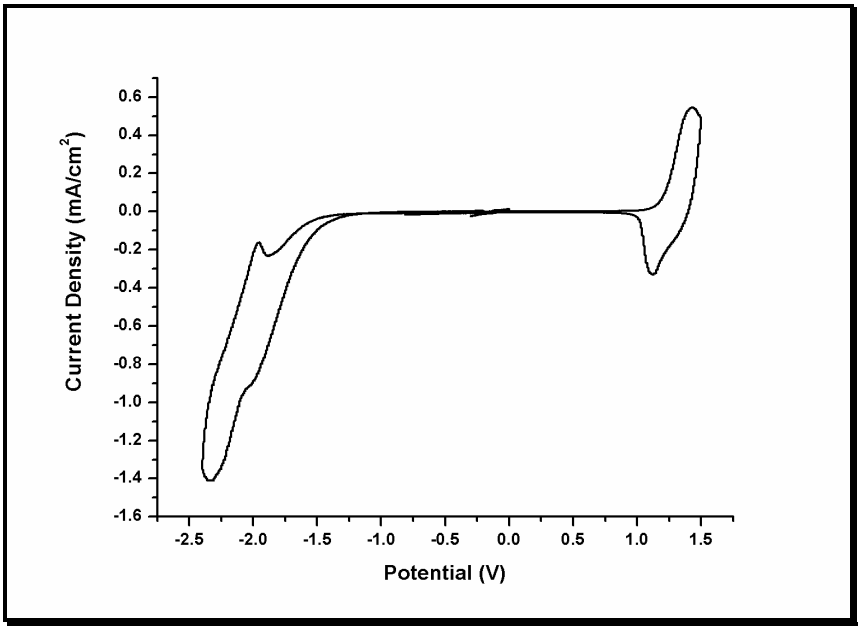


**Figure 3.10** Cyclic voltammogram of P1 for both p and n type doping in the presence of 0.1 M $TBAPF_6$/MeCN solution at a scan rate of 50 mV/s

P1 film revealed reversible redox couple at positive potentials pointed at 1.43 and 1.19 V versus Ag wire pseudo-reference electrode. It has the highest oxidation potential due to its electron poor structure compared to other polymers. P1 is also has n doping property with a reduction peak at -2.35 V and de-doping value of -1.78 V.

Due to P1's dual property, HOMO/LUMO energy levels were calculated precisely from the onset potentials of p and n doping peaks from CV as -5.94 and -2.97

respectively. The onset values were estimated by taking the intersection between the baseline and the tangent line drawn to the increasing side of the current. The reference electrode and the potentials were subsequently calibrated to $Fc/Fc^{+}$ and the band energies were calculated relative to the vacuum level considering that the value of NHE is -4.75 eV versus vacuum. Calculated electrochemical band gap of P1 was comparatively higher than the one estimated from π-π* transition due to the creation of free ions by means of applied potential which requires higher energy than optical absorption [74]. Table 1 summarizes the electrochemical data for polymer P1.

**Table 1** Oxidation potentials and onset values for both p- and n-type doping, estimated HOMO–LUMO energies and band gaps of synthesized polymers P1

| **P1** | Oxidation Potential (V) | | Reduction Potential (V) | | Bandgap (eV) | | Energy Level (eV) (from CV) | |
|---|---|---|---|---|---|---|---|---|
| | $E_{ox}$ | $E_{ox\ onset}$ | $E_{red}$ | $E_{red\ onset}$ | $E_g^{ec}$ | $E_g^{op}$ | HOMO | LUMO |
| | 1.43 | 1.19 | -2.35 | - 1.78 | 2.97 | 2.55 | -5.94 | -2.97 |

### 3.2.2 Spectroelectrochemistry

To examine the spectral change in the polymer during doping and de-doping process, spectroelectrochemistry studies were done. Neutral P1 film was spray coated on ITO coated glass slide from a solution of 3 mg/mL in chloroform. UV–vis–NIR spectrum was recorded for corresponding polymer film in 0.1 M $TBAPF_6$/ACN solution upon gradually increased external bias. Coated film was subjected to subsequent redox cycling by CV to achieve electrochemical stability

prior to spectroelectrochemical analysis. Figure 3.11 exhibits the change in the electronic absorption spectra of P1 upon increasing potentials between 0 V and +1.3 V.

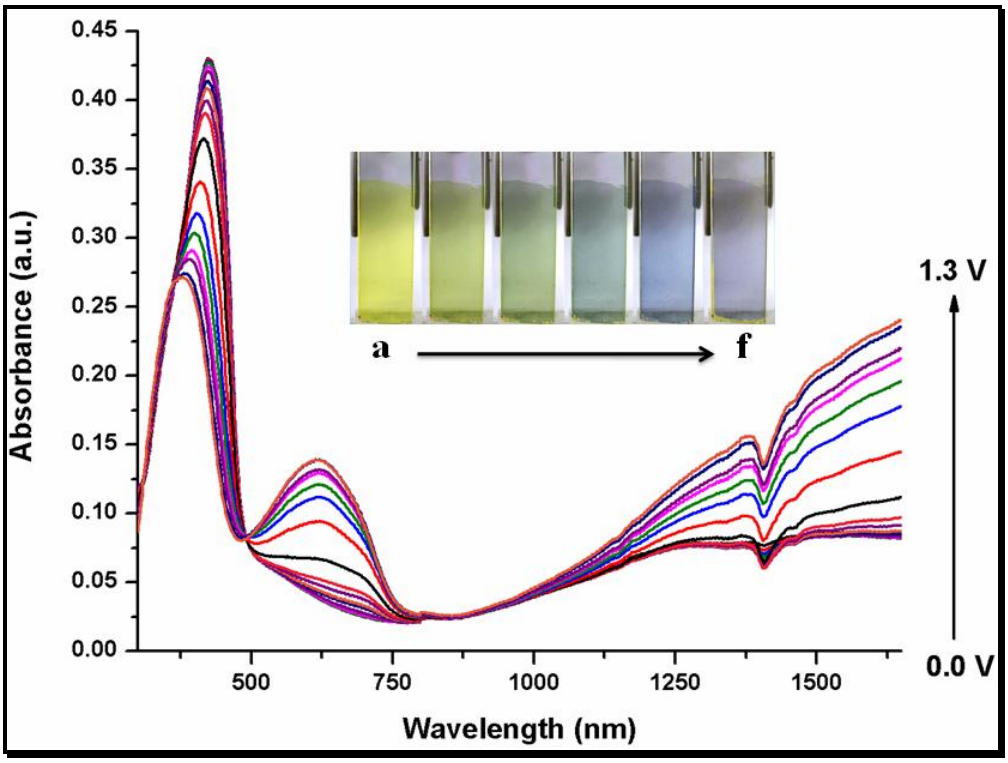


**Figure 3.11** Electrochemical p-type doping electronic absorption spectra of P1 between 0.0 and 1.3 V with 0.1 V potential intervals

P1 is yellow in its neutral form and it turns to a green reflecting state when partially oxidized, then it becomes blue when fully oxidized. At low doping states, the absorption band is centralized at 431 nm and as it diminishes two new absorption bands are observed in the visible and NIR regions with maximum values of 620 nm and 2000 nm due to the formation of charge carriers. The optical band gap of P1 was calculated from the low energy transition as 2.55 eV.

Although the oxidation potential for P1 was determined as 1.43 V, spectroelectrochemical data were recorded up to 1.3 V since at higher potentials no spectral change was observed. Electron poor P1 revealed blue shifted dominant wavelengths both in visible and in NIR regions which were consistent with electrochemical data. Moreover, due to its electron deficient nature the neutral state absorption in the visible region (430 nm) did not reveal a significant depletion but hypsochromically shifted to 380 nm. This indicates the limited formation of polaronic and bipolaronic bands for P1.

### 3.2.3 Kinetic Studies

The electrochemical stability as well as percent transmittance changes can be monitored by successive potential cycling of the polymer films in monomer-free solutions. Optical studies were carried out for P1 in ACN/TBAPF$_6$ solution in order to observe the changes between its neutral and fully oxidized states upon applied external bias. During the experiment, percent transmittance changes were recorded at corresponding wavelengths by means of a UV-vis-NIR spectrophotometer in the potential range of  0 .0 V and +1.3 V within 5 s time intervals (Figure 3.12).

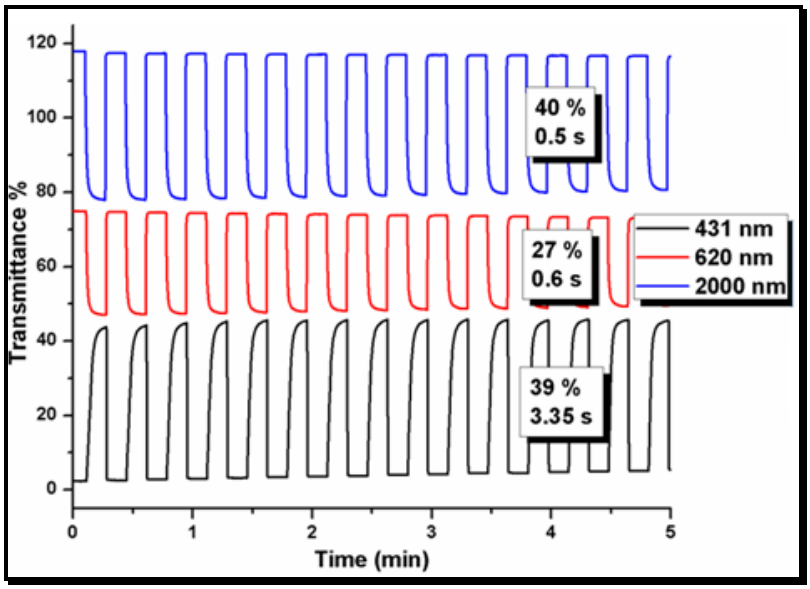


**Figure 3.12** Kinetic switching results in both visible and NIR regions for P1

P1 revealed 39 % optical contrast between its neutral and oxidized states at 431 nm with a switching time of 3.3 s. In NIR region, polymer film showed 40 % transmittance change within 0.6 s which allows the P1 to be used in NIR applications. Since P1 revealed a blue shift for high energy transition upon oxidation, it showed relatively high optical contrast for the one observed at 431 nm.

## 3.3Poly((9,9-dioctylfluorene)-2,7-diyl-(4,7-bis(thien-2-yl)2-dodecyl benzo[1,2,3]triazole)) (P2)

### 3.3.1 Cyclic Voltammetry (CV)

In order to study the redox behavior of P2, polymer was dissolved in chloroform to a concentration of 5 mg/mL and spray coated on indium tin oxide (ITO) coated glass slide. The polymer film on ITO was subjected to cyclic voltammetry (CV) in

ambient conditions to determine the redox potentials in 0.1 M $TBAPF_6$/ ACN solution at a scan rate of 50 mV/s. Initially, polymer film was subjected to a repeated cycling to obtain electrochemically stable and reproducible doping–dedoping. Afterward, potentials were swept between 1.4 and -2.3 V versus Ag wire pseudo-reference electrode (50 mV versus $Fc/Fc^+$). (Figure 3.13).

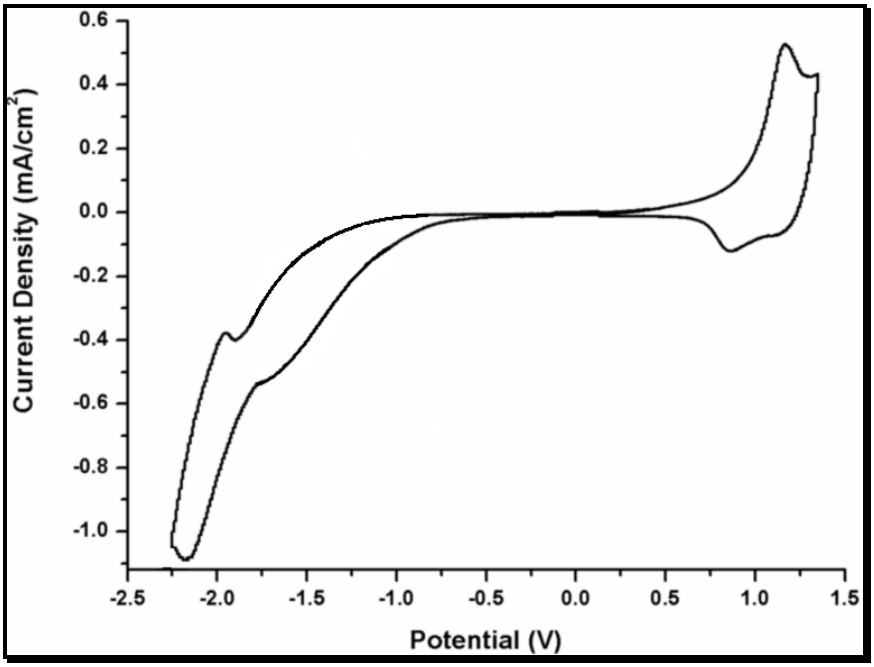


**Figure 3.13** Cyclic voltammogram for spray coated polymer film of P2 in ACN/$TBAPF_6$ solution at a scan rate of 50 mV/s

Due to incorporation of electron donating thiophene rings in P2 chains, polymer film showed lower redox potentials as 1.16 and 0.96 V compared to those of P1 versus the same reference electrode. P2 also has n doping property with a reduction peak at -2.16 V and de-doping value of -1.60 V. Table 2 summarizes the electrochemical data for polymer P2.

**Table2** Oxidation potentials and onset values for both p- and n-type doping, estimated HOMO–LUMO energies and band gaps of synthesized polymers P2

| **P2** | Oxidation Potential (V) | | Reduction Potential (V) | | Bandgap (eV) | | Energy Level (eV) (from CV) | |
|---|---|---|---|---|---|---|---|---|
| | $E_{ox}$ | $E_{ox\ onset}$ | $E_{red}$ | $E_{red\ onset}$ | $E_g^{ec}$ | $E_g^{op}$ | HOMO | LUMO |
| | 1.16 | 0.96 | -2.16 | - 1.60 | 2.56 | 2.16 | -5.71 | -3.15 |

### 3.3.2 Spectroelectrochemistry

The changes in the absorption band of P2 upon stepwise increased potential were investigated by UV-vis spectroscopy in a monomer free solution containing ACN with 0.1 M TBAPF6. The neutral P2 film shows an absorption maximum in the visible region at 574 nm resulting in an optical band gap of 2.16 eV (calculated from the onset of the π-π* transition for the neutral form). Since neutral state absorption for P2 is centralized at around 400 nm and lower energy transition emerged at 700 nm, partially oxidized polymer film revealed green color for which these two absorption maxima are crucial. Further oxidation of polymer films resulted in blue color due to diminishing π-π*transition intensity (Figure 3.14).

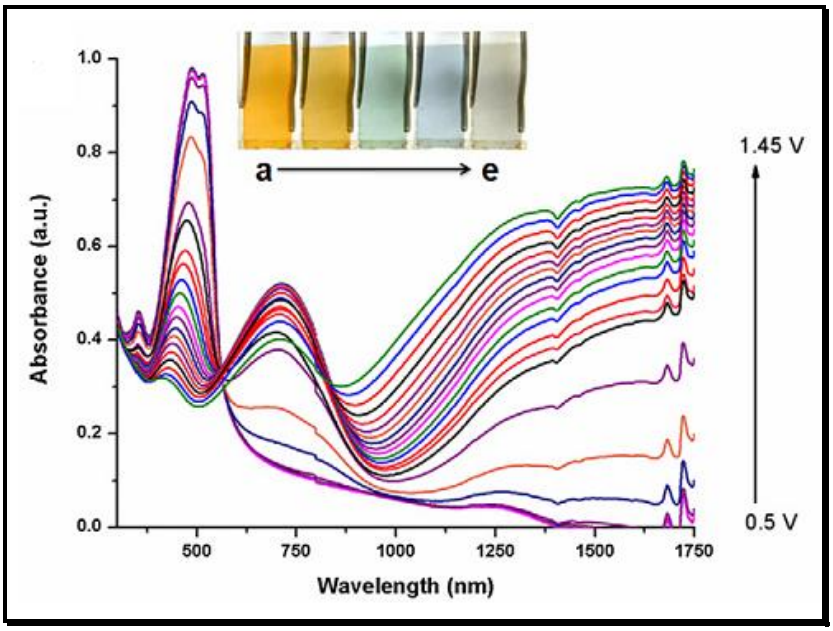


**Figure 3.14** Electrochemical p-type doping electronic absorption spectra of P2 between 0.5 and 1.45 V with 0.1 V potential intervals

In order to have a better understanding on structure–electronic properties relationship, P2 was compared to previously reported parent polymers PFO and PTBT, in terms of its HOMO/LUMO energy levels (Figure 3.15). π-π* interaction between donor and acceptor determines the match between these units and plays a crucial role on the electronic properties of the resulting polymers since it influences the intramolecular charge transfer in these types of polymers [75]. Figure 3.15 shows that the addition of fluorene unit in PTBT did not significantly alter the electronic band gap of the resulting polymer P2 (2.56 eV), but only lowered the HOMO–LUMO levels ca. 0.1 eV.

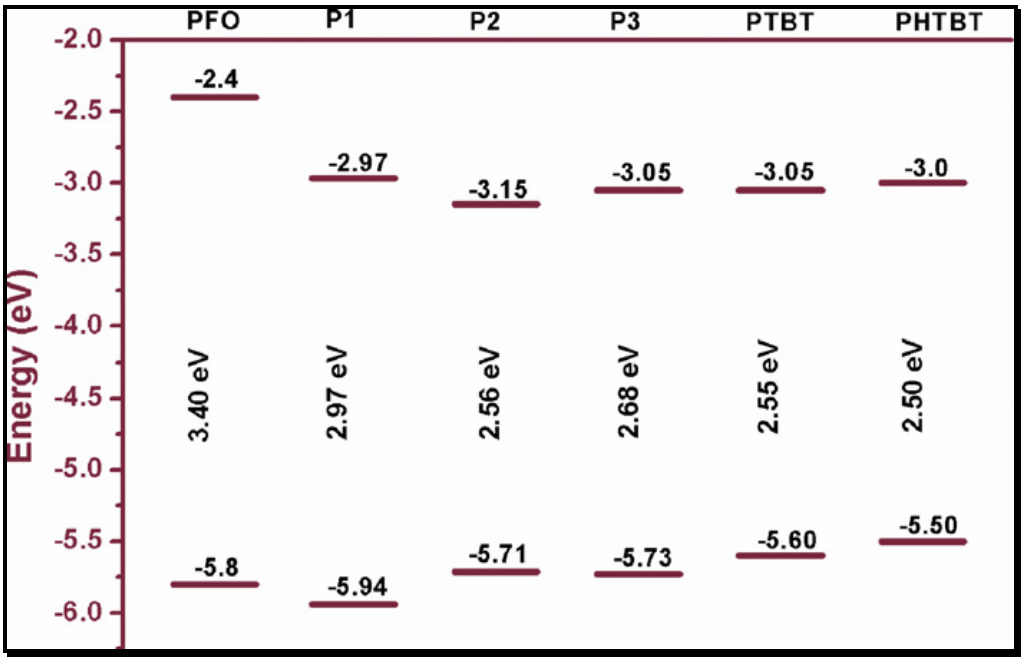


**Figure 3.15** HOMO/LUMO levels and band gaps of related polymers [76]

### 3.3.3 Kinetic Studies

Kinetic studies were conducted in order to determine switching times and percent transmittance changes (ΔT %) of the P2 between its neutral and oxidized states. During the experiment, percent transmittance changes were recorded at corresponding wavelengths by means of a UV-vis-NIR spectrophotometer within 5 s time intervals (Figure 3.12). P2 revealed 22 % transmittance in the visible region at 485 nm. In the near-IR region the optical contrast for the polymer film was found to be 45% which is considerably sufficient for near-IR applications (Figure 3.16).

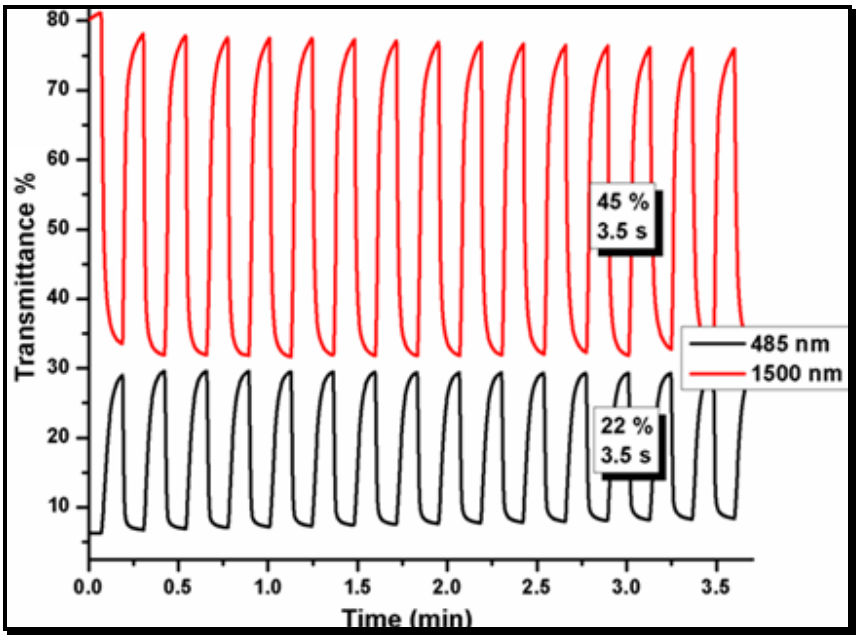


**Figure 3.16** Kinetic switching results in both visible and NIR regions for P2

## 3.4 Poly((9,9-dioctylfluorene)-2,7-diyl-(4,7-bis(3-hexylthien-5-yl) 2-dodecyl-benzo[1,2,3]triazole)) (P3)

### 3.4.1 Cyclic Voltammetry (CV)

In order to investigate the redox properties of P3, same experimental methods and environment as in the case of electrochemical studies of P1and P2 were used. The potential was swept between 1.4 V and -2.1 V for P3. Due to incorporation of electron donating hexylthiophene rings in P3 chains, polymer film showed lower redox potentials as 1.25 and 0.98 V compared to those of P1 versus the same reference electrode. As the CV indicates the polymer is both p and n dopable with a

reduction peak at -2.16 V and de-doping value of -1.60 V. Table 3 summarizes the electrochemical data for polymer P3.

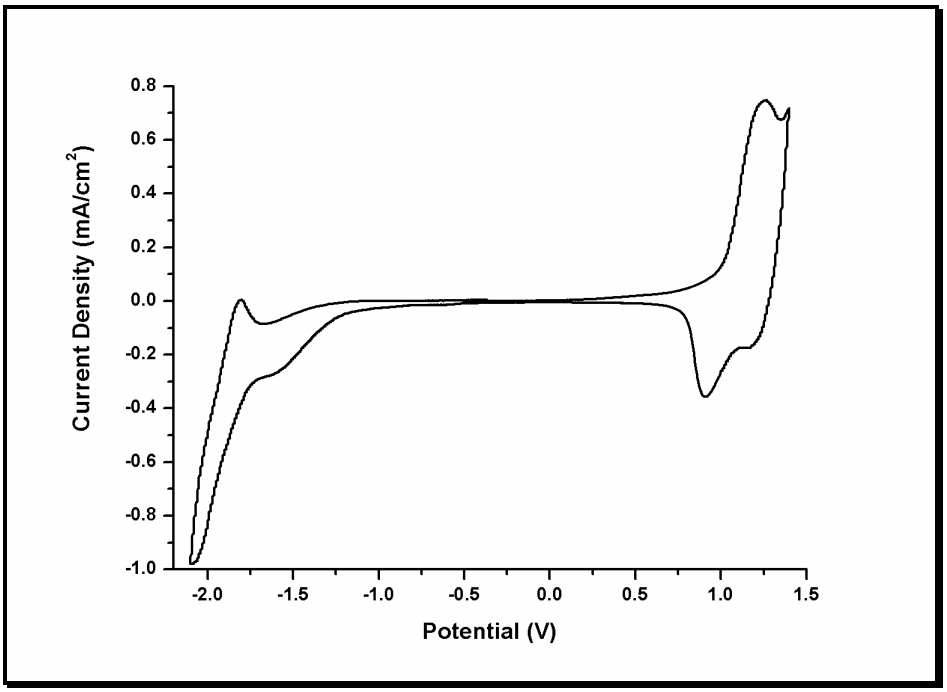


**Figure 3.17** Cyclic voltammogram for spray coated polymer film of P3 in ACN/TBAPF6 solution at a scan rate of 50 mV/s

**Table 3** Oxidation potentials and onset values for both p- and n-type doping, estimated HOMO–LUMO energies and band gaps of synthesized polymers P3

| **P3** | Oxidation Potential (V) | | Reduction Potential (V) | | Bandgap (eV) | | Energy Level (eV) (from CV) | |
|---|---|---|---|---|---|---|---|---|
| | $E_{ox}$ | $E_{ox\ onset}$ | $E_{red}$ | $E_{red\ onset}$ | $E_g^{ec}$ | $E_g^{op}$ | HOMO | LUMO |
| | 1.25 | 0.98 | -2.10 | -1.70 | 2.68 | 2.24 | -5.73 | -3.05 |

### 3.4.2 Spectroelectrochemistry

Spectroelectrochemistry experiments were performed in the monomer free, 0.1 M $TBAPF_6$, ACN solution to monitor the optical changes upon doping and dedoping processes. UV–Vis-NIR spectra were obtained as a function of applied potential between 0.5 V and 1.3 V. The spectral responses of polymer films to stepwise oxidation were recorded as the potential was slowly increased. As Figure 3.18 indicates P3 has absorption wavelengths in the visible region which were centered at 460 and 715 nm. Optical band gap ($E_g$) for **P3** was calculated from the onsets of lower energy transition as 2.24 eV.

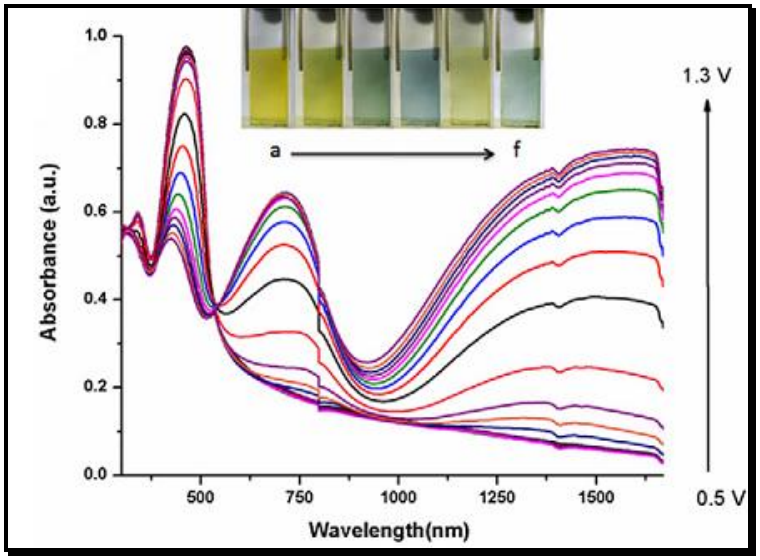


**Figure 3.18** Electrochemical p-type doping electronic absorption spectra of P2 between 0.5 and 1.3 V with 0.1 V potential intervals

With the stepwise oxidation of polymer film, as the visible region absorption diminished, new absorption bands centered as 715 nm and 1560 nm were formed.

These lower energy transitions exhibit the formation of charge carriers such as polarons and bipolarons.

Substitution of 9,9'-dioctyl fluorene units resulted in a blue shifted absorption for P3 compared to its previously studied parent polymer PHTBT [62]. Considering the energy levels of P3, LUMO level was intact upon addition of PFO, however; HOMO of the polymer was lowered due to the contribution of valence band of PFO and resulted in a higher electrochemical band gap. Although PHTBT has slightly lower band gap than PTBT, thiophene containing polymer P2 revealed narrower band gap than that of its hexylthiophene included analogue P3.This may be due to the steric interactions between the hexylgroups and the adjacent fluorene units. The same trend also is the case for benzothiadiazole bearing copolymers [68].

### 3.4.3 Kinetic Studies

Due to the high rigidity in P3 films which stems from the long alkyl chains on both fluorene, thiophene and benzotriazole units, reasonable kinetic values could not be acquired.

## 3.5 Thermal Properties (DSC) & (TGA)

The thermal properties of the polymers were examined by DSC and TGA under nitrogen atmosphere at a heating rate of 10 $^{o}$C/minute. The polymers showed excellent thermal stability indicating $\leq$ 5% weight loss on heating to approximately 400 $^{o}$C. DSC did not show any transition temperatures like glass transition temperature, which may stem from the rigid structure of the polymers. Moreover, the lack of melting transition can be an indication of amorphous structure. The thermal stability of the polymers is significant in terms of their applications in OSCs and other optoelectronic devices.

### 3.6 Photovoltaic Studies

#### 3.6.1 Optical Properties

The photophysical properties of the copolymers were examined via UV-vis absorption spectra. Figure 3.19 shows the UV-vis spectra for polymers P1, P2 and P3 in dilute chloroform solutions and in solid films drop cast on a quartz substrate separately. The $\lambda_{max}$ peaks originate from the internal charge transfer interaction between the electron donor fluorene and electron accepting benzotriazole unit.

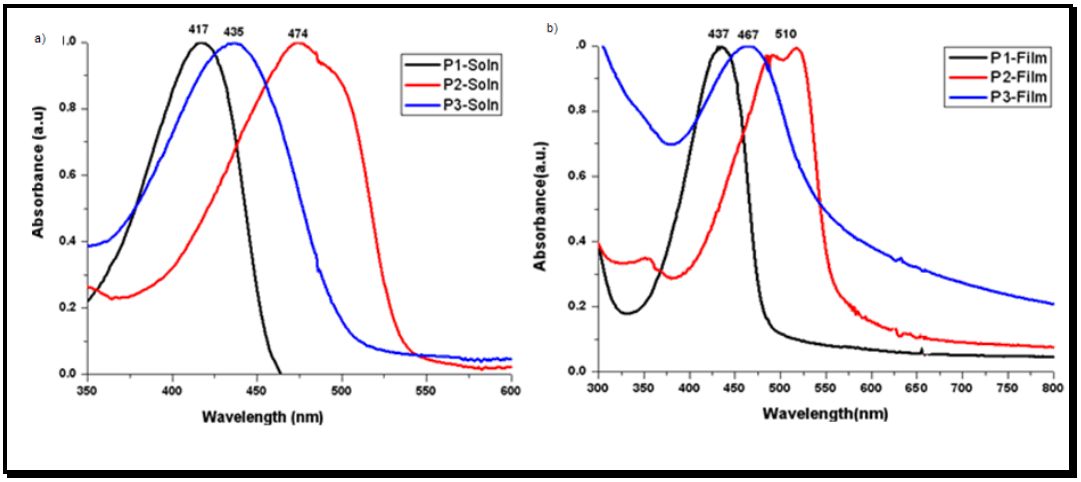


**Figure 3.19** Normalized absorption spectra of P1, P2, P3 in chloroform solution (a) and in thin film (b)

Thin film absorption spectra of the polymers indicate similar properties to that in dilute solution. There is a red shift of *ca.* 20 nm for P1, *ca.* 32 nm for P2 and *ca.* 36 nm for P3. Red shift in the thin film shows the formation of π stacking that can ease harvesting of sunlight for solar cell applications [77].

### 3.6.2 Photoluminescence Studies

The emission spectrum of the three polymers in chloroform solutions is shown in Figure 3.20. Strong emissions in the visible range suggest that the polymers can be applied to OLEDs. P1 emits blue light with a $\lambda_{max}$ of 467 nm. P2 and P3 emit green color with $\lambda_{max}$ values of 518 and 530 nm respectively.

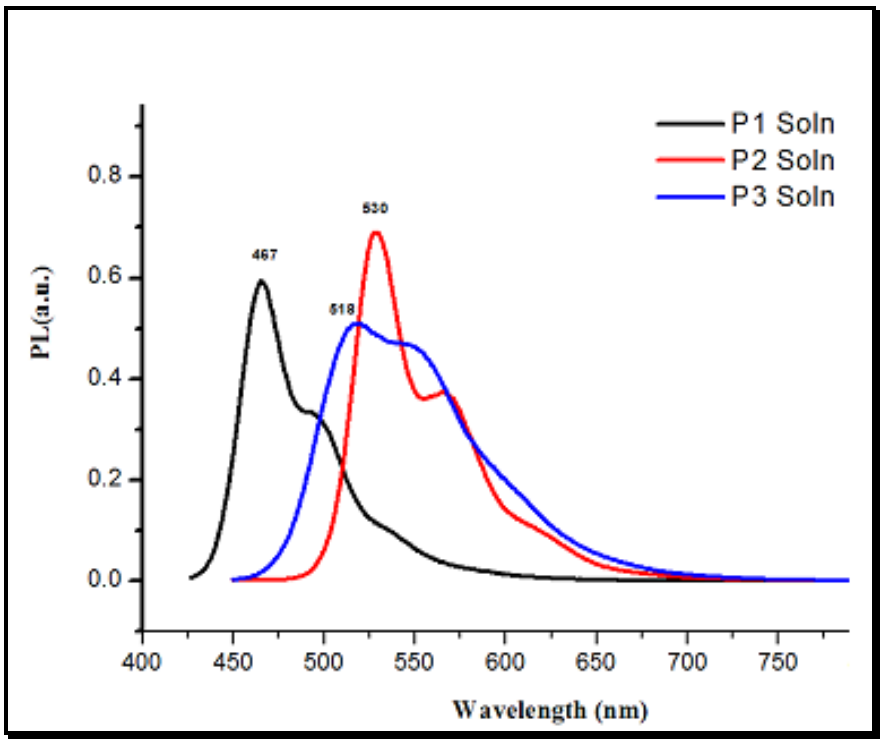


**Figure 3.20** Optical emission spectrum of the targeted polymers in chloroform solutions

### 3.6.3 Photovoltaic properties

The positions of the HOMO and LUMO of the polymers are the basic parameters for the device performance as they qualify the driving force for charge separation and Voc [78]. All three polymers satisfy the HOMO-LUMO energy requirement for OSC device fabrication. These values can be found in Figure 3.15. The high LUMO levels of the polymers enable charge transfer in the resulting devices utilizing $PC_{61}BM$ as the acceptor.

Photovoltaic properties of these polymers were examined in devices with the structure of ITO/PEDOT:PSS active layer/LiF/Al. The active layer contains a blend of P1, P2 or P3 donor and PC61BM acceptor. As solvent, chlorobenzene was used for P1 and P2, chloroform used for P3 for the device fabrication. The ratio of donor to acceptor and the thickness were optimized. Optimum performance was achieved with a ratio of polymer to PC61BM of 1:1 (w/w) for P1 and P2 and 1:2 (w/w) for P3 and active layer thickness in the range of 70 nm to 90 nm. Figure 3.21 displays the current-density voltage characteristics of the devices and corresponding short-circuit current densities (Jsc), open-circuit voltages (Voc), fill factors (FF) and power conversion efficiencies (PCE). At 1:1 weight ratio of P1/$PC_{61}BM$ as active layer, device gave a Voc value of 0.6 V, FF of 28 % and a Jsc value of 0.46 $mA/cm^2$, giving rise to a power conversion efficiency of 0.074 %.

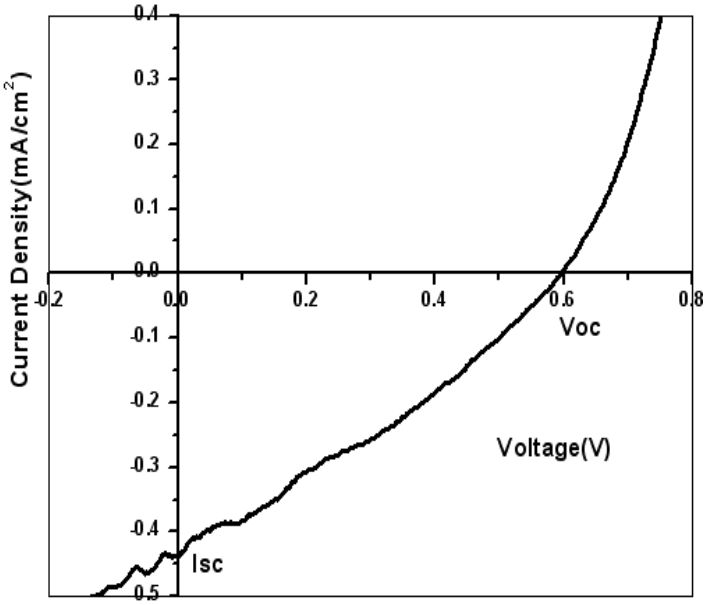


**Figure 3.21** Current density-voltage (*J-V*) characteristics of the P1/PCBM blends of 1:1 under white light illumination (AM 1.5 G conditions)

1:2 weight ratio of P1/$PC_{61}BM$ as active layer was also investigated leading to Voc value of 0.4 V, FF of 23 % and a Jsc value of 0.5 mA/cm$^2$. The low FF values of the devices might be analyzed based on their poor surface morphology.

The devices with 1:1 weight ratio P2/$PC_{61}BM$ as active layer showed a Voc value of 0.6 V, FF of 28 % and a Jsc value of 3.4 mA/cm$^2$, resulted in a power conversion efficiency of 0.56 %. Figure 3.22 shows the I-V characteristics of the device.

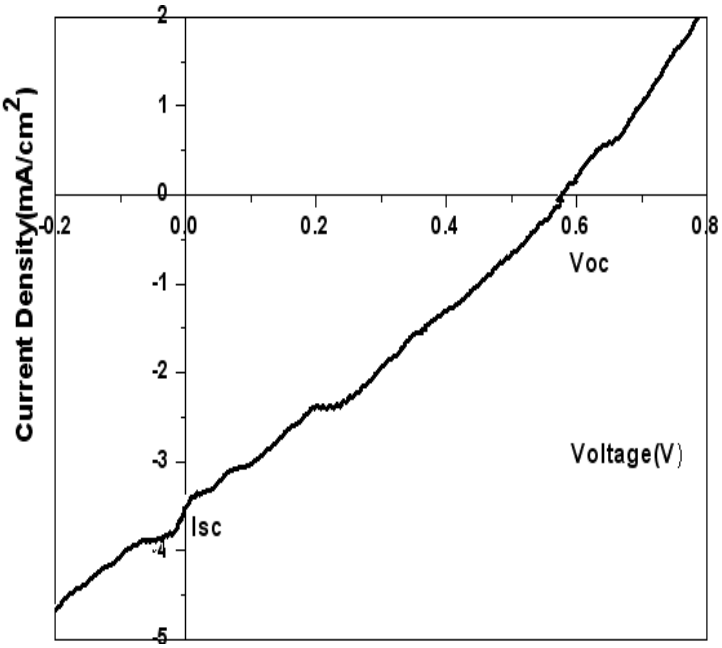


**Figure 3.22** Current density-voltage (*J-V*) characteristics of the P2/PCBM blends of 1:1 under white light illumination (AM 1.5 G conditions)

The devices with 1:2 weight ratios of P2/$PC_{61}$BM as active layer showed a Voc value of 0.66 V, FF of 38 % and a Jsc value of 1.8 mA/$cm^2$. The reduced Jsc value of 1:2 weight ratio polymer: PCBM based devices probably stems from the increased aggregation of PCBM which cause a reduced interfacial area between donor and acceptor phases preventing efficient free charge formation [79].

The devices with 1:2 weight ratio P3/$PC_{61}$BM as active layer showed a Voc value of 0.71 V, FF of 19% and a Jsc value of 0.79 mA/$cm^2$, resulted in a power conversion efficiency of 0.11%. Figure 3.22 shows the I-V characteristics of the device and photovoltaic data are summarized in Table 4.

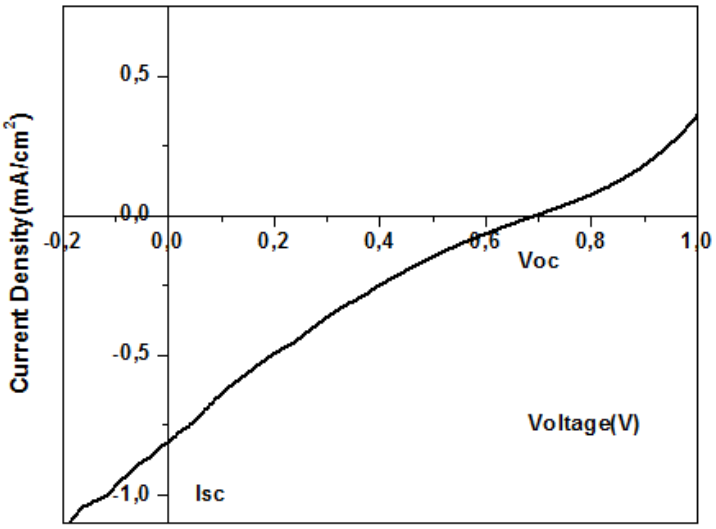


**Figure 3.23** Current density-voltage (*J-V*) characteristics of the P3/PCBM blends of 1:2 under white light illumination (AM 1.5 G conditions)

**Table 4** Photovoltaic performance of the solar cells based on P1:PCBM, P2:PCBM and P3:PCBM

| **Polymer** | **Active layer ratio (Px:PCBM)** | **$V_{oc}$ (V)** | **$J_{sc}$ (mA/cm2)** | **FF** | **PCE (%)** |
|---|---|---|---|---|---|
| **P1** | 1:1 | 0.6 | 0.46 | 0.28 | 0.074 |
| | 1:2 | 0.4 | 0.5 | 0.23 | 0.046 |
| **P2** | 1:1 | 0.6 | 3.4 | 0.28 | 0.56 |
| | 1:2 | 0.66 | 1.8 | 0.38 | 0.42 |
| | 1:3 | 0.65 | 1.75 | 0.28 | 0.32 |
| **P3** | 1:1 | 0.56 | 0.17 | 0.22 | 0.02 |
| | 1:2 | 0.71 | 0.79 | 0.19 | 0.11 |

The better performance of the P2 (PFTBT) can be based on its lower band gap compare to other polymers. Lower band gap means broad absorption of the photon flux and this leads to higher Jsc values. Although P2 and P3 have close Voc values due to their almost same HOMO energy levels, higher efficiency of P2 can be also attributed to higher hole mobility. Since P3 has hexyl groups on its backbone, a steric effect between the adjacent monomer units can arise resulting in a decrease in planar conformation and decreased hole mobility. Further optimizations of the devices such as using solvent additives for achieving better morphologies can lead to better efficiencies.

# CHAPTER 4

# CONCLUSION

Three novel donor-acceptor type alternating conjugated copolymers poly((9,9-dioctylfluorene)-2,7-diyl-(2-dodecyl-benzo[1,2,3]triazole)) (P1), poly((9,9-dioctylfluorene)- 2,7-diyl-(4,7-bis(thien-2-yl) 2-dodecyl-benzo[1,2,3]triazole)) (P2), poly((9,9-dioctylfluorene)-2,7-diyl-(4,7-bis(3-hexylthien-5-yl) 2-dodecyl benzo[1,2,3]triazole)) (P3) were synthesized chemically via Suzuki polycondensation. Structural characterizations of the polymers were carried out by NMR analysis. Cyclic voltammetry experiments, spectroelectrochemistry and kinetic studies for the polymers were conducted in order to explore the electrochemical and electrochromic properties of the copolymers as well as their photovoltaic characterizations.

All three polymers have multicolored electrochromic states, convenient HOMO and LUMO levels, band gaps, and strong absorptions in the visible region and excellent thermal stability in order to be applicable to different optoelectronic studies such as OSCs and OLEDs. Furthermore, the stable kinetic results and multicolored electronic states of P1 and P2 suggest that they can be good candidates for ECD applications.

OSC device fabrications of P1, P2 and P3 were carried out with a device configuration of ITO/PEDOT: PSS/active layer/LiF/Al. Polymers were used as donor materials and $PC_{61}BM$ as acceptor. Polymer:PCBM weight ratios for each polymer and active layer thickness were optimized. Highest efficiency was achieved with P2 as 0.56 % due to its more planar structure and lower band gap.

Optimizations of structures, molecular weights and morphologies of active layer for achieving improved charge carrier mobility might result in higher power conversion efficiencies.

## REFERENCES


[1] G. Inzelt, Conducting Polymers (A New Era in Electrochemistry), **2008**, Berlin Heidelberg, p1.

[2] H. Shirakawa, E. J. Louis, A. G. MacDiarmid, C. K. Chiang, A. J. Heeger, *J. Chem. Soc. Chem. Commun*., **1977**, 578.

[3] H. Shirakawa (Angew Chem Int Ed., **2001**, 40, 257.

[4] F. Jonas, L. Schrader, *Synth.Met.,* **1991,** 41, 831.

[5] a) J. Rault-Berthelot, J. Simonet, *J. Electrochem. Soc.,* **1985,** 182, 187. b) A. G. MacDiarmid, A.J. Epstein, *Farad. Discuss. Chem. Soc.,* **1989,** 88, 317.

[6] A. F. Diaz, J. I. Castillo, J. A. Logan, W. Lee, *J. Electroanal. Chem.*, **1981**, 129, 115.

[7] J. Roncali, *Chem. Rev.*, **1997**, 97, 173.

[8] J. l. Reddinger, J. R. Reynolds, *Advances in Polymer Science*, **1999**, 45, 59.

[9] a) M. J. Rice, *Phys. Lett.,* **1979**, A71, 152. b)W. P. Su, J. R. Schrieffer, A. J. Heeger, *Phys. Rev. Lett.,* **1979**, 42, 1698.

[10] a) X. Li, Y. Jlao, S. Li, *Eur. Polym. J.*,**1991**, 27, 1345.

b) K. Pichler, D. A. Halliday, D. D. C. Bradley, P. L. Burn, R. H. Friend, A. B. Holmes, *J. Phys. Condens. Matter.,* **1993**, 5, 7155.

[11] a) J. L. Bredas, R. R. Chance, R. Silbey, *Phys. Rev. B.,* **1982**, 26, 5843.

b) J. L. Bredas, G. B. Street, *Acc. Chem. Res.,* **1985**, 18, 309.

[12] J.L. Bredas, G. B. Street, *Acc. Chem. Res*., **1985**, 18, 309.

[13] P. Chandrasekhar, Conducting Polymers Fundamentals and Applications, Boston, Kluwer Academic Publishers, (1999) Ch. 2

[14] A. G. MacDiarmid, A. J. Heeger, *Synth.Met.*, **1979**, 1, 101.

[15] A. D. Child, J. R. Reynolds, *Chem. Commun.,* **1991,** 1779.

[16] D. M. de Leeuw, M. M. J. Simenon, A. R. Brown, R. E. F. Einerhand, *Synth. Met.*, **1997**, 87, 53.

[17] K. Gurunathan, A.V. Murugan, R. Marimuthu, U.P. Mulik, D.P. Amalnerkar, *Mater. Chem. Phys.*, **1999**, 61, 173.

[18] C. J. DuBois, F. Larmat, D. J. Irvin, J. R. Reynolds, *Synth. Met.*, **2001**, 119, 321.

[19] C. J. DuBois, K. A. Abboud, J. R. Reynolds, *J. Phys. Chem. B.*, **2004,** 108, 8550.

[20] D. M. de Leeuw, M. M. J. Simenon, A. R. Brown, R. E. F. Einerhand, *Synth. Met*., **1997**, 87, 53.

[21] A. J. Heeger, *Chem. Soc. Rev.*, **2010**, 39, 2354.

[22] P. M. Beaujuge, S. Ellinger J. R. Reynolds, *Adv. Mater*., **2008**, 20, 2772.

[23] a) G. Sonmez, H.B. Sonmez, C.K.F. Shen, R.W. Jost, Y. Rubin, F. Wudl, *Macromolecules,* **2005**, 38, 669. b) M.A. Invernale, Y. Ding, D.M.D. Mamangun, G.A. Yavuz, Sotzing *Adv. Mater.*, **2010**, 22, 1379. c) P.M. Beaujuge, S.V. Vasilyeva, S. Ellinger, T.D. McCarley, J.R. Reynolds, *Macromolecules,* **2009**, 42, 3694. d) A. Durmus, G.E. Gunbas, P. Camurlu, L. Toppare, *Chem. Commun.*, **2007**, 3246. e) G.E. Gunbas, A. Durmus, L. Toppare, *Adv. Mater.*, **2008**, 20, 691.

[24] a) A.C. Grimsdale, K.L. Chan, R.E. Martin, P.G. Jokisz, A.B. Holmes, *Chem. Rev.*, **2009**, 109, 897. b) H. Tsuji, C. Mitsui, Y. Sato, E. Nakamura, *Adv. Mater*., **2009**, 21, 3776. c) K.T. Kamtekar, H.L. Vaughan, B.P. Lyons, A.P. Monkman, S.U. Pandya, M.R. Bryce, *Macromolecules*, **2010**, 43, 4481.

[25] a) S. Gunes, H. Neugebauer, N.S. Sariciftci, *Chem. Rev.*, **2007**, 107, 1324. b) J.C. Bijleveld, A.P. Zoombelt, S.G.J. Mathijssen, M.M. Wienk, M.Turbiez, D.M. Leeuw, R.A.J. Janssen, *J. Am. Chem.Soc.*, **2009**, 131, 16616. c) S.H. Park, A. Roy, S. Beaupre, S. Cho, N. Coates, J.S.M.D. Moses, M. Leclerc, K. Lee, A.J. Heeger, *Nat. Photon.*, **2009**, 3, 297.

[26] a) S. Allard, M. Forster, B. Souharce, H. Thiem, U. Scherf, *Angew. Chem. Int. Ed*., **2008**, 47, 4070. b) L.L. Chua, J. Zaumseil, J.F. Chang, E.C.W. Ou, P.K.H. Ho, H. Sirringhaus, R.H. Friend, *Nature,* 2005, 434, 194.

[27] A. Cirpan, A. A. Argun, C. R. G. Grenier, B. D. Reeves, J. R. Reynolds, *J. Mater. Chem.*, **2003**,13, 2422.

[28] R. J. Mortimer, *Electrochimica Acta*, **1999**, 44, 2971.

[29]A. L. Dyer, M. R. Craig, J. E. Babiarz, K. Kiyak, J. R. Reynolds, *Macromolecules*, **2010**, 43, 4460.

[30] a) A. A. Argun, P. H. Aubert, B. C. Thompson, I. Schwendeman, C. L. Gaupp, J. Hwang, N. J. Pinto, D. B. Tanner, A. G. MacDiarmid, J. R. Reynolds, *Chem. Mater.*, **2004**, 16, 4401. b) G. A. Sotzing, J. L. Reddinger, A. R. Katritzky, J. Soloducho, R. Musgrave, J. R. Reynolds, *Chem. Mater.*, **1997**, 9, 1578. c) S. Beaupre, J. Dumas, M. Leclerc, *Chem. Mater.*, **2006**, 18, 4011. d) A. Balan, G. Gunbas, A. Durmus, L. Toppare, *Chem. Mater.*, **2008**, 20, 7510. e) S.-H. Hsiao, G.-S. Liou, Y.C. Kung, H. J. Yen, *Macromolecules*, **2008**, 41, 2800.

[31] S. Beaupre, P.L. T. Boudreault, M. Leclerc, *Adv. Mater.*, **2010**, 22 , E6.

[32] A. F. B. Braga, S. P. Moreira, P. R. Zampieri, J. M. G. Bacchin, P. R. Mei, *Sol. Energy Mater. Sol. Cells*, **2008**, 92, 418.

[33] M. Helgesen, R. Søndergaard, F. C. Krebs, *J. Mater. Chem.*, **2010**, 20, 36.

[34] J. Chen , Y. Cao, *Acc. Chem. Res.*, **2009**, 42, 1709.

[35] C. Li, M. Liu, N. G. Pschirer, M. Baumgarten, K. Mullen *Chem. Rev.*, **2010**, 110, 6817.

[36] A. K. Ghosh, T. Feng, *J. Appl.Phys.*, **1973**, 44, 2781.

[37] C.W. Tang, *Appl.Phys.Lett.*, **1986**, 48, 183.

[38] a)B. C. Thompson, J. M. J. Frechet, *Angew. Chem, Int. Ed.*, **2008**, 47, 58. b) G. Dennler, M. C. Scharber, C. J. Brabec, *Adv. Mater.*, **2009**, 21, 1323. c) R. A. J. Janssen, J. C. Hummelen, N. S. Sariciftci, *MRS Bull.*, **2005**, 30, 33.

[39] a) S. H. Park, A. Roy, S. Beaupré, S. Cho, N. Coates, S.Moon, D. Moses, M. Leclerc, K. Lee, A. J. Heeger, *Nat. Photon.*, **2009**, 3, 297. b) A. Green, K. Emery, Y. Hishikawa, W. Warta, *Prog. Photovolt: Res. Appl.*, **2010**, 18, 346. c) http://www.solarmer.com (accessed May 2010). d) http://www.heliatek.com. (accessed May 2010)

[40] B. C. Thompson, J. M. J. Frechet, *Angew. Chem. Int. Ed.*, **2008**, 47, 58.

[41] Q. Zheng, B. J. Jung, J. Sun, H. E. Katz, *J. Am. Chem. Soc.*, **2010**, 132, 5394.

[42] C. Soci, I.W. Hwang, D. Moses, Z. Zhu, D. Waller, R. Guadiana, C. J. Brabec, A. J. Heeger, *Adv. Funct. Mater*., **2007**,17, 632.

[43] L. J. A. Koster, V. D. Mihailetchi, P.W. M. Blom, *Appl. Phys. Lett*., **2006**, 88, 093511.

[44] Z. E. Ooi, T.L. Tam, R.Y. C. Shin, Z. K. Chen,T. Kietzke, A. Sellinger, M. Baumgarten, K. Muellen, J. C. deMello, *J. Mater. Chem*., **2008**, 18, 4619.

[45] D. Gedefaw, Y. Zhou, S. Hellström, L. Lindgren, L. M. Andersson, F. Zhang, W. Mammo, O. Inganas, M. R. Andersson, *J. Mater. Chem*., **2009**, 19, 5359.

[46] Y. H. Kim, C. Sachse, M. L. Machala, C. May, L. M. Meskamp, K. Leo, *Adv. Funct. Mater*., **2011**, 21, 1076.

[47] C. J. Brabec, S. E. Shaheen, C. Winder, N. S. Sariciftci, P. Denk, *Appl. Phys. Lett*., **2002**, 80, 1288.

[48] a) J. Roncali, *Chem. Rev*., **1992**, 92, 711. b) ‘‘Handbook of Oligo- and Polythiophene’’, D. Fichou, Ed.,Wiley-VCH, Weinheim **1999**.

[49] J. Roncali, *Macromol. Rapid Commun*., **2007**, 28, 1761.

[50] a) A. V. Patil, W. H. Lee, E. Lee, K. Kim, I. N. Kang, S. H. Lee, *Macromolecules*, **2011**, 44, 1238. b) T. Yamamoto, Z.H. Zhou, T. Kanbara, M. Shimura, K. Kizu, T. Maruyama, Y. Nakamura, T. Fukuda, B.L. Lee, N. Ooba, S. Tomaru, T. Kurihara, T. Kaino, K. Kubota, S. Sasaki, *J. Am. Chem. Soc*., **1996**, 118, 10389. c) S. Akoudad, J. Roncali, Chem. Commun., **1998**, 2081. d) X. Zhang, S.A. Jenekhe, *Macromolecules*., **2000**, 33, 2069.

[51] P.M. Beaujuge, J.R. Reynolds, *Chem. Rev*., **2010**, 110, 268.

[52] F.C. Krebs, *Nat. Mater.*, **2008**, 7, 766.

[53] N. Miyaura, A. Suzuki, *Chem. Rev*., **1995**, 95, 2457.

[54] M. Inbasekaran, E. Woo, W. Wu, M. Bernius, L. Wujkowski, *Synth. Met*., **2000**, 111–112, 397.

[55] R. Po, M. Maggini, N. Camaioni, *J. Phys. Chem*., **2010**, 114, 695.

[56] M. A. Green, K. Emery,Y. Hishikawa,W. P. Warta, *Res. Appl*., **2009**, 17, 85.

[57] S. C. Price, A. C. Stuart, L. Yang, H. Zhou,W. You, J. *Am. Chem. Soc*., **2011**, 133, 4625.

[58] a) Y. Liang, D. Feng, Y. Wu, S. T. Tsai, G. Li, C. Ray, L. Yu, J. *Am. Chem. Soc*., **2009**, 131, 7792. b) S. H. Park, A. Roy, S. Beaupre, S. Cho, N. Coates, J. S. Moon, D.Moses, M. Leclerc, K. Lee, A. J. Heeger, *Nat. Photonics*, **2009**, 3, 297.

[59] Y. Zhang, J. Zou, H. L.Yip, K. S. Chen, J. A. Davies, Y. Sun, A. K.Y. Jen, *Macromolecules*, **2011**, 44, 4752.

[60] Y. Liang, Z. Xu, J. Xia, S.T.Tsai,Y. Wu, G. Li, C. Ray, L. Yu, *Adv. Mater*., **2010**, 22, E135.

[61] A. Balan, D. Baran, L. Toppare , *Polym. Chem*., **2011**, 2, 1029.

[62] D. Baran, A. Balan, S. Celebi, B. M. Esteban, H. Neugebauer, N. S. Sariciftci, L. Toppare, *Chem. Mater*., **2010**, 22, No-9.

[63] B. Peng, A. Najari, B. Liu, P. Berrouard, D. Gendron, Y. He, K. Zhou, M. Leclerc, Y. Zou, *Macromol. Chem. Phys*., **2010**, 211, 2026.

[64] a) A. Cirpan, L. Ding, F.E. Karasz, *Polymer*, **2005**, 46, 811. b) R. Kroon, M. Lenes, J.C. Hummelen, P.W.M. Blom, B. Boer, *Polym. Rev*., **2008**, 48, 531. c) A. Cirpan, L. Ding, F.E. Karasz, *Synth. Met*., **2005**, 150, 195.

[65] C. Deibel, V. Dyakonov, *Rep. Prog. Phys*., **2010**, 73, 096401.

[66] P. M. Beaujuge, J. R. Reynolds, *Chem. Rev*., **2010**, 110, 268.

[67] a) F. Huang, L. Hou, H. Shen, J. Jiang, F. Wang, H. Zhen, Y. Cao, *J. Mater. Chem*., **2005**, 15, 2499. b) S. Ko, R. Mondal, C. Risko, J. K. Lee, S. Hong, M. D. McGehee, J. L. Bredas, Z. Bao, *Macromolecules*, **2010**, 43, 6685.

[68] W. Li, R. Qin, M. Andersson, F. Li, C. Zhang, B. Li, Z. Liu, Z. Bo, F. Zhang, *Polymer*, **2010**, 51, 3031.

[69] J. K. Lee, H. H. Fong, A. A. Zakhidov, G. E. McCluskey, P. G. Taylor, M. S. Berrios, H. D. Abruna, A. B. Holmes, G. G. Malliaras, C. K. Ober, *Macromolecules*, **2010**, 43, 1195.

[70] E. R. Kötz, H. Neff, K. J. Müller, *Electroanal. Chem*., **1986**, 215, 331.

[71] A. Balan, D. Baran, G. Gunbas, A. Durmus, F. Özyurt, L. Toppare, *Chem. Commun*., **2009**, 6768.

[72] A Balan, G. Gunbas, A. Durmus, L. Toppare, *Chem. Mater*., **2008**, 20, 7510.

[73] L. Bonoldi, A. Calabrese, A. Pellegrino, N. Perin, R. Po, S. Spera, A. Tacca, *J. Mater Sci*., **2011**, 46, 3960.

[74] C.Q. Ma, M. Fonrodona, M.C. Schikora, M.M. Wienk, R. A. J. Janssen, P. Bauerle, *Adv. Funct. Mater*., **2008**, 18, 3323.

[75] T. Yamamoto, Z.H. Zhou, T. Kanbara, M. Shimura, K. Kizu, T. Maruyama, Y. Nakamura, T. Fukuda, B.L. Lee, N. Ooba, S. Tomaru, T. Kurihara, T. Kaino, K. Kubota, S. Sasaki, *J. Am. Chem. Soc*., **1996**,118, 10389.

[76] E. Kaya, A. Balan, D. Baran, A. Cirpan, L. Toppare, *Organic Electronics*, **2011**, 12, 202.

[77] J. Pei, S. Wen, Y. Zhou, Q. Dong, Z. Liu, J. Zhang , W. Tian, *New J. Chem.*, **2011**, 35, 385.

[78] E. Wang, L. Hou, Z. Wang, Z. Ma, S. Hellstrom, W. Zhuang, F. Zhang, O. Ingan, M. R. Andersson, *Macromolecules*, **2011**, 44, 2067.

[79] J. H. Huang, Z.Y. Ho, D. Kekuda, Y. Chang, C. W. Chu, K. C. Ho, *Nanotechnology*, **2009**, 20, 025202

# APPENDIX A

## DSC AND TGA DATA

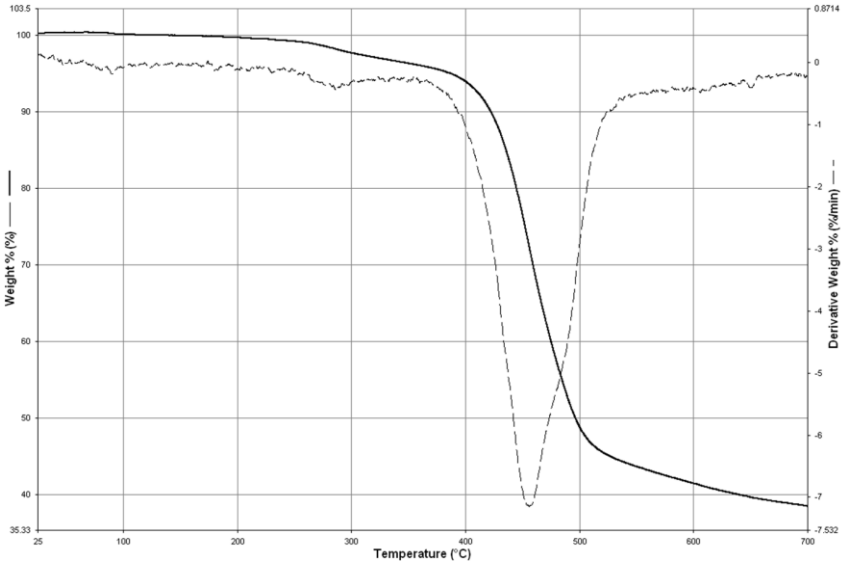


**Figure A.1** TGA result of P1

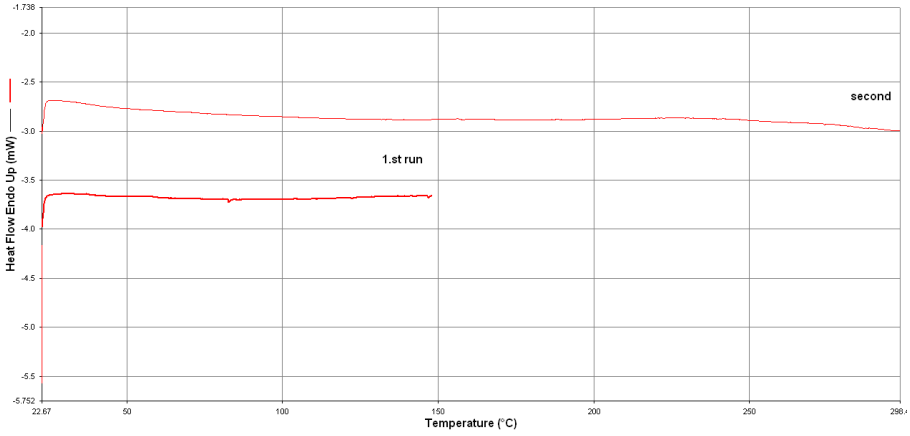


**Figure A.2** DSC result of P1

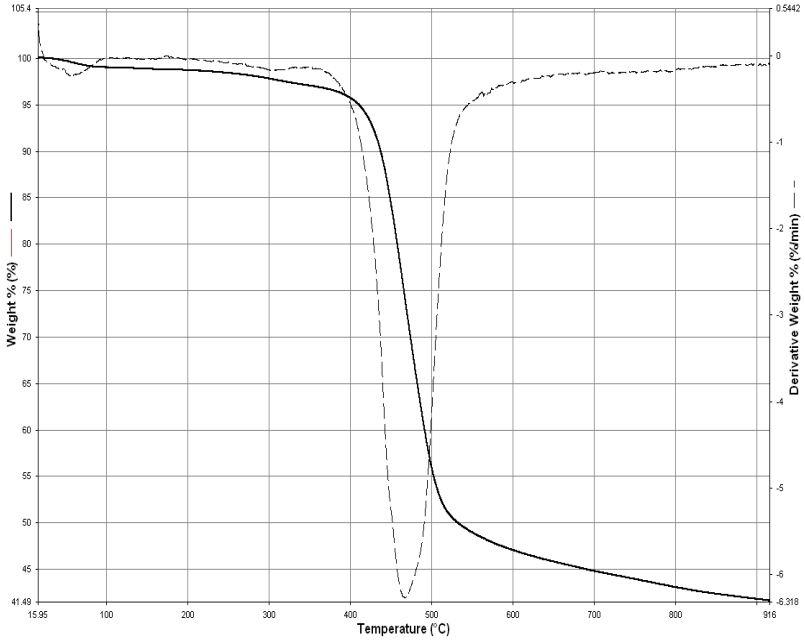


**Figure A.3** TGA result of P2

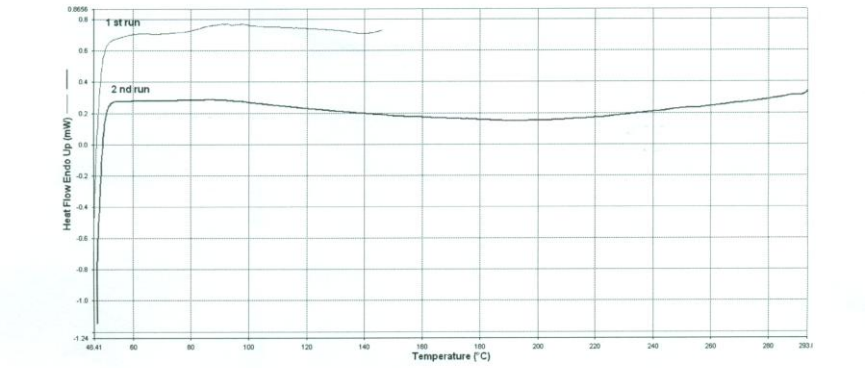


**Figure A.4** DSC result of P2

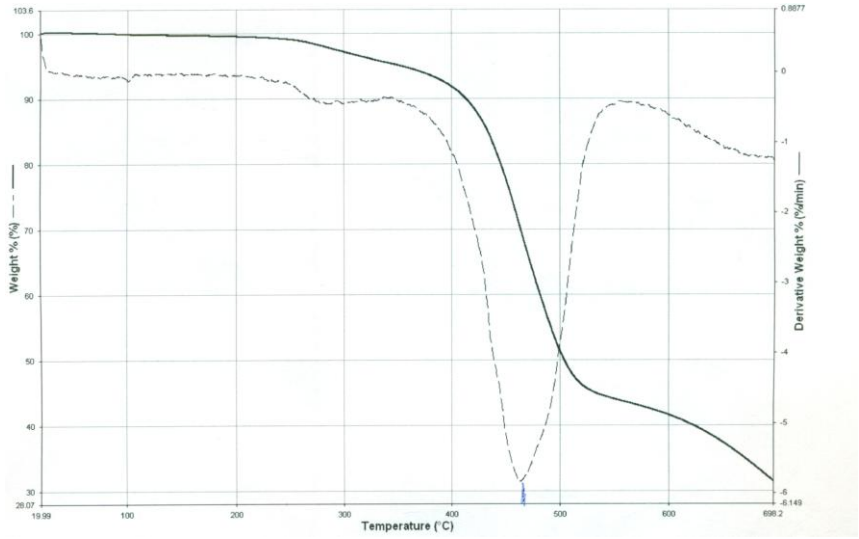


**Figure A.5** TGA result of P3

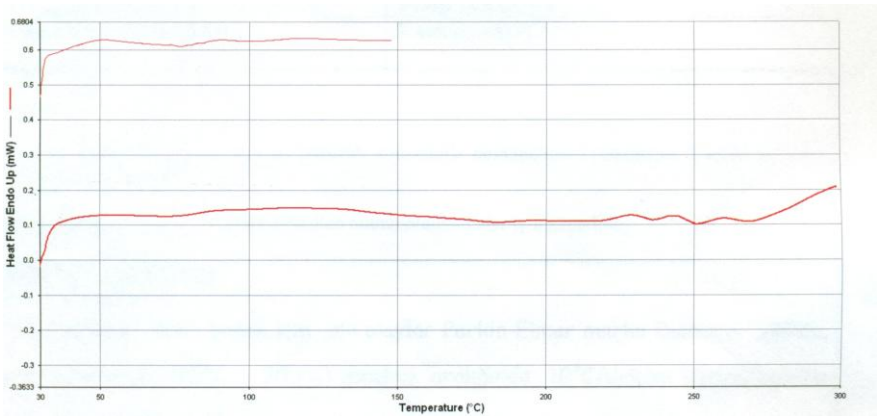


**Figure A.6** DSC result of P3